Circuit Level Modelling of a Capacitive Electric Field Sensor

Faheem Mahomed

Johannesburg, 2012

A dissertation submitted to the Faculty of Engineering and the Built Environment, University of Witwatersrand, for the degree of Master of Science in Engineering.

Declaration

I declare that this dissertation is my own, unaided work, unless otherwise acknowledged. It is being submitted for the degree of Master of Science of Engineering at the University of Witwatersrand, Johannesburg. It has not been submitted before for any degree or examination at any other university.

Signed on: ____ day of _____ 20___

_____

Abstract

This work addresses the problem of modelling an electric field detection device. The modelling of the device was approached from two different perspectives. The first approach entailed using the physics principles which describe the operation of the electric field sensor, the contemporary theory which is used to analyze electric field sensors and its limitations. The second approach used the theory which describes the capacitive interaction of a four-bodied system. A robust circuit model was derived using both cases and shown to be interchangeable under the assumptions that the electrodes generating the electric field are sufficiently large and far enough from the sensor.

An experimental apparatus was designed which could verify this model. This apparatus was composed of two major parts, namely the field generation device, and the field detection system. Considerations in the construction of the field generation device involved uniformity of the generated field and a ground reference of the supply. This influenced the design of the sensor system. The sensor system had to operate as a free-body system with no ground reference connection in order for the uniformity of the generated field to remain intact. The differences between the model prediction for the expected measurements and the actual physical measurements are small. Reasons for this difference are presented and they include non-uniformities in the generated field and non-ideal characteristics of the components and devices used for the experiment. Possible improvements to the model and sensor device are discussed and they include installation of an attachment which allows maneuverability of the sensor, such as an insulated handle and a further derivation which would result in a more geometrically independent model.

Özet

Bu çalışma bir elektrik alan bulma aletini yapmanın sorununa hitap eder. Cihazın yapılmasına iki farklı açıdan yaklaşildı. İlk yaklaşım elektrik alan algılayıcısının çalışmasını tanımlayan fizik ilkelerini kullanmayı gerektirdi ki bu elektrik alan algılayıcıları ve onun sınırlamalarını analiz etmek için kullanılan çağdaş bir teoridir. İkinci yaklaşım, dört-vücutlu bir sistemin kapasitif etkileşimini tanımlayan teoriyi kullandı. Her iki yaklasım kullanılarak türetillen sağlam bir devir modeli, elektrik alanını oluşturuyor olan elektrotların algılayıcıdan yeterince büyük ve yeteri kadar uzak olduğu farz edilerek yer değiştirebilirligi gösterildi.

Bu modelin doğruluğunu gosteren deneysel bir cihaz tasarlandı. Bu cihaz, alan üretim aleti ve alan bulma sistemi isimli iki ana parçadan oluşturuldu,. Alan üretim aletinin inşasında dikkatler, oluşturulan alanın düzenliliği ve tedariğin bir yer referansını karıştırdı. Bu algılayıcı sisteminin tasarımını etkiledi. Algılayıcı sistemi, oluşturulan alanın düzenliliği için emirde yer referans bağlantısı olmadan el sürülmemiş kalması için bir özgür-vücut sisteminin olduğu gibi çalıştırmak zorundaydı. Beklenen ölçümler için örnek tahmin ve asıl fiziksel ölçümlerin arasında farklar küçüktür. Bu farkin sebepleri oluşturulan alanda düzenlilik olmamasi ve deney için kullanılan alet bileşenlerinin ideal olmayan karakteristiklerindendir. Modele ve algılayıcı aleti olası iyileştirmeler tartışıldı, ve onlar, daha geometrikçe bağımsız bir modelle sonuçlanacak olan algılayıcının, yalıtılmis bir kulp ve daha fazla bir köken gibi manevra yapılabilirliğine izin verecek olan bir ek parcanin yerleştirmesini kapsar.

مُلخَّص

يتناول بحث الماجستير هذا، مسألة وضعِ نموذجٍ لجهازِ رصدٍ أو كشفٍ لمجالٍ كهربائيٍ. لهذا الغرض تمّ التطرُّقُ والتقريبُ لهذه المسألةِ من زاويتينِ مختلفتينِ. أولاهما تعتمد على استخدام مبادئ الفيزياء لتوضيح عمل مكشافِ المجالِ الكهربائي، أي النظريّة الحديثة المستخدمة في تحليل مجال الكهرباء لأجهزة الاستشعار وكذلك محدوديتها. أمّا الثانية فقد أُستخدِمت النظريّة التي تصف التفاعل السّعوي لنظام الأربعِ أجسام. نموذج دارة قويّة يعتمد على إستعمال كِلتا الحالتين، يُظهِرُ التبادل تحت فرضيّات أنّ الأقطاب الكهربائية لتوليد المجال الكهربائي هم كِبارٌ و بعيدي بما فيه الكفاية عن جهاز الكشف. جهازٌ تجريبي صُمِّم بإمكانه التأكُّد والتثبُّت من هذا النّموذج. هذا الجهاز يضم قسمين رئيسيين وهما، جهاز توليد المجال و نظام كشف المجال. لبِناء جِهاز توليد المجال أُخِذَت في الإعتبار التّماثل في المجال المولَّد و كذلك مرجعيّة أساسيّة للإمداد. هذا وقد أثَّر على تصميم نظام الاستشعار.

إنَّ نظام الاستشعار يجِب أن يعمل على نظام الإستِقلاليَّة بدون ارتِباط مرجعيَّة أرضيَّة حتَّى نحافظ على خصائص المجال المُولَّد. إنَّ الفروقات بين تكهُن النموذج للمقاييس المُتوقَّعة و المقاييس الفزيائيَّة الفعليَّة هي صغيرة. إنَّ أسباب هذا الاختلاف موضَّحة في هذا البحث ومنهاُيعود إلى عدم التماثل في توليد المجال وكذلك عدم مِثاليَّة خصائِص المكوِّنات والأجهزة المُستعملة مي هذه التجربة. إمكانية تحسين الأداة على النموذج و جهاز الإستشعار نوقشت وقدِّمت وهي تشمل تركيب مُرفقٍ من شأنِه إجازُ مرونة لجهاز الإستشعار، مثل مقبضٍ معزول ومزيد من الاشتقاق الذي من شأنه أن يسفر عـ لى نموذج أكثر إستقلالاً هندسياً.

Abstrait

Le travail de cette thèse porte sur le problème de la modélisation d'un dispositif de detection d'un champ électrique. La modélisation de l'appareil a été approchée de deux perspectives différentes. La première approche impliquait la physique utilisant les principes qui décrivent le fonctionnement du champ électrique du capteur, la théorie contemporaine qui est utilisé pour analyser détecteurs de champ électrique et de ses limitations. La deuxième approche utilisée la théorie qui décrit l'interaction capacitive d' un système a quatre organes . Un modèle solide de circuit a été calculé utilisant les deux cas et montré être interchangeables selon les hypothèses que les électrodes du champ électrique produit sont suffisamment grandes et espacées du capteur.

Un appareil expérimental a été conçu qui pourrait vérifier le modèle. Cet appareil a été composé de deux parties principales, à savoir le périphérique de la génération du champ et le système de detection du champ. Des Considérations dans la construction de la périphérique de la génération du champ impliqué l'uniformité du champ généré et un terrain de référence du fourni. Ca, a influencé la conception du système de capteurs. Le système de capteurs doive fonctionner comme un système libre avec aucune connexion au référence du sol et ca pour l'uniformité du champ généré qui doit rester unchangeable. Les différences entre la prédiction du modèle pour les mesures attendu et les mesures physiques réelles sont petites. Les raisons de cette différence sont présentées et ils comprennent les non-uniformités dans le champ généré et les caractéristiques non idéales des composantes et dispositifs utilisés pour l'expérimentation. Des améliorations possibles au modèle du capteur et périphérique sont examinées et comprises notamment l'installation de la pièce jointe qui vous permet de manoeuvrer le capteur, tels qu'une isolation de poignée et une nouvelle dérivation qui résulterait en une modèle plus géométriquement indépendant.

Acknowledgements

I would firstly like to thank my parents, who always, to the best of their abilities assist, motivate and support me. My supervisor, Prof. Ivan Hofsajer, who was almost always available to provide guidance or encouragement, and for being patient with me, to him I am immensely grateful. I would also like to thank my wife, who was tolerant and supportive. I would like to thank those friends of mine, in particular Abdul-Khaaliq Mohamed, and Yusuf Mahomed, who always took time out of their lives to help or advise me when I needed help and advice. I also acknowledge Emile Brink for his work in the field of electromagnetics. Finally, I would like to show appreciation to all of those who were there to keep me sane and “force” me to take breaks, even when I needed to work.

Contents

List of Figures

Chapter 1

Chapter 2

Chapter 3

Chapter 4

Chapter 5

No Figures.

Appendix A

Appendix B

Appendix C

List of Tables

Chapter 1

No Tables.

Chapter 2

Chapter 3

No Tables.

Chapter 4

Chapter 5

No Tables.

Appendix A

No Tables.

Appendix B

No Tables.

Appendix C

Chapter 1

Introduction

1.1 Introduction

A description of the problem statement and a basic outline of the methods used are provided in this chapter. This chapter will also provide some insight into the contemporary methods that are used for electric field detection and the operation of capacitive sensors. An explanation of the methodology and approach undertaken in order to successfully model, design, construct and test a parallel plate uniform electric field sensor is also documented here.

Low frequency AC electric field detection in a uniform field situation is a widely covered topic and is performed for various applications [1-3]. There already exists a variety of sensor types and procedures in order to perform such measurements [1].

The standards [1, 2] document the most common of these measurement devices, which are optical electric field sensors and capacitive electric field probes. Brief descriptions of these devices will be provided in this chapter; however, focus will be placed on capacitive electric field probes.

Electric field measurement is important and can be used for various purposes. Wijeweera et al [4], designed an electric field sensor which can be used for both AC and DC systems and summarizes a few of the applications for electric field measurements. These include providing safety for equipment and their operators during live line maintenance [5] and the design of insulation systems [6]. Other applications include simple, inexpensive and safe measurement of voltage in power systems [7], and partial discharge detection [8].

Capacitive probes are commonplace in various categories of measurements including electrocardiograms [9], proximity detection [10], flow rate [11], and many other applications. There are also various types of capacitive probes which are used for electric field detection under AC and DC conditions [1, 2, 4]. The principles on which these devices function and their limitations will be discussed.

1.2 Problem Statement

It is important to realise that although various documents exist which describe the functionality and operation of capacitive electric field detection devices, there exists no general simple circuit model which can be used to design a particular sensor for a required application or to accurately predict the behaviour of the sensor in a particular field environment on a circuit level.

This document focuses on the modelling at a circuit level and the design of a specific capacitive electric field probe (a simple parallel plate sensor) and its predictability in simulation and actual measurement for a uniform field using this circuit model. This model is designed with limitations of the geometry of the sensor and field generation device. It is based on the circuit model which represents a four bodied capacitively coupled system. This circuit model represents an electric field transformer, which can be described as a dual to the magnetic transformer, however, this model has a voltage as an input, and this is limited. By modifying this model to have an electric field instead of voltage as an input, the voltage potential, which generates the field for a particular conductor geometry, is unimportant and hence the model can function effectively as an electric field sensor circuit model. This will result in a more complete circuit representation which can approximate the fringing electric fields in the region of the sensor.

1.3 Methodology

In order to derive a simple circuit model which represents a sensor in an electric field a comprehensive understanding of the contemporary theory that describes parallel plate sensors had to be achieved.

This involved investigating the concepts of charge, electric field and capacitance from a physics as well as a circuit analysis point of view. The method of analysis which is currently present in the IEEE standards [1 – 3] is discussed and its limitations are presented. Thereafter, the circuit model which is derived from four conducting bodies is shown, and this four terminal, or two-port model, is shown to be useful. Under certain conditions, it can be simplified to a two-terminal representation of a sensor present in an electric field.

An entire measurement system is then designed which comprises of an electric field generation device (which are simply two large parallel conductor plates) and a sensor system (which consists of an amplifier and voltage measurement device). Various considerations had to be addressed in the design of this system and they included uniformity of the electric field that was generated as well as the effects of parasitic self-capacitances present in the system.

Thereafter, experiments were conducted where the generated field was varied in terms of its magnitude and frequency and the voltages were measured across the parallel plates of the sensor. Results of this are presented and then compared to the model prediction for these voltages. An evaluation of this comparison is then provided and future work is discussed.

1.4 Literature Review

1.4.1 Common Device Types for AC Field Measurement

As mentioned earlier, the standards [1, 2], describe the two most common types of electric field sensors, capacitive and optical. The capacitive sensors are broken up into two categories, namely free-body meters and ground-reference meters. The following subsections summarize the contents of the standards [1, 2].

1.4.1.1 Free-Body Meters

The sensor system designed in this document is a free body-meter. Detailed reasoning for this is shown in chapter three.

Free body meters are defined by [1, 2] to operate by measuring the induced current, or fluctuating charge, between the conductors of the sensor or probe when it is inserted into an electric field. This measurement of the steady state current is taken above the ground plane and typically used in survey type measurements. This type of probe *must* be electrically isolated. This means that there is no ground reference connection to the probe. In other words, a "floating" measurement is taken. Figure 1.4-1 illustrates this. Any type of conductor and separating dielectric arrangement or geometry is allowed for free-body meters, however, for simplicity, the parallel plate type drawn in Figure 1.4-1 is used. The display device does not have to be attached to the sensor or probe, and even remote display and on-board sensor measurement storage devices exist.

The theory describing the physics of operation of free-body meters is explored in further detail in section 2.4 of chapter two.

.

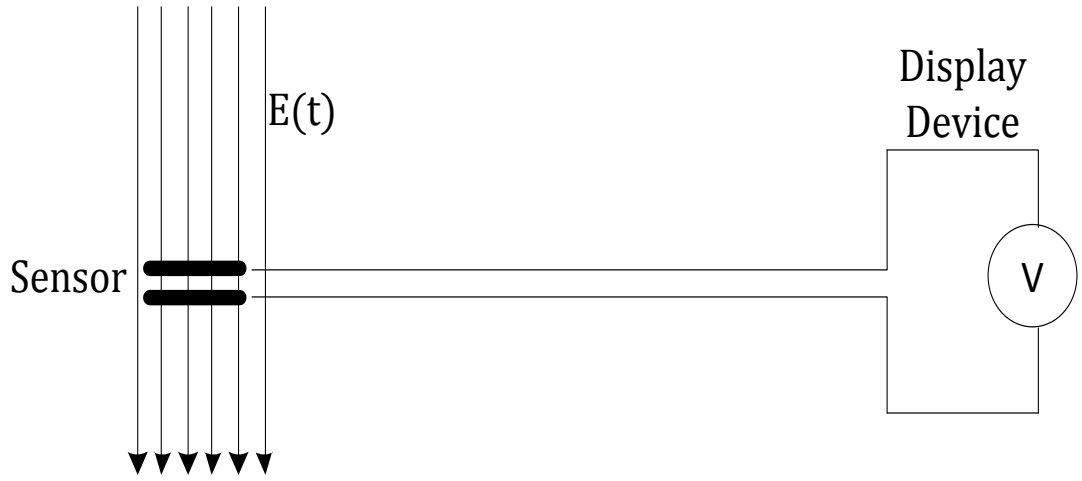

Figure 1.4-1: Typical setup of a free-body type probe.

1.4.1.2 Ground-Reference Meters

These meters are defined by [1, 2] to operate by measuring the charge or current induced by the electric field at ground level, or on the surface of a flat conductor plate

at ground potential. This means that one conductor acts as the sensing surface, while the other is at ground potential. This is shown by Figure 1.4-2.

When a planar surface is energized and the sensor is operated at the same potential as the surface, the measurement of the field strength can be achieved using this type of meter [1, 2].

The theory of operation is similar to that of the free-body sensor and will not be discussed. The most important difference is that this meter requires a connection to ground for it to operate effectively [1, 2].

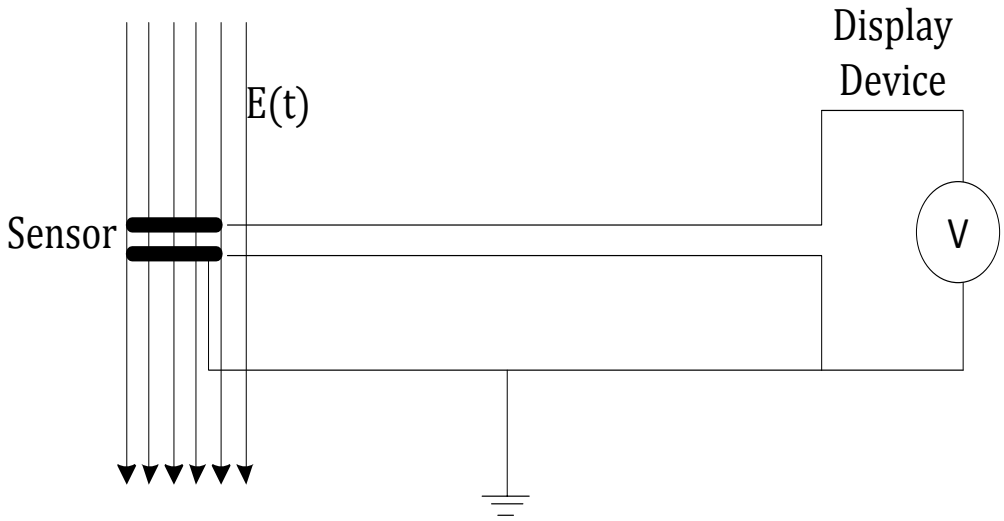

Figure 1.4-2: Typical setup of a ground-reference type probe.

1.4.1.3 Optical Sensors

The most common optic field sensor is described by [1, 2] to operate on the principle of Pockel's effect when there exists an electric field around it. Unlike the ground-reference meter, these devices can be operated without a ground connection, and can therefore be employed for tasks that are similar to the free-body meters. It is, however, not feasible to utilize this device for applications where the field strength is below approximately 5 kV/m. These probes are advantageous in size and

manoeuvrability to their typical free-body counterparts, and can be placed very close to conductors using insulating handles.

The general principle of operation is that light is passed through a dual refractive crystal, termed as a Pockel's crystal, and the presence of an electric field changes the intensity of the linearly polarized light. The relationship of this transmitted light to the incident light is described in terms of the electric field mathematically and can be predicted according to the properties of the crystal, namely, its refractive index, thickness, and its electro-optic coefficient. Fiber-optic cables are normally used in order to transmit and receive this light, and a separate unit is required for signal analysis outside the field.

These meters are complicated and expensive to fabricate. There are, however, advantages to this type of meter and they are listed below [12]:

- Immunity to electromagnetic influence.
- Galvanic isolation from sensors to the ground potential.
- This type of meter is suitable for HV applications since it provides the required sensitivity, manoeuvrability and bandwidth for these applications.

This type of sensor will not be considered for the investigation because it has a very limited sensitivity and is expensive.

1.4.2 DC Field Measurement

DC field measurement is slightly more complicated than AC measurements. DC field meters generally convert the field into an AC field by mechanically rotating or vibrating the conductors. There are two types of DC field meters described by the standard [13], namely field mills (also known as generating voltmeters) and vibrating plate electric field meters. Field mills are also broken up into two categories, namely the shutter type and the cylinder type. The following discussion on DC field meters is made with reference to [13].

Both of the DC field meter types, i.e. field mill and vibrating plate meters, measure the modulated currents or charges which are induced capacitively by the sensing conductors. They also both contain motors in order to mechanically manipulate the exposure of these sensing conductors or electrodes to the field so as to create an AC measurement.

Field mills contain a fan-like structure which is rotated and the exposure to the field is intermittently varied according to this frequency of rotation. The vibrating plate meters, however, operate by oscillating the linear position of one of the parallel sensor plates, and this results in an AC field dependent on the frequency of this oscillation.

The sensor model which is derived in this document considers only AC electric fields, and cannot be applied to DC sensors.

1.4.3 Existing Method of Modelling a Sensor in Circuit Form

Solving for the AC electric field strength is in general performed using the methods describes by the standards [1, 2]. However, there is an interesting application specific model used by Mehdizadeh [14], which describes the inter-plate dielectrics, especially in the case of stratified or layered dielectrics via a circuit model. This does not, however, show the effect of the electric field on the sensor plate system on a circuit level. It simply describes the sensor as a capacitor and analyses the system from an impedance point of view as shown by Figure 1.4-3. Here the circuit model simplifies analysis of the two complex impedances caused by the two different dielectrics between the sensor plates.

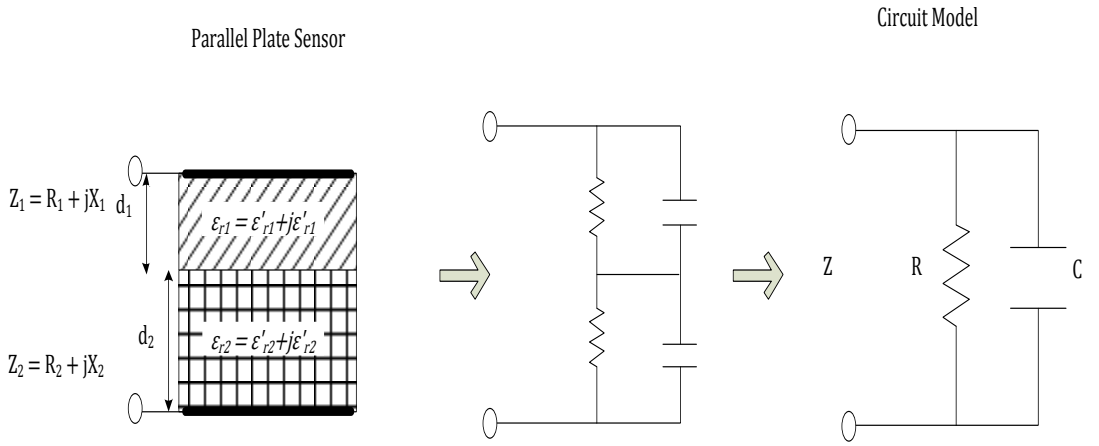

Figure 1.4-3: Impedance transformation model [14].

The purpose of this method is to represent the complex impedance (Z) between the sensor plates in terms of the complex permittivities (ε_{r1} and ε_{r2}) of the dielectric materials present between the sensor plates. This method is useful in terms of analysing the impedances of the system, especially when there is more than one dielectric between the sensor plates; however, it does not provide an insightful description which allows for the complete analysis of a parallel plate sensor in an electric field on a circuit level.

It is not comprehensive since it cannot be applied to account for parasitic capacitances of the sensor plates or fringing electric fields. It also does not provide for a clear representation on a circuit level of the external electric field.

1.4.4 Circuit Model of a Four Bodied System

Chapter two describes this model and its derivation in further detail. It has been shown that a four-bodied system can be represented from a circuit analysis perspective [15 - 18]. The four bodied system in terms of its inter-capacitances is shown as Figure 1.4-4. By considering bodies one, two, three and four as terminals, the simplified circuit model representation of this system is shown as Figure 1.4-5.

This system can be used to determine an AC electric field that is caused by a potential between bodies one and two (for example if they are parallel plates, this electric field will be uniform), when bodies three and four are present in the field.

The four bodied system model can be manipulated mathematically in order to be dependent on the field between bodies one and two instead of the voltage potential between them. This means that by simplifying this model, a general model for a capacitive electric field detection device can be derived.

The circuit model for this system can be described as an electric field transformer model [15 - 18]. It has an input and output port. The input port is dependent on an absolute potential, and this is, however, not always practical in an electric field detection situation. This is because, in order to calculate the field due to the voltage between bodies one and two, complicated electromagnetic analysis is required which depends on the geometrical position, shape, and size of the conducting bodies. This potential is also not always known, for example in the case of measuring fields near equipment.

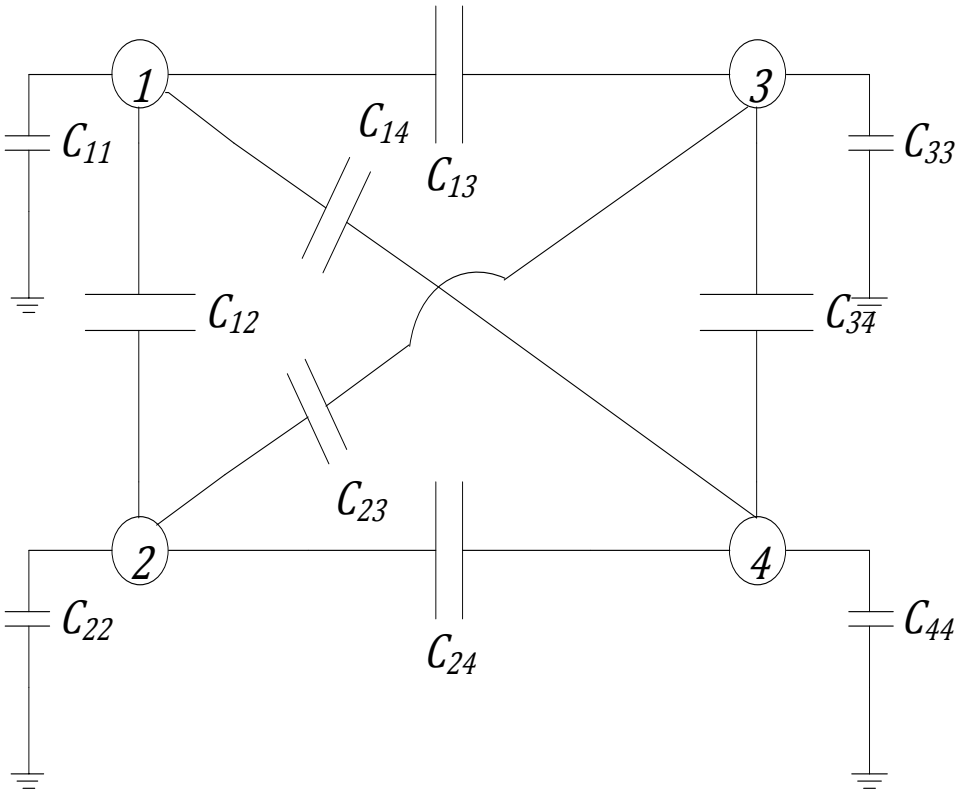

Figure 1.4-4: Four bodied system [16].

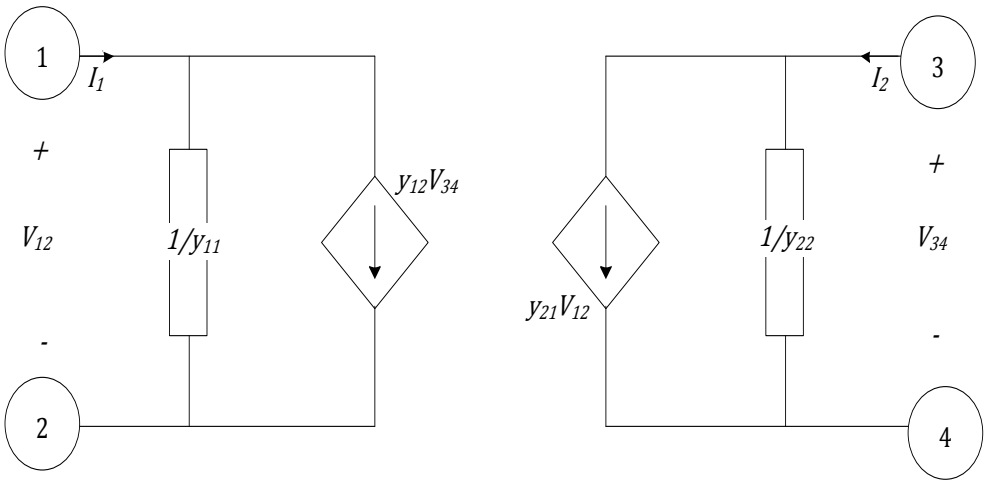

Figure 1.4-5: Circuit model representation of a four bodied system.

1.5 Conclusion

Various methods and devices exist which allow for the effective measurement of uniform AC and DC electric fields and this chapter has summarized the most common of these methods. These include capacitive and optical probes. Many applications exist for the measurement of electric fields and they include partial discharge detection and proximity detection. Capacitive probes provide better sensitivity and are more economical in terms of cost. They are also simple to construct and are divided into two categories, namely free-body sensors and ground-reference sensors. Free body sensors are shown to be more versatile in terms of measurement applications because of their independence of a direct connection to ground. Also outlined in this chapter is the lack of a general circuit model which describes a parallel plate sensor in a uniform AC electric field which can account for effects of fringing fields in the region of the sensor. The description of the methodology entails rigorous analysis of the theory available as well as the simulation, derivation and experimental validation of a model which can be used to predict the effects of an external field on a parallel plate sensor from a circuit analysis perspective.

1.6 References

[1] IEEE Standard Procedures for Measurement of Power Frequency Electric and Magnetic Fields From AC Power Lines, Transmission and Distribution Committee Of The IEEE Power Engineering Society, IEEE Std. 644™-1994 (R2008) December 1998.

[2] IEEE Recommended Practice for Magnetic Flux Density and Electric Field Strength Meters—10 Hz to 3 kHz, Transmission and Distribution Committee Of The IEEE Power Engineering Society, IEEE Std. 1308™-1994, August 2011.

[3] *Transmission Line Reference Book-45 kV and Above*, second edition, Palo Alto, Calif.: Electric Power Research Institute, 1982.

[4] Wijeweera, G., Bahreyni, B., Shafai, C., Rajapakse, A., Swatek, D., "Micromachined electric field sensor to measure AC and DC fields in power systems," *Power & Energy Society General Meeting, 2009, IEEE*, pp. 1-26, 30 July 2009.

[5] C. J. Miller, "The measurement of electric fields in live line working," *IEEE Trans. Power App. Syst.*, vol. PAS-86, no. 4, pp. 493–498, Apr. 1967.

[6] G. H. Vaillancourt, J. P. Bellerive, M. St-Jean, and C. Jean, "New live line tester for porcelain suspension insulators on high-voltage powerlines," *IEEE Tran. Power Del.*, vol. 9, no. 1, pp. 208–219, Jan. 1994.

[7] Gerrard, C.A., Gibson, J.R.; Jones, G.R.; Holt, L., Simkin, D., "Measurements of power system voltages using remote electric field monitoring," *Generation, Transmission and Distribution, IEEE Proceedings*, vol. 145, no. 3, pp. 217-224, May 1998.

[8] Lee, K.W.; Park, S.H.; Lim, K.J.; Kang, S.H.; , "Design and application of electric-field sensor for measuring PD signals in high voltage equipments," *Proceedings of the 7th International Conference on Properties and Applications of Dielectric Materials, 2003*, pp. 828- 830 vol.2, 1-5 June 2003.

[9] Maruyama, T.; Makikawa, M.; Shiozawa, N.; Fujiwara, Y.; , "ECG Measurement Using Capacitive Coupling Electrodes for Man-Machine Emotional Communication," *IEEE/ICME International Conference on Complex Medical Engineering, 2007. CME 2007*, pp. 378-383, 23-27 May 2007.

[10] Hyung-Kew Lee; Sun-Il Chang; Euisik Yoon; , "Dual-Mode Capacitive Proximity Sensor for Robot Application: Implementation of Tactile and Proximity Sensing Capability on a Single Polymer Platform Using Shared Electrodes," *Sensors Journal, IEEE* , vol. 9, no. 12, pp. 1748-1755, Dec. 2009

[11] Cheng-Ta Chiang; Yu-Chung Huang; , "A Semicylindrical Capacitive Sensor With Interface Circuit Used for Flow Rate Measurement," *Sensors Journal, IEEE* , vol. 6, no. 6, pp. 1564-1570, Dec. 2006.

[12] Rahmatian, F.; Jaeger, N.A.F.; , "High accuracy optical electric field and voltage sensors," *Optical Fiber Sensors Conference Technical Digest, 2002. Ofs 2002, 15th*, pp. 411- 414, vol. 1, 2002.

[13] IEEE Guide for the Measurement of DC Electric-Field Strength and Ion Related Quantities, *IEEE Std 1227-1990*, pp. 1, 1990.

[14] M. Mehdizadeh, *Microwave/RF Applicators and Probes for Material Heating, Sensing, and Plasma Generation: A Design Guide*. Elsevier, Oxford, first edition, chapter 3, 2010

[15] Y. Mahomed. “Derivation of an electric transformer circuit model based on electric field coupling” 4th Year Project Report 10P03, School of Electrical and Information Engineering, University of the Witwatersrand, South Africa, 2004.

[16] F. Mahomed. “Definition and application of a new capacitive coupling technique: Electromagnetic considerations.” 4th Year Project Report 10P03, School of Electrical and Information Engineering, University of the Witwatersrand, South Africa, 2010.

[17] Chao Liu; Hu, A.P.; Budhia, M.; , "A generalized coupling model for Capacitive Power Transfer systems," *IECON 2010 - 36th Annual Conference on IEEE Industrial Electronics Society*, pp. 274-279, 7-10 Nov. 2010.

[18] Y. Mahomed, I. Hofsajer. “A Discussion on the Duality Principle Applied to Mutual Inductance”, School of Electrical and Information Engineering, University of the Witwatersrand, In preparation.

Chapter 2

Uniform Electric Field Sensor Model

2.1 Introduction

In this chapter the investigation of the theory which describes uniform electric field parallel plate sensors is documented. Existing analysis techniques which represent these types of sensors are shown to be dependent on the physics which describes the system from a field perspective. This is complicated and a circuit model provides the means to easily design for a sensor which is suitable for a specific application. It also allows for the simplification and hence the accountability of external effects which may affect the measurement of an electric field.

The circuit model of a four-bodied system was initially considered as it completely describes the interaction of a typical electric field detection case. This model, although displaying feasibility and potential, was shown to not clearly represent the influence of an electric field in the system. Hence, a simpler model was derived using FEM simulations. The two models are then shown to be mathematically equivalent under certain conditions, and this chapter documents the process followed in order to achieve this.

An investigation was conducted which provides an understanding of the relationship between the external uniform field and the resulting current that flows and the voltage that manifests between the sensor plates under various conditions. A brief background is provided which describes the theory and approach of the investigation from the point of view of the contemporary theory, the four bodied system model, as well as the final model for the electric field sensor. This is followed by the results which describe the models, discussions which define their limitations and conditions for which they are valid, and finally, conclusions are provided.

Figure 2.1-1 shows a block diagram representation of the sensor modelling sections in this chapter and the links between these sections that are presented here are shown.

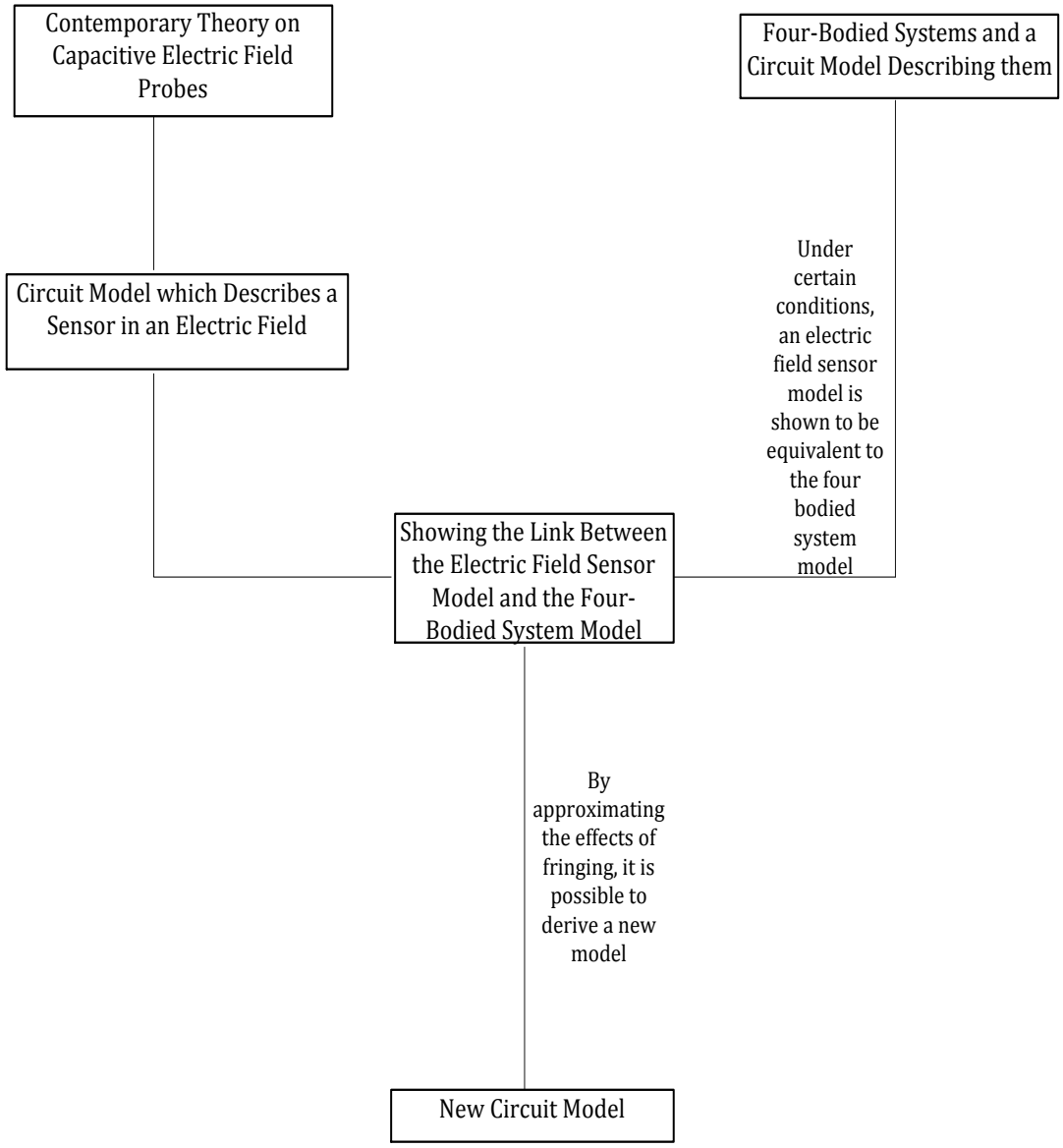

Figure 2.1-1: Block diagram explaining the links between the modelling sections of this chapter.

2.2 Electric Fields and Potential Differences or Voltages

In this section, an explanation of the definition of an electric potential is provided. The voltage or electric potential that is calculated between two points, for capacitors or resistors, from a fundamental physics perspective and its difference in sign to the voltage calculated from a circuit perspective is explored. A circuit model which describes the interaction of conductors in an electric field will have to account for this

difference in sign and hence, an understanding of the analysis of voltage from both these points of view is critical in the derivation of such a model.

In other words, the voltage that would be calculated across the sensor plates due to its interaction with an electric field around it, from a circuit analysis perspective and from a fundamental electromagnetics perspective will have a difference is sign. This section addresses this difference in sign so that the model that will be derived can account for it. This section is written with reference to Brink [1].

2.2.1 The Fundamental Physics Perspective of Voltage

Voltage is the term used to describe the potential difference between two points and it has the units of volts. Equation 2.1 shows this mathematically in terms of an electric field present between those two points (x_1 and x_2).

$$V = -\int_{x1}^{x2} \boldsymbol{E}.d\boldsymbol{s} \tag{2.1}$$

Considering Figure 2.2-1, the two oppositely charged plates produce an electric field between them. If a positive unit test charge is placed inside this field, the energy of the system is measured in terms of potential energy. By converting from potential energy to another form of energy, for example, kinetic energy or thermal energy, is considered to be a loss of potential energy to the system. It can be deduced that since the charge is motionless, the energy of the entire system is found between the electric potential energies of the field and the charge relative to its position in the field. This charge is assumed to be small enough to not distort the field distribution. The electric potential, or voltage, is defined as the energy difference of the field-charge system due to the movement of this unit test charge within the field.

Due to the properties of charge explained in Appendix A, if the unit charge is released it will accelerate away from the positively charged plate and travel a distance *d*. Thus, the potential energy of the system will be reduced or converted into kinetic energy and equation 2.1 will have a negative solution. However, by forcing the charge from

the negative to the positive plate (against the direction of the electric field) utilising an external source will cause the potential energy of the system to increase, hence a positive solution to equation 2.1.

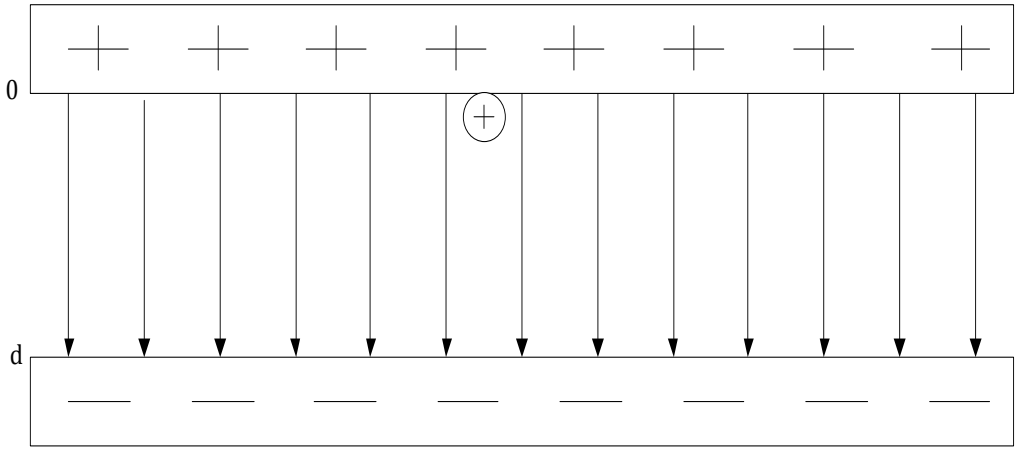

Figure 2.2-1: Positive charge in a field between two plates.

In order to illustrate the analysis of a circuit from the fundamental electromagnetics perspective, Figure 2.2-2 represents a basic circuit consisting of a source loaded by a resistor.

The voltage source is considered to be connected through the load via ideal conductors, this is not important for the analysis of this problem. To illustrate the flow of current, two positive unit test charges are considered. Their starting points are as indicated on the diagram. These charges will move through the load and source concurrently. In order to understand this concept, the other charges in the system will be ignored.

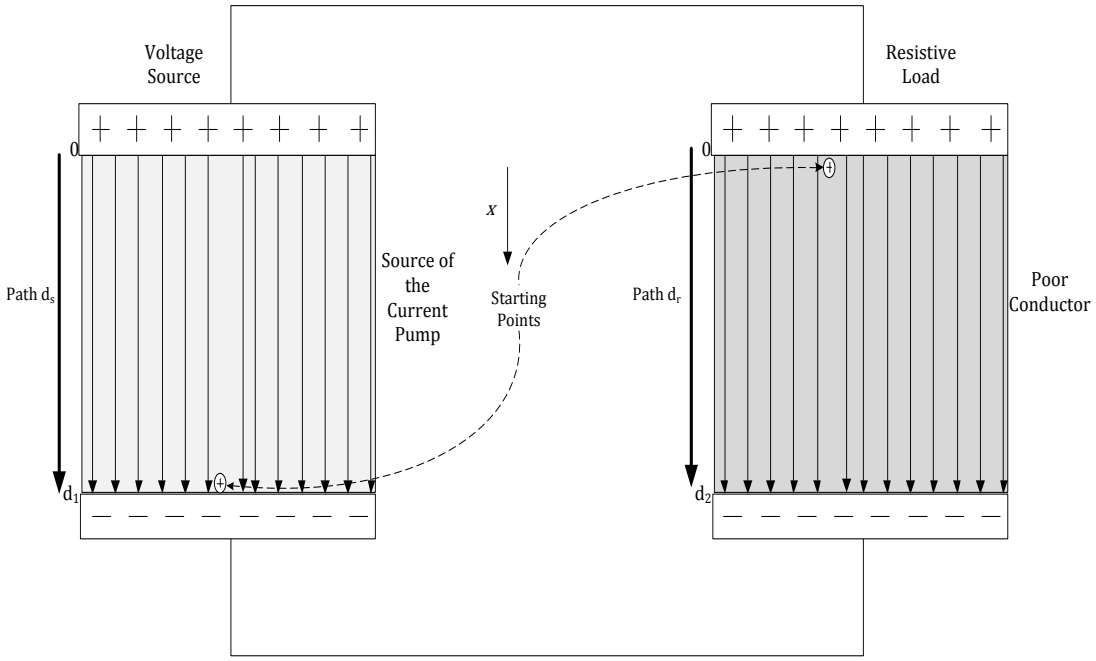

Figure 2.2-2: Field analysis perspective of a simple electric circuit.

Considering the resistive load as two ideal plates with opposite charges that create a field, and placing the test charge at the positive plate, the change in potential energy will be negative. Thus, the solution for the voltage or the electric potential difference will have a negative solution. This is shown by equation 2.2, where the subscript *R* is associated with the resistive load.

$$V_R = -\int_0^{d_2} \boldsymbol{E}_R . d\boldsymbol{s}_R \tag{2.2}$$

Writing the vectors *E* and *ds* in terms of their magnitude and direction, it can be seen that they are both parallel in the same direction. This is shown by equations 2.3 and 2.4. Therefore equation 2.2 simplifies to equation 2.5. Where $\hat{\imath}$ is the direction of the vector quantities.

$$\boldsymbol{E}_R = E_R \, \hat{\imath} \tag{2.3}$$

$$d\boldsymbol{s}_R = ds_R \, \hat{\imath} \tag{2.4}$$

$$V_R = -\int_0^{d_2} E_R . ds_R = -E_R . [d_2 - 0] = -E_R . d_2 \quad (2.5)$$

The solution for the voltage is negative, this means that due to the movement of the test charge in the field-charge system, the system has lost potential energy. The potential energy was converted into kinetic energy (described by the motion of the charge) and this in turn was converted into thermal energy (heat dissipation or I^2R).

In a similar way, the test charge situated in the voltage source will move through it. Figure 2.2-2 shows that the source can be described as positive and negative plates with a charge or current pump situated between them. This pump applies a force to the test charge, against the opposing force from the electric field. It is now possible to solve for the potential difference of the field-charge setup of the voltage source. This is shown by equation 2.6.

$$V_S = -\int_{d_1}^{0} \boldsymbol{E}_S . d\boldsymbol{s}_S \quad (2.6)$$

It is clear already that since the limits of integration are in the opposite direction from the resistor's field-charge system, the integral will result in a change in sign of the solution to the equation.

Therefore, since the field and displacement vectors are again parallel and in the same direction, shown by equations 2.7 and 2.8, equation 2.9 shows that the solution for voltage in the source is positive.

$$\boldsymbol{E}_S = E_S \, \hat{\imath} \quad (2.7)$$

$$d\boldsymbol{s}_S = ds_S \, \hat{\imath} \quad (2.8)$$

$$V_S = -\int_{d_2}^{0} E_S . ds_S = -E_S . [0 - d_1] = E_S . d_1 \quad (2.9)$$

This positive potential is expected, since the total energy of the field-charge setup of the source has gained potential energy. This energy originated from the current or charge pump, which is due to the characteristics of the source (for example, the chemical reaction of a battery). The energy supplied by this pump is then transferred to the load where it is converted into kinetic energy and finally thermal energy.

2.2.2 The Circuit Analysis Perspective of Voltage

Considering the circuit shown in Figure 2.2-2 from a circuit analysis point of view, it can be redrawn as Figure 2.2-3.

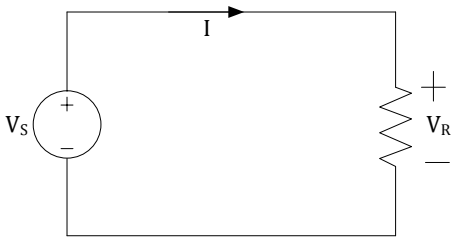

Figure 2.2-3: Circuit analysis perspective of a simple circuit.

By taking KVL around the circuit, equation 2.10 is obtained. Multiplying this by the current, equation 2.11 shows the power of the system.

$$-V_S + V_R = 0 \tag{2.10}$$

The subscript *C* denotes from a circuits perspective.

$$-P_{S_C} + P_{R_C} = 0 \tag{2.11}$$

By multiplying the actual numerical values for the test charges which are moved through the electric fields into equations 2.5 and 2.9, the change in potential energy is obtained, and adding a denominator of time to these equations will result in the power that is delivered or lost by the source and the resistive load. In other words, by simply multiplying the potentials calculated by equations 2.5 and 2.9 by the current (or charge per time) the power of the source and load can be determined. The addition of

these calculated powers results in equation 2.12. Here the subscript *F* denotes from a fundamentals perspective.

$$P_{S_F} - P_{R_F} = 0 \tag{2.12}$$

There is a clear difference in sign between equations 2.11 and 2.12. In both cases, source and resistor, the power calculated from a fundamentals perspective and that calculated from circuit analysis perspective have opposing signs.

The difference in the definition of the conventions can be used to explain this difference in sign. From a circuits perspective, the resistor absorbs power, and the conversion to thermal power is ignored, therefore a positive sign. From a fundamental point of view, the potential energy per time, or power is lost by the resistive system and hence it has a negative sign.

It is therefore evident that the reference conventions are different in these approaches and therefore if voltage is calculated from a fundamental perspective and is required to be converted to a circuit analysis perspective, the sign will need to be changed.

2.3 Electric Fields and Conductor Charge Distribution

Understanding fundamentally what happens to the charge distribution inside the conductors which form the parallel plate sensor is important to describe how the currents and voltages manifest between these plates.

The presence of the sensor in the uniform electric field causes the charge that develops on the sensor plates to change, and this change is dependent on the sensor conditions. This means that if the sensor is supplying power to a load, the charge that develops on the plates will change.

2.3.1 Open Circuited Conditions

If the sensor plates are placed in a uniform electric field, and all the dielectrics are air, then the surface charge distribution that will manifest on the surfaces of the open

circuited sensor plates is shown by Figure 2.3-1. This causes an electric field E_1, between the sensor plates. This field is equal to the electric field generated by the outer plates.

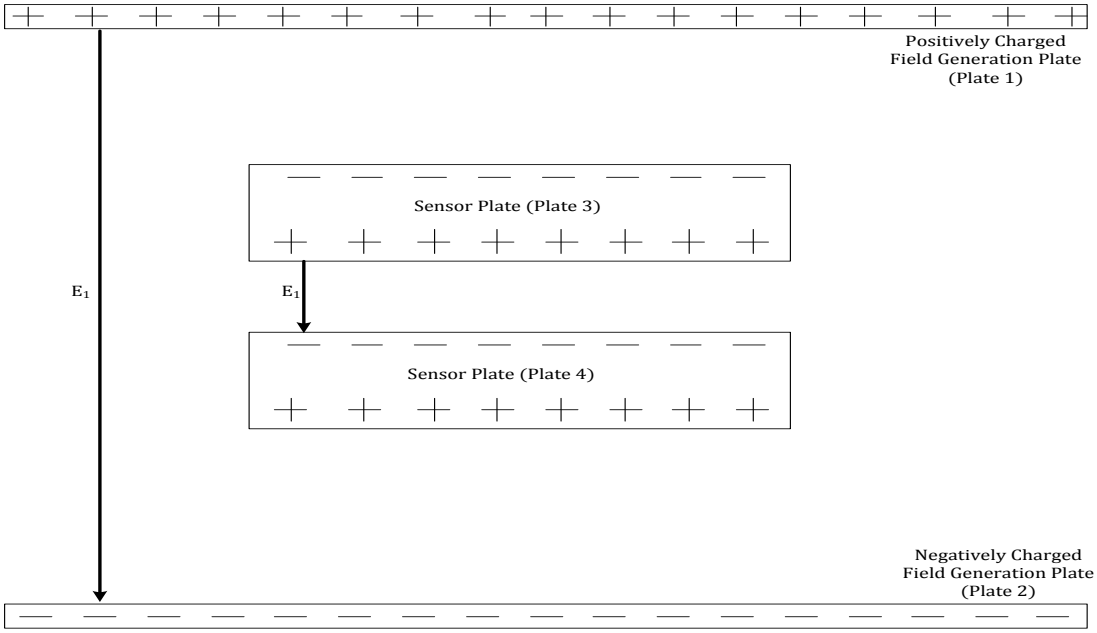

Figure 2.3-1: Charge distribution of the system under open circuited conditions.

Considering either just the top or the bottom sensor plate shown in Figure 2.3-1, it can be seen that the charge at the upper side of the plate is equivalent to the negative of the charge at the lower side of the plate. Under these conditions, there is no current flowing out of the sensor plates since they are open circuited. To state this differently, if the field E_1, is a time varying field, and the charge between the upper and lower surfaces of each of the sensor plates with respect to time is added, the result will be zero. This is referred to as the charge difference between the upper and lower surfaces of the sensor plates. The term difference is used simply because the one quantity is positive and the other is negative.

2.3.2 Short Circuit and Loaded Conditions

If a load is added to the sensor plates, the surface charge distribution of these plates will change. This means that the magnitude of the surface charge difference between the upper and lower surfaces of the sensor plates will change and become linearly

larger as the load is decreased from an open circuit to a short circuit. Or, in terms of current, under conditions of a time varying field, the magnitude of the current supplied by the sensor plates will become larger as the impedance between the plates becomes smaller (inversely proportional relationship between charge and impedance).

This means that the electric flux density and electric field is also different at the upper and lower sides of the plate in Figure 2.3-2 which shows the special case of a short circuit. Therefore, the electric field between the plates is the negative of the supplied electric field E_1 and the total field between the sensor plates, which is the addition of these two quantities, is zero. Under AC conditions this means that a maximum current flows between the plates when the sensor is short circuited and no current flows when it is open circuited. Stated differently, a maximum voltage can be measured between the sensor plates when they are open circuited and a zero voltage is measured across them when they are short circuited.

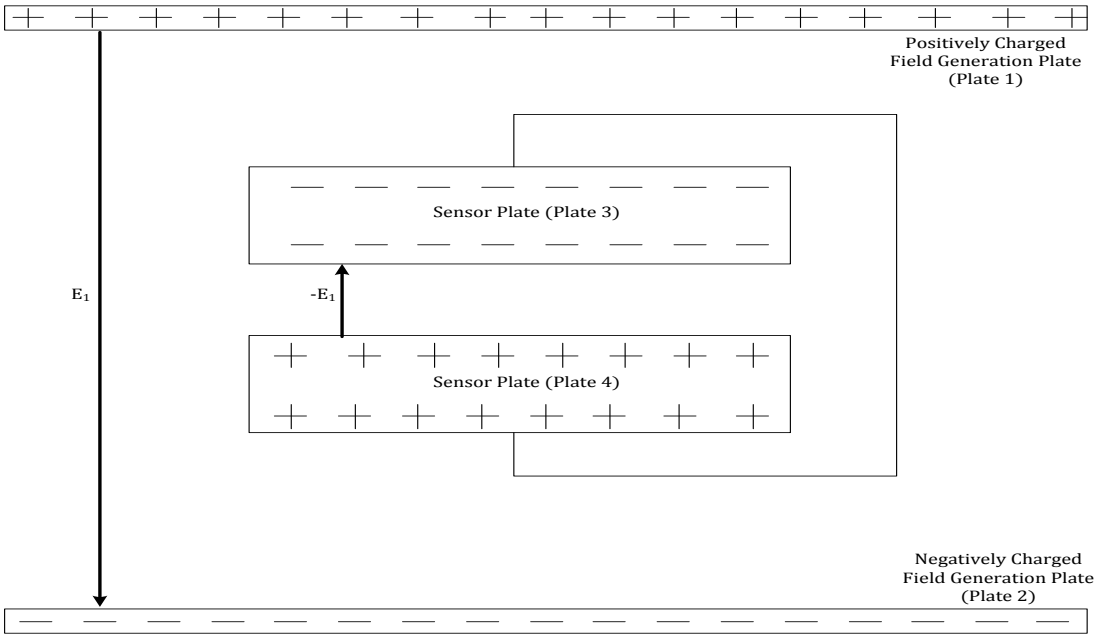

Figure 2.3-2: Charge distribution of the system under short circuited conditions.

2.3.3 Inclusion of Dielectric Materials

When a dielectric is introduced between the sensor plates, the uniform electric field that is generated becomes slightly distorted. This is because the dielectric results in a confinement, or concentration, of this field between the sensor plates. This means that

if the open circuited case is considered, and if the dielectric separating the sensor plates has a permittivity larger than that of the separating dielectric of the plates generating the field, there is a difference in the amount of flux lines entering and leaving each plate of the sensor plate system. In terms of the electric field strength, the electric field that is present between the sensor plates, E_2, will be different from the electric field generated, E_1 (refer to Figure 2.3-3). This, in an ideal case, forms a proportional relationship and hence the field strength between the sensor plates is proportional to the generated field by the permittivity of the dielectric present between the plates generating the field compared to that of the dielectric separating the sensor plates. This is represented mathematically in equation 2.13.

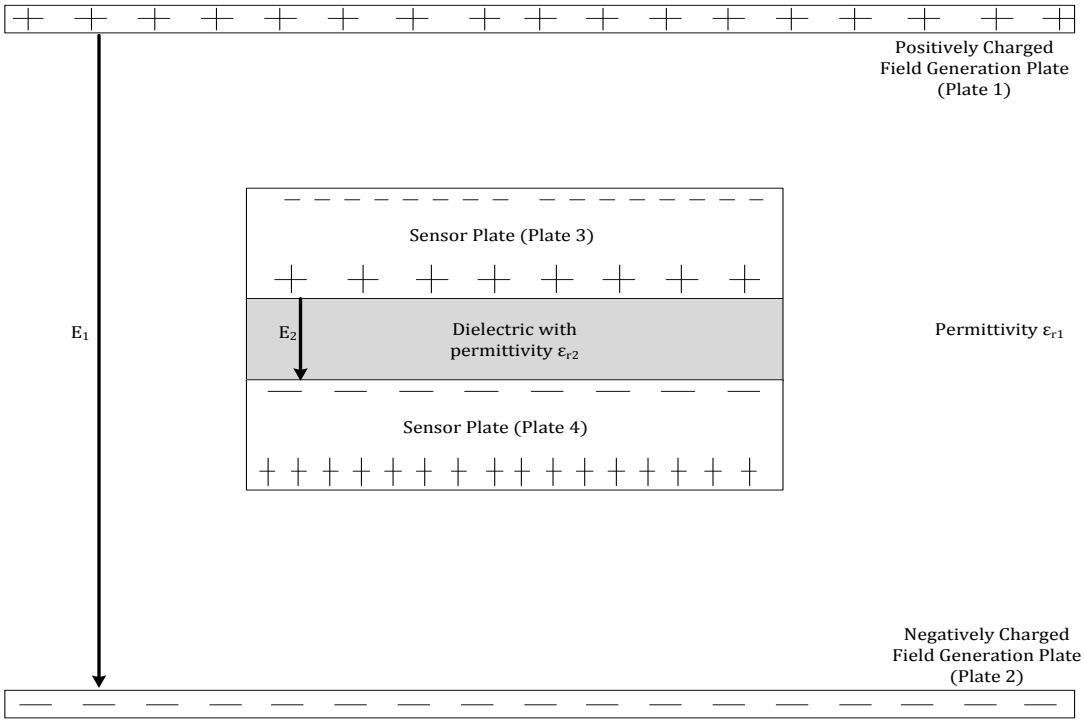

Figure 2.3-3: Charge distribution of the system with a different sensor dielectric.

$$E_2 = \frac{\varepsilon_{r_1}}{\varepsilon_{r_2}} E_1 \tag{2.13}$$

Due to the introduction of a dielectric to the system, the charge distribution of the sensor plates changed. This imbalance in the distribution of the charge on the surface of the plates is due to the confinement of the electric field due to the properties of the

dielectric material. This is the reasoning which allows for the dielectric material to be modeled as a reactive load to the sensor system [2].

2.4 Contemporary Theory on Electric Field Sensor Analysis

Figure 2.4-1 depicts a typical uniform electric field detection scenario. The large outer plates provide a uniform electric field pattern for the sensor to detect, where plates three and four are the sensor plates. The plates are all considered to be 1 m in breadth in order to simplify the problem. All the theory shown is this section is adapted from [3- 5].

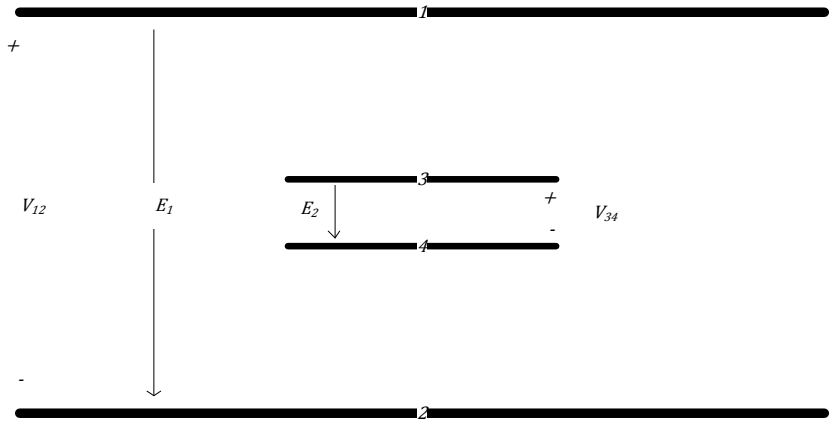

Figure 2.4-1: Geometrical representation of a uniform electric field detection scenario.

Placing a voltage potential, V_{12}, across the outer plates (or by forcing plates one and two to become oppositely charged) gives rise to an electric field (between plates one and two), E_1, as represented by equation 2.14. This is because the fundamental equation for voltage, shown as equation 2.1 simplifies due to the electric field and displacement vectors being parallel and in the same direction. Thus equation 2.14 is the solution in terms of the electric field due to a potential.

$$E_1 = V_{12}/d_{12} \tag{2.14}$$

Where d_{12} is the separation distance between plates one and two.

As explained in section 2.3, a charge separation within the conducting sensor plates occurs. If the surface charge, *Q*, on plate three (the top sensor plate in figure 2.4-1) is considered under the condition that the sensor plates are open circuited, it can be calculated using equation 2.15.

$$Q = \int D \cdot dA = C_{34}V_{34} \tag{2.15}$$

Where C_{34} is the capacitance between plates three and four, V_{34} is the open circuit voltage between those plates, *D* is the displacement flux or displacement charge, and *A* is the area of overlap of the plates which the flux lines of the field flow to and from.

Therefore the open circuit voltage, V_{34}, across the sensor plates can be written as equation 2.16. The displacement flux, *D*, can be written in terms of the electric field and the dielectric which confines the field. All dielectrics in the system are considered to be air, and the relative permittivity of air is approximately 1. This is shown as equation 2.17. Hence, the surface charge on plate three, shown by equation 2.15 can be written in terms of the electric field E_1, as equation 2.18 shows.

$$V_{34} = \frac{Q}{C_{34}} \tag{2.16}$$

$$D = \varepsilon_0 \varepsilon_r E_1 = \varepsilon_0 E_1 \tag{2.17}$$

$$Q = \varepsilon_0 \int E_1 \cdot dA \tag{2.18}$$

By substituting this definition for the surface charge in terms of the electric field into equation 2.16, and by evaluating the integral under the assumption once again that the field and displacement vectors are both parallel and in the same direction, the voltage, V_{34}, can be written in terms of the electric field generated by the outer plates, E_1. This is shown by equation 2.19. Hence, the field between the sensor plates (plates three and four, is equal to the field that is generated by plates one and two). This is described in section 2.3.

$$V_{34} = E_1 d_{34} \tag{2.19}$$

Where d_{34} is the separation distance of the two sensor plates.

These equations make the assumption that the dielectric material between the sensor plates, plates three and four, is air (refer to Figure 2.4-1). If this dielectric material is not air, then it will influence the field between the plates, as pointed out in section 2.3, by a factor of the dielectric permittivity ratio.

When the generated electric field, E_1, is an AC sinusoidal field, the short circuit current which flows between the sensor plates can be calculated. This current is simply the rate of change of charge between the upper and lower surfaces of the sensor plate conductors. Thus if the equation of charge in terms of the electric field is considered (equation 2.18), the short circuit sinusoidal current between the sensor plates, *I*, assuming an unperturbed electric field, is given by 2.20.

$$I = \frac{dQ}{dt} = j\omega\varepsilon_0 E_1 A \tag{2.20}$$

Where ω is the angular frequency of the electric field, E_1. This term is present because the time derivative of the sinusoidal electric field is taken.

Equation 2.20 implies that if the short circuit current, *I*, flowing through the sensor plates is measured, the electric field, E_1, is trivial to calculate. Similarly equation 2.19 implies that if the open circuit voltage is measured, the electric field can be calculated for a known separation distance between the sensor plates, d_{34}.

2.4.1 Limitations

The above-mentioned method is well-established and extensively documented [3, 5]. It is, however, also the most limited method. It does not allow for the design of a sensor for a specific application, for example, if the sensor is required to drive a load, or if the size of the sensor is relevant, this method does not provide a technique to design the sensor. This method also requires the separate inclusion of the effects of the dielectric separating the sensor plates. It also does not take into account the effects

of loading the sensor and isolated circuit analysis is required for this. Another major limitation is the lack of representation of the system as a circuit model which simplifies the analysis to a large extent since an understanding of the fundamental physics principles which determine the interaction of fields within the system is required in this method. This method also does not provide a means to account for the fringing electric field that occurs in the region of the sensor plates.

2.5 Four-Bodied System Model

2.5.1 Multicapacitor Systems

This section explains the interaction of multiple conductive bodies in terms of potentials and charges. There exists a network of definable capacitances between multiple conductive bodies arranged in any arbitrary fashion. The theory of the definition of such a system is fully described by Elliot in [6] and summarized here with reference to [6, 7].

Considering a system which has a number of N conductors, and making the assumption that one of the bodies is infinitely large (it is an infinite container of both positive and negative charges) and it is at the zero or ground potential (this body is considered as earth), two statements about the system can be made. Firstly, if the potential of each conductor is known, the distribution of the surface charge on the conductors can be determined, and secondly this charge distribution can be determined if the total charge on each conductor is known as well.

Now, by placing a positive unit test charge onto one conductor, leaving all of the other conductors floating, or uncharged, will result in the potentials, p_{11}, p_{21}, … , p_{N1}, on all the conductors in the system. These terms are simply a geometrical quantification of a potential (dependent on the orientation, shape and size of the conducting bodies), due to the effect that placing a charge on the conductor has on the other conductors. Hence, if a positive charge is placed on the nth conductor, leaving the other conductors floating, the potentials p_{1n}, p_{2n}, … , p_{Nn}, will be produced. Also, by placing a charge Q_1 on the first conductor, with a positive charge placed on it, the resulting potentials will be $p_{11}Q_1$, $p_{21}Q_1$, … , $p_{N1}Q_1$, and hence if Q_n is placed on S_n

(which is the surfaces of the bodies), when the positive test charged is placed on the *n*th conductor, the potentials $p_{1n}Q_n$, $p_{2n}Q_n$, … , $p_{Nn}Q_n$, are formed. Thus, it can be said that the total potential of a body is the sum of the potentials between itself and the other bodies in the system. Hence, it is possible to write the potentials of each body of the entire system, V_1, V_2, … , V_N, as shown by equation 2.21. It is shown by Elliot [6] in detail that the potential on one body due to its effect on another is equal to the potential of the second body on the first, or $p_{ij} = p_{ji}$. Therefore, the potential of a conductor is increased if a charge is placed on both itself or on another conductor in the system

$$\begin{pmatrix} V_1 \\ V_2 \\ \vdots \\ V_N \end{pmatrix} = \begin{pmatrix} p_{11}Q_1 + p_{12}Q_2 + \cdots + p_{1N}Q_{1N} \\ p_{21}Q_1 + p_{22}Q_2 + \cdots + p_{2N}Q_N \\ \vdots \\ p_{N1}Q_1 + p_{N2}Q_2 + \cdots + p_{NN}Q_N \end{pmatrix} \tag{2.21}$$

Making charge the subject of equation 2.21, it can be written in terms of the voltage, shown by equation 2.22. Here, the *c* coefficients represent geometrical quantities which can be written mathematically as the ratios of the two determinants involving the *p* quantities. These coefficients are called the coefficients of capacitance.

$$\begin{pmatrix} Q_1 \\ Q_2 \\ \vdots \\ Q_N \end{pmatrix} = \begin{pmatrix} c_{11}V_1 + c_{12}V_2 + \cdots + c_{1N}V_{1N} \\ c_{21}V_1 + c_{22}V_2 + \cdots + c_{2N}V_N \\ \vdots \\ c_{N1}V_1 + c_{N2}V_2 + \cdots + c_{NN}V_N \end{pmatrix} \tag{2.22}$$

By describing the system in terms of potential differences between bodies, as opposed to the absolute potentials of the bodies, the equation for charge in terms of voltage can now be written with a new geometrically dependent constant *C* (termed the inter-body capacitance) shown as 2.23.

$$\begin{pmatrix} Q_1 \\ Q_2 \\ \vdots \\ Q_N \end{pmatrix} = \begin{pmatrix} C_{11}V_1 + C_{12}(V_1 - V_2) + \cdots + & C_{1N}(V_1 - V_N) \\ C_{21}(V_2 - V_1) + C_{22}V_2 + \cdots + & C_{2N}(V_2 - V_N) \\ \vdots & \\ C_{N1}(V_N - V_1) + C_{N2}(V_N - V_2) + \cdots & + C_{NN}V_N \end{pmatrix} \tag{2.23}$$

A four bodied system is shown in Figure 2.5-1 along with all the possible capacitances that may be defined between the conductors, as well as the self-

capacitance of each conductor. The mathematical description of this system is known as the capacitance or C-matrix, and is given by equation 2.24 which is simply equation 2.23 rewritten where *N* is four. Using 2.24, and considering pairs of terminals as ports with connection to an external system this network can be modeled as a two port network and compared to a conventional magnetic transformer [7 - 10].

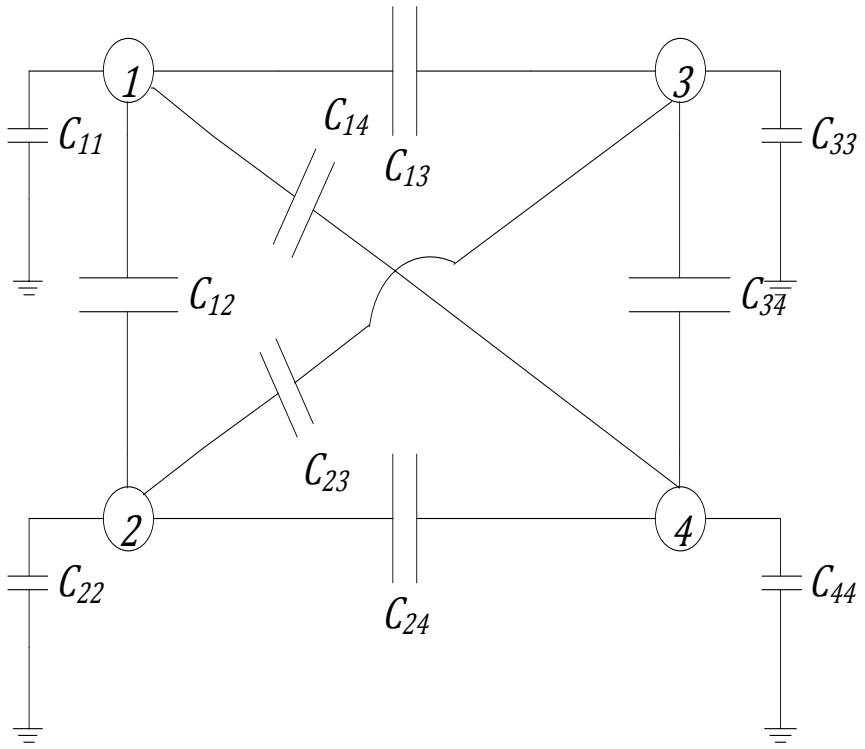

Figure 2.5-1: Four-bodied multicapacitor system [8].

All ten capacitors that exist due to the interaction of the four bodies are included in the C-matrix. The self-capacitances of the bodies, seen on the diagonal of the matrix representation of equation 2.24 are much smaller than the inter-body capacitances for this application and can be neglected in the derivation of the transformer model.

$$\begin{aligned} Q_1 &= C_{11}V_1 + C_{12}(V_1 - V_2) + C_{13}(V_1 - V_3) + C_{14}(V_1 - V_4) \\ Q_2 &= C_{21}(V_2 - V_1) + C_{22}V_2 + C_{23}(V_2 - V_3) + C_{24}(V_2 - V_4) \\ Q_3 &= C_{31}(V_3 - V_1) + C_{32}(V_3 - V_2) + C_{33}V_3 + C_{34}(V_3 - V_4) \\ Q_4 &= C_{41}(V_4 - V_1) + C_{42}(V_4 - V_2) + C_{43}(V_4 - V_3) + C_{44}V_4 \end{aligned} \tag{2.24}$$

Where Q is charge and V is voltage. The C- matrix is symmetrical about the diagonal, i.e. $C_{MN} = C_{NM}$.

2.5.2 System Model

By considering the system shown in Figure 2.5-1 as a two port, or four terminal system, it is possible to derive a circuit model describing the system [7 - 10]. This means that the conducting bodies, bodies one and two are considered as the input port, and bodies three and four are considered as the output port. This implies that applying terminal analysis circuit techniques, i.e. evaluating the short circuit currents, open circuit voltages and Thevenin equivalent impedances from both ports, results in a two-port network model of the system which can be analyzed from a circuits perspective. It is important to note that in the derivation of this model, the assumption is made for both ports that the current that enters a terminal must be equal to the current that leaves the other terminal of that port [10]. Stated differently, the charge on the surface of body one added to that of body two must be zero, and the addition of the surface charge of body three to body four must be zero [10].

The y-parameter two port network model of the four bodied system described above is shown as Figure 2.5-2 [7, 8]. This two port network is governed by equations 2.25 to 2.27 when self-capacitances are neglected [10]. The self-capacitances are neglected because as mentioned in the preceding section, they are much smaller than the inter-body capacitances. These equations are all written in terms of inter-body capacitances.

In this system, the input voltage is defined to be the voltage (V_{12}) between conductors one and two, and the output is defined to be the voltage (V_{34}) between conductors three and four.

$$y_{11} = j\omega \left[\frac{(C_{13} + C_{14})(C_{24} + C_{23})}{(C_{13} + C_{24} + C_{23} + C_{14})} + C_{12} \right] \tag{2.25}$$

$$y_{22} = j\omega \left[\frac{(C_{13} + C_{23})(C_{24} + C_{14})}{(C_{13} + C_{24} + C_{23} + C_{14})} + C_{34} \right] \tag{2.26}$$

$$y_{12} = y_{21} = j\omega \frac{(C_{23}C_{14} - C_{24}C_{13})}{(C_{13} + C_{24} + C_{23} + C_{14})} \tag{2.27}$$

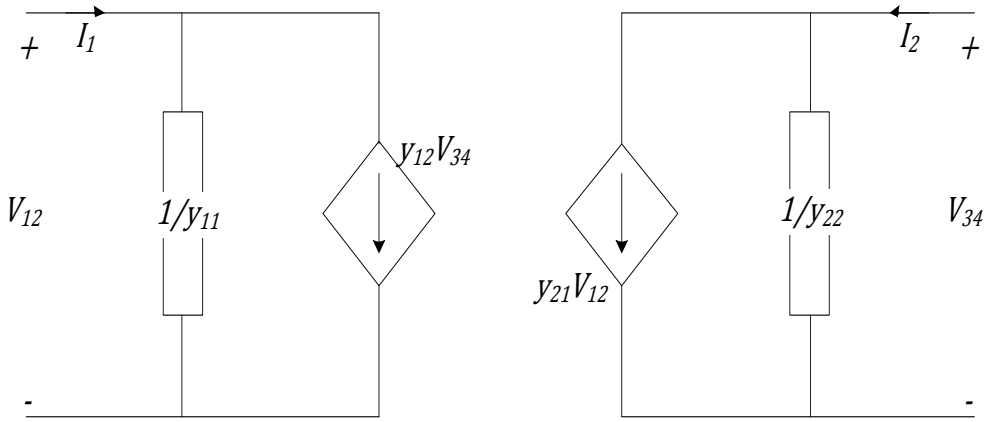

Figure 2.5-2: Two port network model [7, 8]

This model can predict an output voltage, $V_{34,}$ and current, I_2, for a given input voltage, $V_{12,}$ in a four bodied system. The four-bodied system circuit model is a complete description of the model of an electric field transformer which under certain conditions can be described as a dual to the magnetic field transformer [7 - 10]. This means that if a potential is placed between bodies one and two, an electric field is generated. When sensor is inserted into the field, this model provides predictability in the measurement of the field. Stated differently, for a parallel plate sensor present in an electric field, the voltages and currents between the sensor plates can be predicted by the model, provided the geometries or inter body capacitances and the potential present between the bodies generating the field are known.

2.5.3 Limitations

This method can allow for the specific design of a sensor for a required application. By sizing the inter-plate capacitor of the sensor correctly, the sensor can be designed specifically to drive a load or as an open circuit voltage detection device. The limiting factor is the inability to take into account the applied electric field directly as an input. This means that for this method to work, the voltage between the outer plates, V_{12}, must be known. The dimensions of the system must also be known, i.e. the separation

distances, shapes and sizes of all the bodies. This is so the inter plate capacitances can be calculated. The voltage, V_{12}, between the bodies generating the field is not always known when measuring an electric field, for example, when measuring the field near a machine. The geometrical structure may be complicated, where the inter body capacitances can only be determined via simulation or complicated field analysis. This is not practical in most electric field detection situations. This model, therefore, must be modified in order to operate with the electric field that is to be measured as the input of the system.

2.6 Electric Field Sensor Model

2.6.1 Modelling Procedure

The geometry shown in Figure 2.4-1 was simulated using FEM (finite element method) software. In order to simulate the effects of a load, or even the effects of a short circuited sensor, the voltage between plates three and four was forced to a certain value. The outer plates of the structure or plates one and two were made much larger than the inner plates. This allowed for minimal distortion of the field by the presence of the sensor. The resulting flux densities, charges and electric fields were noted.

This procedure was followed for four cases of uniform electric field, where the sensor conditions were varied four times in each case. This provided enough information to show the effects of the variation of the field as well as the sensor conditions. The FEM simulations were conducted iteratively for various fields generated by the outer plates, and various loading conditions. This allowed for the different charge differences (ΔQ) to be calculated in order for a trend to be noticed. The results are shown in the subsequent section.

2.6.2 Results and Model

Figure 2.6-1 shows that the V-ΔQ curves are all straight lines with a gradient of the inter plate capacitance of the sensor. As the external electric field changes the x- and y- intercept points change, but the gradient remains the same.

The curves on the graph show a linear relationship of inverse proportion between the resulting charge difference and the forced voltage between the sensor plates. Table 2.6-1 to Table 2.6-4 documents the charges produced by the simulation for the forced voltages between the sensor plates at the particular field levels, these were the values used to plot the graph. This is unlike a typical two plate capacitor which has a proportional relationship between the voltage and charge difference. A typical capacitor would exhibit a voltage-charge relationship that is described by equation 2.15 as an increase in voltage results in an increase in the charge difference with the proportion of the size of the capacitor, or that the voltage-charge relationship is linear with a positive gradient due to the capacitance. These results show the voltage-charge relationship to be linear with a negative gradient of the inter-plate capacitance and an added term which denotes the influence of the external electric field on the two sensor plates.

The curves shown in Figure 2.6-1 form the basis for the derivation of a model based on an electric field as an input to the system, where the voltage generating the electric field is unknown. The equation that can be derived from the curves that are shown in Figure 2.6-1, which describes the system, is shown as equation 2.28.

$$\Delta Q = -\frac{Q_1 V_{34}}{\left(\frac{\varepsilon_{r_1} E_1 d_{34}}{\varepsilon_{r_2}}\right)} + Q_1 \tag{2.28}$$

Where ΔQ represents the addition between the charge at the upper and lower sides of plate three (which is the top sensor plate). This addition of the surface charges is explained in section 2.3 and is referred to as the charge difference. This charge difference on the upper plate is equivalent to the addition of the charge at the upper and lower sides of the bottom plate. V_{34} is the sensor plate voltage, d_{34} is the distance between the sensor plates, and E_1 is the external electric field. The relative permittivities, ε_{r_1} and ε_{r_2}, represent the relative permittivity of the dielectric separating the outer plates and that separating inner (sensor) plates respectively. The denominator represents the internal field of the sensor plates. Thus the equation which describes the current between the plates can therefore be derived from this charge difference and this is shown by equations 2.29 to 2.34.

Table 2.6-1: Simulated load voltages and charges obtained at 50 V/m.

Voltage (V)	Charge Below (C)	Charge Above (C)	Magnitude of Charge Difference (C)
0	-3.82E-14	-4.51E-11	4.51E-11
0.01	8.81E-12	-4.50E-11	3.62E-11
0.025	2.21E-11	-4.47E-11	2.26E-11
0.05	4.44E-11	-4.44E-11	0.00E+00

Table 2.6-2: Simulated load voltages and charges obtained at 100 V/m.

Voltage (V)	Charge Below (C)	Charge Above (C)	Magnitude of Charge Difference (C)
0	-7.63E-14	-9.02E-11	9.01E-11
0.01	8.77E-12	-9.01E-11	8.13E-11
0.05	4.42E-11	-8.95E-11	4.53E-11
0.1	8.90E-11	-8.90E-11	0.00E+00

Table 2.6-3: Simulated load voltages and charges obtained at 150 V/m.

Voltage (V)	Charge Below (C)	Charge Above (C)	Magnitude of Charge Difference (C)
0	-1.15E-13	-1.35E-10	1.35E-10
0.05	4.41E-11	-1.35E-10	9.05E-11
0.1	8.84E-11	-1.34E-10	4.56E-11
0.15	1.33E-10	-1.33E-10	0.00E+00

Table 2.6-4: Simulated load voltages and charges obtained at 200 V/m.

Voltage (V)	Charge Below (C)	Charge Above (C)	Magnitude of Charge Difference (C)
0	-1.53E-13	-1.80E-10	1.80E-10
0.075	6.62E-11	-1.79E-10	1.13E-10
0.125	1.10E-10	-1.79E-10	6.90E-11
0.2	1.78E-10	-1.78E-10	0.00E+00

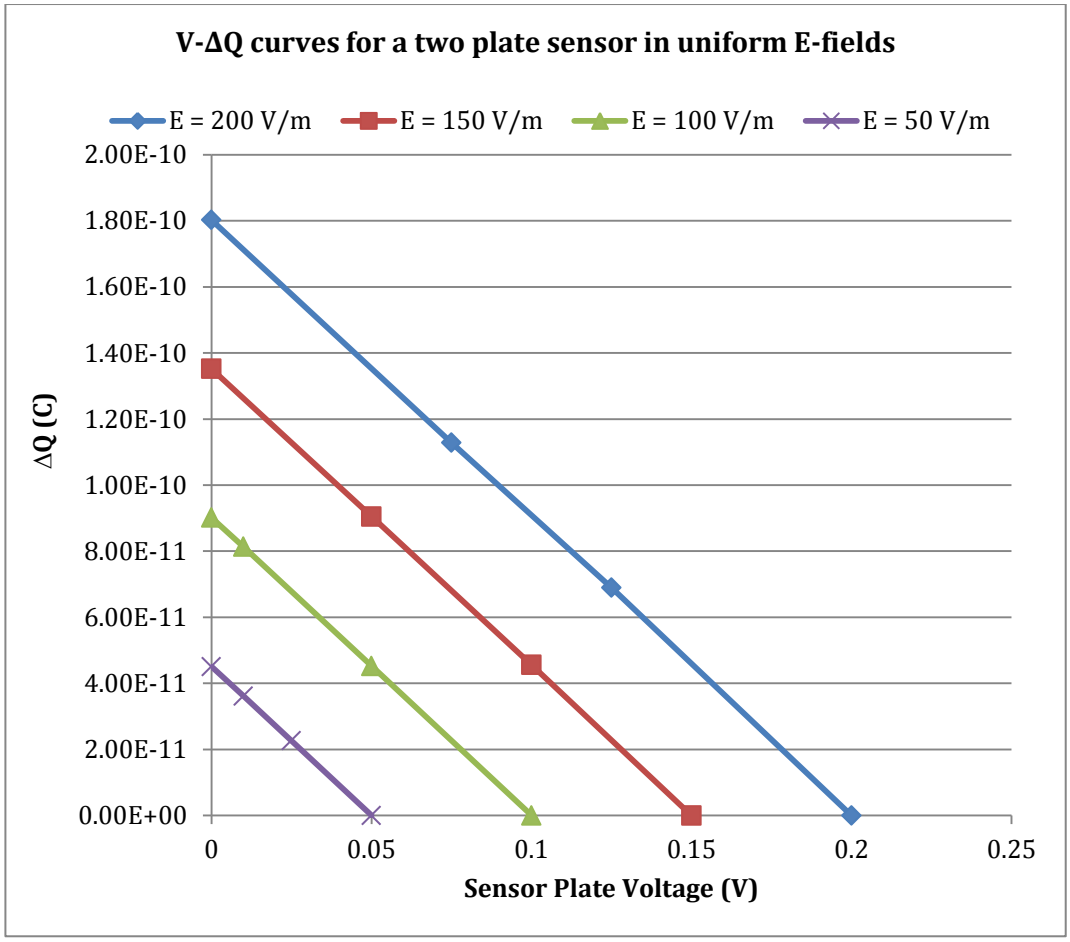

Figure 2.6-1: Graph showing the voltage-current relationship for a two plate sensor in a uniform electric field

$$\Delta Q = -\frac{(\int D_1 . dA)\, V_{34}}{\left(\frac{\varepsilon_{r_1} E_1 d_{34}}{\varepsilon_{r_2}}\right)} + (\int D_1 . dA) \tag{2.29}$$

Where D_1 is the flux density on the upper side of plate 3. The integral is therefore over the surface of this plate. (Equation 2.29 is obtained by substituting equation 2.15 into equation 2.28.)

$$\Delta Q = -\frac{(\int \varepsilon_0 \varepsilon_{r_1} E_1 . dA)\, V_{34}}{\left(\frac{\varepsilon_{r_1} E_1 d_{34}}{\varepsilon_{r_2}}\right)} + (\int \varepsilon_0 \varepsilon_{r_1} E_1 . dA) \tag{2.30}$$

By substituting equation 2.17 into equation 2.29, equation 2.30 is obtained. The term ε_{r_1}, the relative permittivity of the dielectric which separates the outer plates is air for almost all practical cases and will be considered as 1. This term can be re-introduced if it is necessary.

By solving the integrals, equations 2.31 and 2.32 show that the charge difference can be represented in terms of the inter-plate capacitance, external field and the sensor plate voltage.

$$\Delta Q = -\frac{\varepsilon_0 E_1 A_{34} V_{34}}{\left(\frac{E_1 d_{34}}{\varepsilon_{r_2}}\right)} + \varepsilon_0 E_1 A_{34} \tag{2.31}$$

Where A_{34} is the surface area of the conductor for which the surface charges described earlier are distributed over. The subscript 34 is used as this area is the same as the overlapping area between the sensor plates (plates three and four).

$$\Delta Q = -C_{34} V_{34} + \varepsilon_0 E_1 A_{34} \tag{2.32}$$

Equation 2.33 applies the fact that current is the time derivative of charge (shown as equation 2.20), hence, a V-I representation of the sensor equation is shown as equation 2.34.

$$I = -C_{34} \frac{d}{dt}[V_{34}] + \varepsilon_0 A_{34} \frac{d}{dt}[E_1] \tag{2.33}$$

Where I represents the current between plates three and four.

$$I = -jwC_{34} V_{34} + j\omega \varepsilon_0 E_1 A_{34} \tag{2.34}$$

Equation 2.34 differs from the one conventionally used (equation 2.20) because it provides a prediction of current out of short circuit conditions, i.e., when a load is being driven by the sensor.

The circuit model described by equation 2.34 can be represented as a dependant current source in parallel with a capacitor. This is shown as Figure 2.6-2.

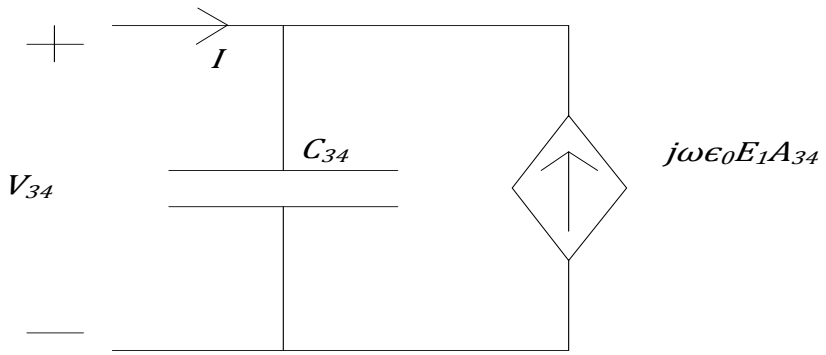

Figure 2.6-2: Circuit model representation of sensor in an electric field.

2.6.3 Limitations

The two-terminal circuit model shares one limitation with both the four body system method and the contemporary method. This is the lack of accountability of external parasitic effects and interference. This will be addressed in further detail in chapter 3.

2.7 Simplification of Four-Bodied Model to Electric Field Sensor Model

The two-terminal model can be shown to be a representation of the four-terminal (two-port or four-bodied) model under certain conditions.

The assumption that must be made geometrically for a uniform electric field to be present is that the outer plates which generate this field must be infinitely large, and since the field is uniform, the fringing is negligible. Another assumption is that the parallel plate sensor is constructed such that that there is no overlapping area between plates two and three, or plates one and four. This is illustrated in Figure 2.7-1 and Figure 2.7-2. It can also be stated that the case for no fringing can be represented by Figure 2.7-1 and a case where slight fringing occurs for the same structure shown can be approximated by Figure 2.7-2.

These figures depict the structure from a side view. Care should be taken so as to not confuse the separation thickness with the overlapping area of the plates. It is important to notice that when this assumption is valid (refer to Figure 2.7-1) the overlapping area of plates one and three, A_{13}, is equivalent to the overlapping area of plates three and four, A_{34}, as well as that of plates two and four, A_{24}.

Each y-parameter described in section 2.5.2, equations 2.22 to 2.24 can be rewritten since the assumptions mentioned above affect them directly. The assumptions are made in order to effectively compare the electric field sensor model to the four bodied system model under the conditions of an electric field as an input to the system instead of voltage. This means that by making the assumptions of large overlapping area and a large distance between the field generating plates and the sensor plates, the input voltage can be shown to be unimportant in the prediction of the output voltage.

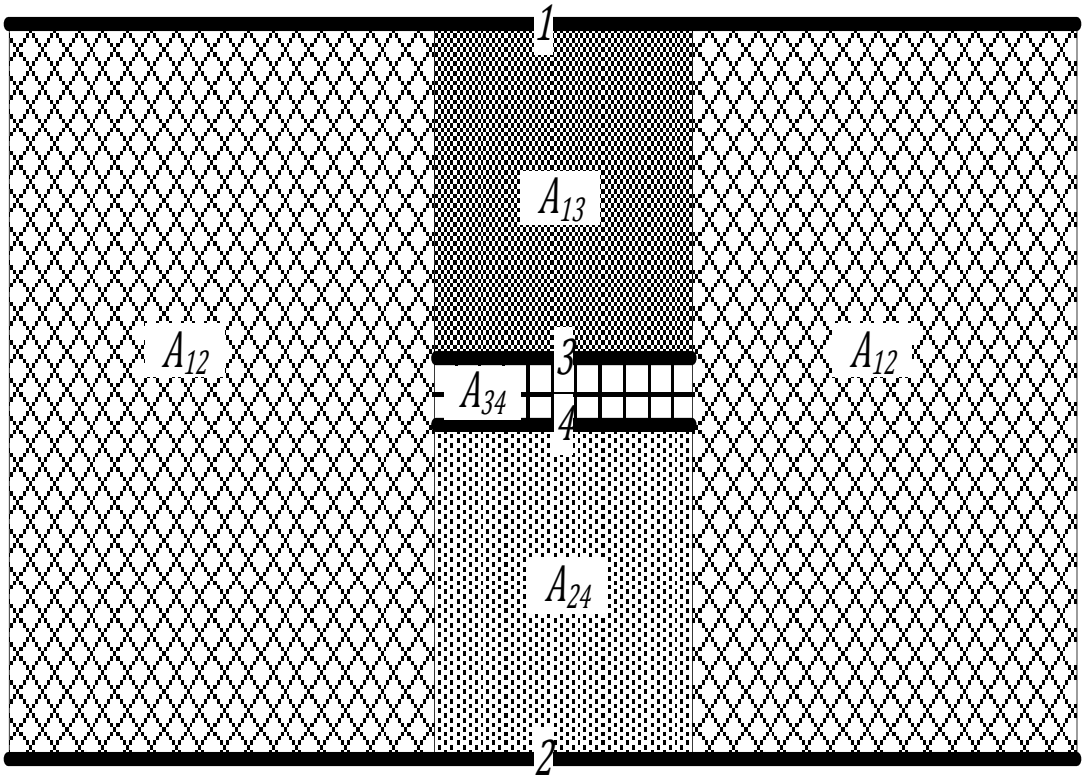

Figure 2.7-1: Side view showing no overlapping area between plates one and four, as well as plates two and three.

By changing the overlapping area of the plates, the resulting inter-plate capacitance also changes according to equation 2.32. This equation provides a general description

for all the inter plate capacitances that exist in the system. It allows for the y-parameter equations (equations 2.25 to 2.27) to be re-written in terms of the geometry of the system.

$$C_{ab} = \frac{\varepsilon_0 \varepsilon_r A_{ab}}{d_{ab}} \tag{2.35}$$

Where C_{ab} is the inter-plate capacitor between plates *a* and *b*. A_{ab} is the area of overlap of the plates *a* and *b*, and d_{ab} is the distance between the plates *a* and *b*.

Thus, increasing an overlapping area, A_{ab}, will result in the proportional increase of the capacitor C_{ab}.

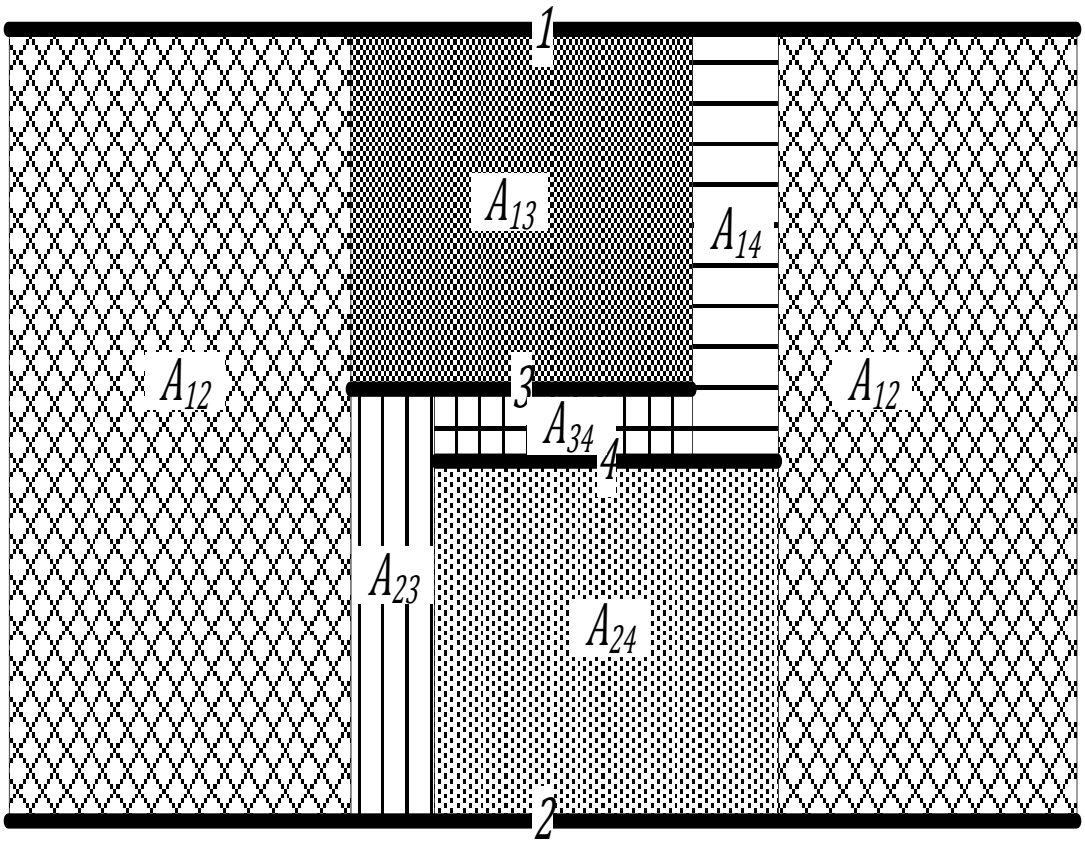

Figure 2.7-2: Side view showing overlapping area between plates one and four, as well as plates two and three.

2.7.1 Fringing and Ground Capacitances Neglected

With reference to the Figure 2.5-1, which describes the inter-body capacitances of a four bodied system, the first assumption stated above affects the capacitor C_{12} (A_{12} becomes infinitely large, and hence C_{12} becomes infinitely large), this capacitor is only present in the first of the y-parameters, as shown by equation 2.25. The second assumption affects all the parameters, since it requires A_{23} and A_{14} to be zero, this will result in the change of both C_{23} and C_{24} according to equation 2.35 to zero as well. The y-parameter equations can be rewritten now, and are shown as equations 2.36 to 2.38.

$$y_{11} = j\omega\left[\frac{(C_{13})(C_{24})}{(C_{13}+C_{24})} + \infty\right] = \infty \tag{2.36}$$

$$y_{22} = j\omega\left[\frac{(C_{13})(C_{24})}{(C_{13}+C_{24})} + C_{34}\right] \tag{2.37}$$

$$y_{12} = y_{21} = j\omega\frac{(-C_{24}C_{13})}{(C_{13}+C_{24})} \tag{2.38}$$

Equation 2.36 shows that the first y-parameter becomes very large. In the circuit model, this translates to a very small impedance, approximately a short circuit, present in the parallel branch on the input side. This is illustrated in Figure 2.7-3. This would imply that the potential between the outer plates, V_{12}, is zero in terms of the model. This is, however, a simple representation of the fact that the input side is not affected or influenced by the interaction of the sensor plates with the generated field.

Figure 2.7-3 shows that the voltage on the input side is no longer dependent on the circumstances of the output side. Thus, if the sensor is driving a load, or even if a short-circuit is placed between the sensor plates, the input side of the uniform field will be unaffected. In other words the modification of the input voltage by the change of the output voltage will be zero.

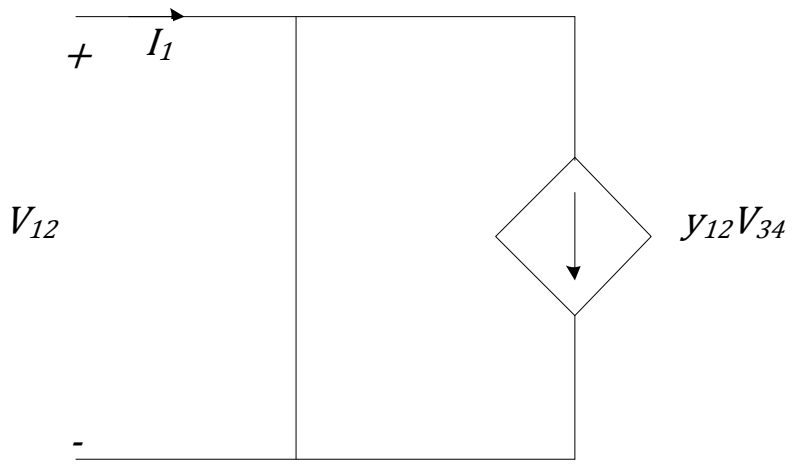

Figure 2.7-3: Input side of y-parameter model assuming outer plats to be infinitely large

It is therefore possible to consider the output side only. Here, by considering the remaining parameters, a common term, *t*, is found (shown by equation 2.39). Equations 2.40 and 2.41 show the simplification of this term.

$$t = \frac{(C_{13})(C_{24})}{(C_{13} + C_{24})} \tag{2.39}$$

$$t = \frac{\left(\frac{\varepsilon_0 \varepsilon_{r_1} A_{13}}{d_{13}}\right)\left(\frac{\varepsilon_0 \varepsilon_{r_1} A_{24}}{d_{24}}\right)}{\left(\frac{\varepsilon_0 \varepsilon_{r_1} A_{13}}{d_{13}} + \frac{\varepsilon_0 \varepsilon_{r_1} A_{24}}{d_{24}}\right)} \tag{2.40}$$

It was mentioned earlier, according to Figure 2.7-1 that A_{13} and A_{24} are both equal to A_{34}. This allows equation 2.40 to be rewritten as 2.41. The dielectric separating the outer plates from the inner plates is shown with a permittivity of ε_{r_1}. This dielectric is, as mentioned earlier, for most cases of electric field detection, air, and will be considered as 1. If it is required it can be included.

$$t = \frac{\varepsilon_0 A_{34}}{d_{13} + d_{24}} \tag{2.41}$$

Therefore the remaining y-parameters shown by equations 2.37 and 2.38 can be re-written as 2.42 and 2.43.

$$y_{22} = j\omega[\frac{\varepsilon_0 A_{34}}{d_{13} + d_{24}} + C_{34}] \tag{2.42}$$

$$y_{12} = y_{21} = j\omega \frac{\varepsilon_0 A_{34}}{d_{13} + d_{24}} \tag{2.43}$$

Figure 2.7-4 shows a comparison of the output side of the two-port model to the electric field sensor model. By comparing the terms separately, the conditions for which the models are equivalent will become evident.

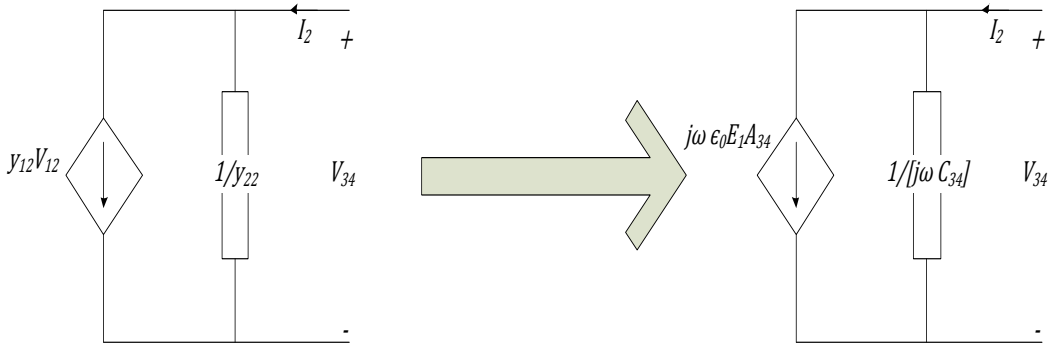

Figure 2.7-4: Comparison of models.

Thus, comparing the dependent source terms yields equation 2.44 with the two-port output side representation on the left and the electric field sensor model on the right.

$$-\frac{\varepsilon_0 A_{34}}{d_{13} + d_{24}} V_{12} \leftrightsquigarrow \varepsilon_0 E_1 A_{34} \tag{2.44}$$

E_1 can be rewritten as the negative of the linear derivative of the input voltage taken over the separation of the outer plates shown by equation 2.45 [1, 5]. This is explained clearly in section 2.2.

$$-\frac{\varepsilon_0 A_{34}}{d_{13} + d_{24}} V_{12} \leftrightsquigarrow A_{34}\varepsilon_0[-\frac{V_{12}}{d_{12}}] \tag{2.45}$$

Therefore in order for the models to become equivalent, d_{12}, the separation distance between the outer plates must be approximately the same as the distance between the outer plates and the sensor (d_{13} added to d_{24}). This is graphically presented in Figure 2.7-5. For this to be valid the condition that the separation distance between the two sensor plates (plates three and four) be much smaller than that between the outer plates and the sensor (plates one and three as well as plates two and four) must hold. This is mathematically represented by equation 2.46.

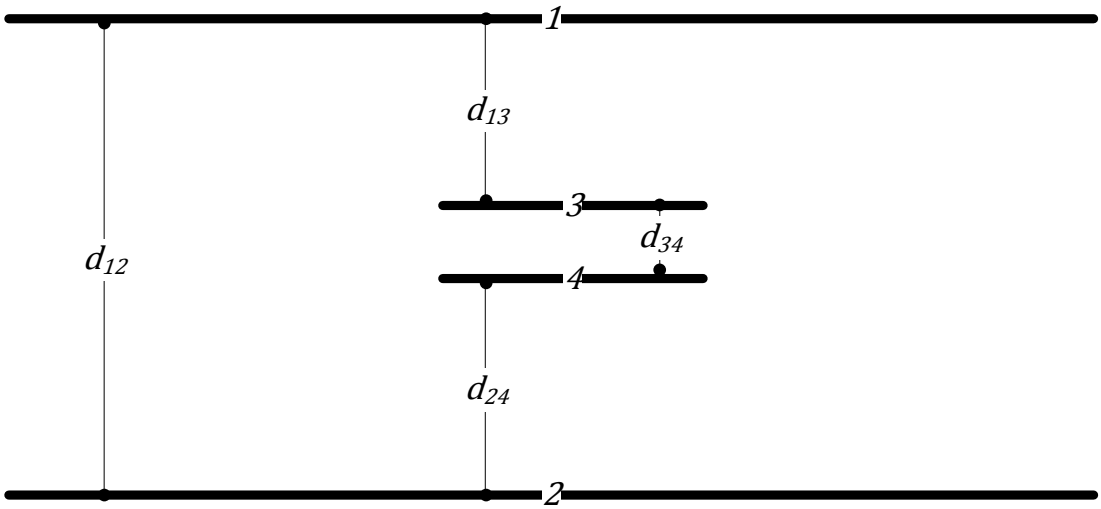

Figure 2.7-5: Side view showing the separation distances of the plates.

$$d_{34} \ll d_{13} + d_{24} \tag{2.46}$$

Comparing the impedance branch of the circuit models in Figure 2.7-4 yields equation 2.47. Again, the two-port output side representation on the left and the electric field sensor model on the right.

$$[\frac{\varepsilon_0 A_{34}}{d_{13} + d_{24}} + C_{34}] \leftrightsquigarrow C_{34} \tag{2.47}$$

By simply applying the criteria shown by equation 2.46, and from the knowledge that the capacitance is inversely proportional to the distance, given by equation 2.35, it is evident that the C_{34} term on the left hand side of equation 2.47 is much larger than the

t term on the right. This is because the denominator of C_{34} is d_{34} which is much smaller than d_{13} added to d_{24} which is the denominator of the *t* term.

2.7.2 Ground Capacitances Taken into Consideration

The effects of including the ground capacitances to the model under the assumptions of zero fringing and uniform electric field is shown in this section. The complete model including these capacitances to ground is derived by Mahomed and Hofsajer [10]. This complete model simply has different y-parameters which include the capacitances to ground as shown by Figure 2.5-1. These self-capacitances of the bodies are shown in this figure as C_{11}, C_{22}, C_{33}, and C_{44}. The complete parameters are shown by equations 2.48 to 2.53.

$$y_{11} = j\omega\left[\frac{X(C_{13}+C_{14})(C_{24}+C_{23})+Y_1}{(X(C_{13}+C_{24}+C_{23}+C_{14})+(C_{33}+C_{44})(C_{11}+C_{22})}+C_{12}\right] \tag{2.48}$$

$$y_{22} = j\omega\left[\frac{X(C_{13}+C_{14})(C_{24}+C_{23})+Y_2}{X(C_{13}+C_{24}+C_{23}+C_{14})+(C_{33}+C_{44})(C_{11}+C_{22})}+C_{34}\right] \tag{2.49}$$

$$y_{12}=y_{21} = j\omega\left[\frac{X(C_{23}C_{14}-C_{24}C_{13})+C_{11}(C_{24}C_{33}-C_{23}C_{44})+C_{22}(C_{13}C_{44}-C_{14}C_{33})}{(X(C_{13}+C_{24}+C_{23}+C_{14})+(C_{33}+C_{44})(C_{11}+C_{22})}\right] \tag{2.50}$$

$$X=(C_{11}+C_{22}+C_{33}+C_{44}) \tag{2.51}$$

$$Y_1=(C_{13}+C_{24}+C_{23}+C_{14}+C_{33}+C_{44})C_{11}C_{22} +(C_{33}+C_{44})(C_{11}(C_{23}+C_{24})+C_{22}(C_{13}+C_{14})) \tag{2.52}$$

$$Y_2=(C_{13}+C_{24}+C_{23}+C_{14}+C_{33}+C_{44})C_{11}C_{22} +(C_{33}+C_{44})(C_{11}(C_{23}+C_{24})+C_{22}(C_{13}+C_{14})) \tag{2.53}$$

Considering just the denominators of the fractions in all of the parameters, it is evident that they are the same. It is also possible to deduce that the left hand side terms of these denominators are much larger than the right hand side terms. This is

because the self-capacitances are much smaller than the inter-plate capacitances and the right hand side term multiplies these small capacitances together, this means that the right hand side term will result in a very small numerical value. It is also possible to approximate the capacitors C_{14} and C_{23} to zero in all the equations. This is explained in the preceding section as fringing is neglected in this analysis. Therefore the denominators can be approximated as shown by equation 2.54.

$$\begin{aligned} &X(C_{13}+C_{24}+C_{23}+C_{14})+(C_{33}+C_{44})(C_{11}+C_{22}) \\ &\cong X(C_{13}+C_{24}+C_{23}+C_{14}) \cong X(C_{13}+C_{24}) \end{aligned} \tag{2.54}$$

The numerators and the X and Y terms simplify as well, and the y-parameters can be re-written as equations 2.55 to 2.60.

$$y_{11} = j\omega\left[\frac{X(C_{13}C_{24})}{X(C_{13}+C_{24})}+\frac{Y_1}{X(C_{13}+C_{24})}+ C_{12}\right] \tag{2.55}$$

$$y_{22} = j\omega\left[\frac{X(C_{13}C_{24})}{X(C_{13}+C_{24})}+\frac{Y_2}{X(C_{13}+C_{24})}+ C_{34}\right] \tag{2.56}$$

$$y_{12} = y_{21} = j\omega\left[\frac{X(-C_{24}C_{13})}{(X(C_{13}+C_{24})}+\frac{C_{11}(C_{24}C_{33})}{(X(C_{13}+C_{24})}+\frac{C_{22}(C_{13}C_{44})}{(X(C_{13}+C_{24})}\right] \tag{2.57}$$

$$X = (C_{11}+C_{22}+C_{33}+C_{44}) \tag{2.58}$$

$$Y_1 = (C_{13}+C_{24}+C_{33}+C_{44})C_{11}C_{22}+(C_{33}+C_{44})(C_{11}C_{24}+C_{22}C_{13}) \tag{2.59}$$

$$Y_2 = (C_{13}+C_{24}+C_{33}+C_{44})C_{11}C_{22}+(C_{33}+C_{44})(C_{11}C_{24}+C_{22}C_{13}) \tag{2.60}$$

It is now simpler to consider each parameter individually. For the first y-parameter, the assumption that the outer plates are infinitely large results in the same outcome as when the system was analysed without the ground capacitances in the preceding section, i.e., the capacitance C_{12}, becomes infinitely large, hence, the entire term, y_{12}, will become infinitely large and the analysis of this case shown with reference to Figure 2.7-3 is the same as in section 2.7.1.

The second parameter y_{22}, has three terms. The left hand side term is identical to the *t*-term described in section 2.7.1 (this is because the *X* terms cancel each other out). The middle term, however, is new. This term, when analysed carefully shows a larger denominator than numerator. This is deduced from the analysis of the term Y_2.

By observing Y_2, which has left and right hand side terms, it is evident that this term will result in a small numerical value. When expanded, both the left and right hand side terms are shown to be comprised of multiples of at least two self-capacitances. As explained above, the multiple of two self-capacitances which are both small, results in a much smaller numerical value. Now, analysing the denominator of the middle term of the second y-parameter, it can be seen that each term simply has the multiple of one of the self-capacitances. It is therefore possible to conclude that this middle term, which has a very small numerator and a larger denominator, will result in an almost insignificant numerical value compared to both the left and right hand side terms in this parameter.

Therefore, the terms in the bracket of this parameter, y_{22}, simplifies to C_{34} using the analysis shown in section 2.7.1.

Finally, the third parameter, y_{12} or y_{21}, can be considered. Using the same logic which allowed for the simplification of the middle term of the second y-parameter, the middle and last terms of this third y-parameter can be shown to be so small that they become insignificant when compared to the first term. This first term is now also identical to the *t*-term shown by equations 2.39 to 2.41 in the preceding section. This means that the simplification of this parameter will produce the same result as shown in the preceding section.

By simplifying the y-parameters making the logical assumption of the self-capacitances to be much smaller than the other capacitances of the system, the complicated circuit model which takes these self-capacitances into account is shown to be equivalent to the electric field sensor model which ignores them.

2.7.3 Fringing Taken into Consideration

In this case, the generated field is assumed to be slightly distorted by the presence of the sensor, meaning that fringing occurs and that the overlapping areas which result in the capacitances C_{14}, and C_{23}, exist and hence need to be accounted for. This approximation of these capacitances that arise due to a fringing field as absolute values is reasonable since they influence the model in the same way. The capacitances to ground are neglected for this approximation. Thus, the y-parameters are written as they were originally derived, shown by equations 2.25 to 2.27.

By assuming infinitely large outer plates, the first parameter, y_{11}, simplifies, as shown by equation 2.36, to an infinitely large capacitance. Thus the implications of fringing fields in the region of the sensor do not affect the generated field.

The second parameter (y_{22}), however, simplifies differently. Certain assumptions must be made for the simplification of this parameter when considering the first term. This is because the first term includes the capacitances due to fringing (C_{14} and C_{23}), and these capacitances in this term are considered to contribute more than the other capacitances present in it.

First, referring to Figure 2.7-6, the distance between the sensor plates (d_{34}) is considered to be small enough so that the distance between plates one and four (d_{14}) is approximately equal to the distance between plates one and three (d_{13}). Similarly, the distance between plates two and four (d_{24}) is approximately the same as that between plates two and three (d_{23}). This assumption has the same implications of the assumption represented by equation 2.46, i.e. the distance between the sensor plates is far smaller than the distance between the outer plates and the sensor.

The second assumption that must be made may be difficult to visualise or represent graphically. Referring to Figure 2.7-2, this assumption states that the areas of overlap due to the fringing effect (A_{14} and A_{23}) are equal, and that they are greater than the areas of overlap between the sensor plates (plates three and four) and the outer plates (plates one and two), or in terms of the diagram, A_{13} and A_{24}. What this implies is that the effect that fringing has on the model prediction is greater than the effects of the

capacitances due to these overlapping areas (A_{13} and A_{24}). In other words, the influence on this first term, y_{22}, that the capacitances due to the occurrence of fringing (C_{14} and C_{23}) is larger than the influence of the inter-body capacitances (C_{13} and C_{24}).

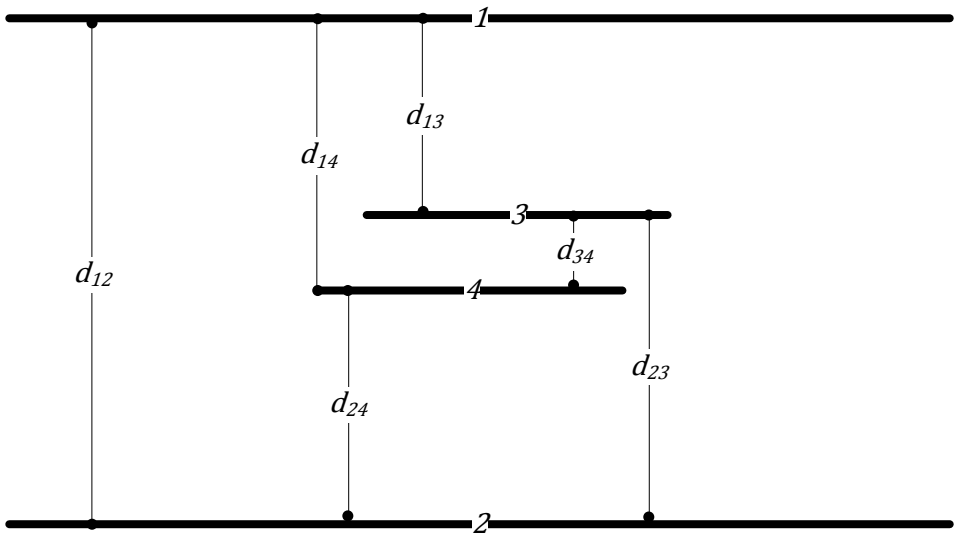

Figure 2.7-6: Separation distances between the plates including overlap for fringing.

Equations 2.61 to 2.63 summarise the assumptions.

$$d_{13} \cong d_{14} = d_t \text{ , } d_{23} \cong d_{24} = d_b$$
$$\text{or} \qquad (2.61)$$
$$d_{34} \ll d_{13} + d_{24}$$

$$A_{14} = A_{23} = A_f \text{ , } A_{13} = A_{24} = A_o \qquad (2.62)$$

$$A_f \gg A_o \qquad (2.63)$$

The subscripts *t*, *b*, *f*, and *o*, denote top, bottom, fringing, and outer-overlap respectively.

Hence, by writing the second y-parameter in terms of the equation describing a parallel plate capacitor, and by substituting the notations shown in equations 2.61 and

2.62, equation 2.64 represents the complete description of the first term of this parameter (y_{22}).

$$\frac{\varepsilon_0 A_f A_o d_t}{d_b(d_t(A_f + A_o) + d_b(A_f + A_o))} + \frac{\varepsilon_0 A_f A_o d_b}{d_t(d_t(A_f + A_o) + d_b(A_f + A_o))} + \frac{\varepsilon_0({A_f}^2 + {A_o}^2)}{(d_b(A_f + A_o) + d_t(A_f + A_o))} \tag{2.64}$$

By applying the assumption stated in equation 2.63 to this term, which is represented by equation 2.64, equation 2.65 is obtained. By inspecting this equation it can be deduced that the first two terms represent a ratio of the areas, where the smaller area A_o is the numerator and the larger area A_f is the denominator. This means that both these terms are much smaller than the third term, and can be considered as insignificant compared to it. The complete y-parameter is now shown with the inclusion of this term as equation 2.66.

$$\frac{\varepsilon_0 A_o d_b}{d_t A_f(d_b + d_t)} + \frac{\varepsilon_0 A_o d_b}{d_t A_f(d_b + d_t)} + \frac{\varepsilon_0 A_f}{(d_b + d_t)} \tag{2.65}$$

$$y_{22} = j\omega\left[\frac{\varepsilon_0 A_f}{(d_b + d_t)} + C_{34}\right] = j\omega\left[C_f + C_{34}\right] \tag{2.66}$$

The term, C_f, indicates that the first term in the bracket is an equivalent capacitance due to fringing. It is possible to analyse the system using y_{22} as it is written in equation 2.26, but this is a much simpler form which allows for the inference of the effect of the fringing capacitance directly without the need for the inclusion of the other internal capacitances of the system.

Finally, considering the last y-parameter (equation 2.27), it is possible to split this parameter into two terms, as shown by equation 2.67.

$$y_{12} = y_{21} = \frac{C_{23}C_{14}}{(C_{13} + C_{24} + C_{23} + C_{14})} - \frac{C_{24}C_{13}}{(C_{13} + C_{24} + C_{23} + C_{14})} \tag{2.67}$$

It can be seen that the numerator of the first term is entirely dependent on the capacitances due to fringing (C_{14} and C_{23}), while that of the second term is dependent on the other inter-body capacitances in the system (C_{13} and C_{24}). If the assumption is made that the contribution to the first term by the other capacitances which are not due to fringing is unimportant (C_{13} and C_{24}), as they are accounted for in the second term, and similarly for the second term, where, in this term the capacitances due to fringing are neglected (C_{14} and C_{23}), equation 2.67 simplifies to 2.68.

$$y_{12} = y_{21} = \frac{C_{23}C_{14}}{(C_{23}+C_{14})} - \frac{C_{24}C_{13}}{(C_{13}+C_{24})} \tag{2.68}$$

It can therefore be said that there is now a term present which is purely due to fringing, and a term present which is purely due to the internal capacitances of the system.

Simplifying these terms in terms of the equation for parallel plate capacitors, (the second term is equivalent to the *t*-term encountered in section 2.7.1), equation 2.69 is obtained.

$$y_{12} = y_{21} = \frac{\varepsilon_0 A_f}{d_{13}+d_{24}} - \frac{\varepsilon_0 A_{34}}{d_{13}+d_{24}} \tag{2.69}$$

The complete representation of the current supplied by the current source in the model can now be represented by equation 2.70, which is simply the outer plate voltage multiplied by the third y-parameter.

$$I_{source} = j\omega[V_{12}\frac{\varepsilon_0 A_f}{d_{13}+d_{24}} - V_{12}\frac{\varepsilon_0 A_{34}}{d_{13}+d_{24}}] \tag{2.70}$$

Now, by applying the assumption of the sensor plate separation distance being sufficiently small, represented by equations 2.46 and 2.61, it is possible to write the current in terms of E_1, which, as mentioned earlier is the negative of the linear derivative of the input voltage taken over the separation of the outer plates. This is represented as equation 2.71.

$$I_{source} = j\omega[E_1\varepsilon_0 A_{34} - E_1\varepsilon_0 A_f] \quad (2.71)$$

By placing these new y-parameters in the model, a new model, which can be used to account for fringing, is obtained. This is shown by Figure 2.7-7.

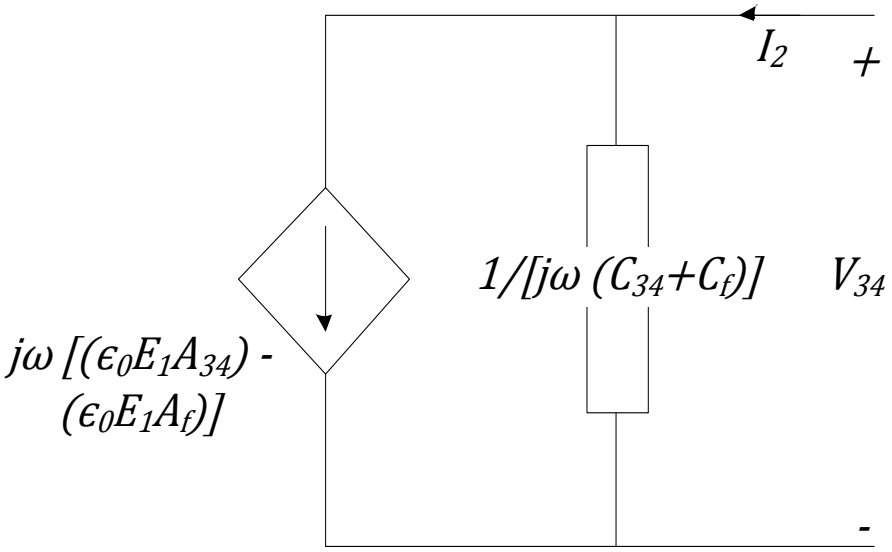

Figure 2.7-7: Model which accounts for fringing.

When considering the effect of inserting the sensor in the field at the angle, the fringing approximation will still be valid, but the value for C_f will be different since by moving one side closer to the bodies generating the field, the separation distances which influence C_f, i.e. d_{14} and d_{23} will change, referring to Figure 2.7-5. This angular position will also influence the calculated field between the plates. The result will now be the dot product of the source field with the unit normal vector to the upper sensor plate. This can be accounted for mathematically in the model shown by Figure 2.7-7.

2.8 Conclusion

A simple circuit model was derived which describes the behavior of a parallel plate sensor in a uniform electric field. This model was shown to be a representation of the circuit model of a four bodied system under the conditions where the outer plates which are used to generate the electric field are sufficiently far enough apart and they

are considered to be infinitely large or much larger than the sensor plates. This defines how little the sensor behavior modifies the generation of the uniform electric field. The limitations of each method are outlined and a common limitation is the lack of consideration for external parasitic effects and interference. The electric field sensor model however, allows for a simple and effective sensor design method which can account for sensor loading conditions as well as dimensioning a sensor when size is a constraint.

2.9 References

[1] E. Brink, "Different perspectives on the potential difference or voltage", School of Electrical and Information Engineering, University of the Witwatersrand, Internal Report, March 2010.

[2] M. Mehdizadeh, *Microwave/RF Applicators and Probes for Material Heating, Sensing, and Plasma Generation: A Design Guide*. Elsevier, Oxford, first edition, chapter 3, 2010

[3] IEEE Standard Procedures for Measurement of Power Frequency Electric and Magnetic Fields From AC Power Lines, Transmission and Distribution Committee Of The IEEE Power Engineering Society, IEEE Std. 644™-1994 (R2008) December 1998.

[4] Lee K W, Park S H, Kim K J, Kang S H. "Design and Application of Electric-Field Sensor for measuring PD signals in High Voltage Equipment", *Proceedings of the 7th International Conference on Properties and Applications of Dielectric Materials*, Nagoya, pp. 828 – 830, June 2005.

[5] *Transmission Line Reference Book-45 kV and Above*, second edition, Palo Alto, Calif.: Electric Power Research Institute, 1982.

[6] R. S. Elliot, *Electromagnetics: History, Theory and Applications*. IEEE Press, New York, first edition, chapter 3, pp. 98- 215, 1999.

[7] Y. Mahomed. "Derivation of an electric transformer circuit model based on electric field coupling" 4th Year Project Report 10P03, School of Electrical and Information Engineering, University of the Witwatersrand, South Africa, 2010.

[8] F. Mahomed. "Definition and application of a new capacitive coupling technique: Electromagnetic considerations." 4th Year Project Report 10P03,

School of Electrical and Information Engineering, University of the Witwatersrand, South Africa, 2010.

[9] Hu, A P, Budhia M, Liu C. "A Generalized Coupling Model for Capacitive Power Transfer Systems." *IECON 2010 - 36th Annual Conference on IEEE Industrial Electronics Society.* pp. 274-279, 2010.

[10] Y. Mahomed, I. Hofsajer. "A Discussion on the Duality Principle Applied to Mutual Inductance", School of Electrical and Information Engineering, University of the Witwatersrand, In preparation.

Chapter 3

Apparatus and Measurement Device

3.1 Introduction

A measurement device was fabricated for which the model derived in chapter two could easily predict behaviour in a uniform AC electric field. This procedure and its rationality are discussed in this chapter.

In order for reliable measurements to be taken, the measurement device, i.e. the parallel plate sensor, as well as the electric field generation apparatus needed to be carefully constructed.

A testing apparatus was constructed in order to accommodate the requirements of generating a reliable near uniform AC electric field at the chosen frequencies of operation. Cautious consideration was taken in order to design the apparatus for the minimisation of external interference on the generated field. This was assembled in accordance with the requirements of the IEEE standards [1 - 3]. The measurement device itself had to perform adequately when placed in a physical environment, and effects such as parasitic self-capacitances had to be considered in its design.

3.2 Uniform AC Electric Field Generation Device

According the IEEE standards [1 - 3], an almost uniform, or "nearly uniform" electric field can be generated using parallel plates under the condition that the dimensions of these plates is much larger than the separation distance between them. Two large copper plates (single sided board used for printed circuits) were therefore used in order to achieve this.

It is also stated in [2] that for maximum uniformity, the probe should be placed at the center of the two plate field generation system. The field generated is then given by equation 3.1 [2]. Guard wires were not included in the test structure simply because the plates that were used were sufficiently large that when a sensor is placed at the center of the system, there is minimal distortion to the uniformity and integrity of the generated field.

$$E = V/d \tag{3.1}$$

Where E (V/m) is the field produced by the plates separated by a distance d (m), with a voltage potential of V (V) across them.

There are therefore two ways of varying the magnitude of the field, i.e. by shifting the plates (either closer or farther), this will change d, or by changing the voltage, V. However, as mentioned earlier, changing the distance between the plates, in particular increasing it, will compromise the uniformity of the generated field. It was therefore chosen to fix the distance between the plates.

3.2.1 Dimensions of the System

A photograph of the structure is shown as Figure 3.2-1. The plates were separated and fixed together using threaded nylon rods and bolts. This allowed for maneuverability of the sensor between the plates and provided a rigid structure.

Figure 3.2-2 shows the dimensions of the structure that was constructed in order to produce the uniform electric field. It can be seen that the separation distance of 100 mm is far smaller than both the other dimensions of the plates.

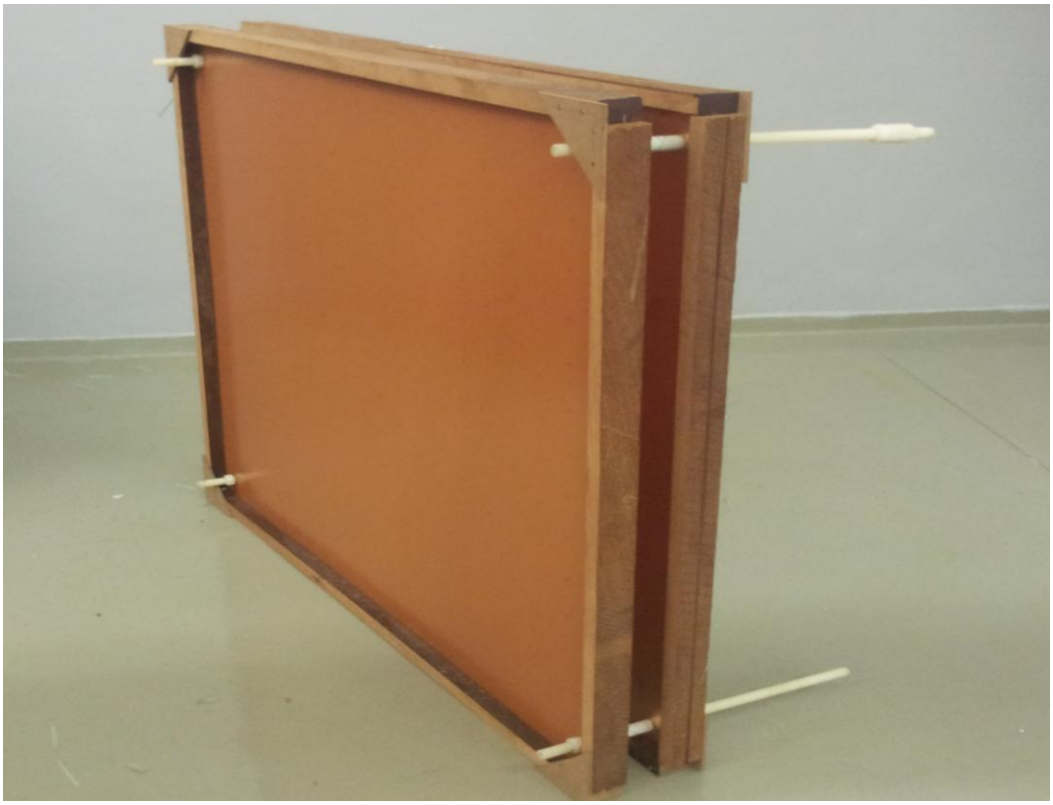

Figure 3.2-1: Photograph of the apparatus used to generate the field.

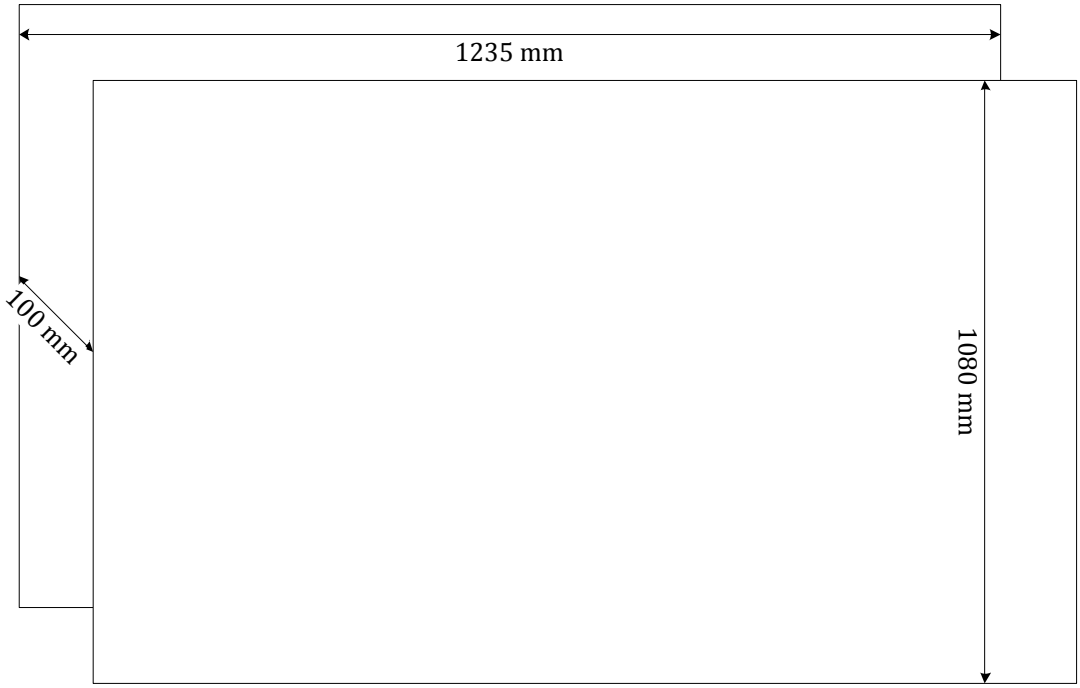

Figure 3.2-2: Dimensions of the two-plate structure.

3.2.2 Supply of the System

The voltage and frequency which was applied across the plates was required to be variable. This voltage also had to be large, i.e. between 10 V and 100 V. The chosen frequency range was between 50 Hz and 500 Hz. The amplifier that was used to achieve these requirements was the Krohn-Hite Model 7500. This amplifier directly energized the plates as shown in Figure 3.2-3.

It is important to note that one of the plates was grounded. This means that a ground-reference meter, as described by [1, 2], cannot be operated in this structure as it will cause a distortion of the electric field which is generated. A ground-reference meter is described by [1, 2] to measure the field using the current or charge present on the plate surface. This measurement requires a connection to ground. This is described in some detail in the subsequent sections.

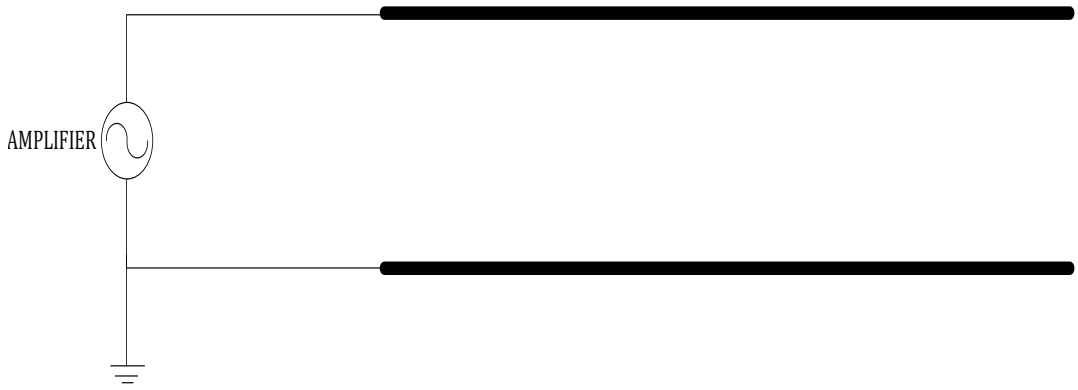

Figure 3.2-3: Diagram showing the supply to the plates.

3.3 Measurement Device

A parallel plate capacitor constructed of two pieces of copper separated by a dielectric, i.e. double sided board used for printed circuits, was used as the measurement probe. The dielectric between the plates is FR-4 (which is a type of material composed of fiberglass). The chosen operating frequency specifications of this sensor are the same as that of the field generation device, as mentioned above, from 50 Hz to 500 Hz.

The probe had to function as a "free-body meter" described by [1, 2], since, as mentioned earlier, a ground connection to one of the probe plates would result in distortion of the field due to the supply characteristics of the system. An oscilloscope or bench voltmeter could therefore not be used to measure the voltage across the plates. The diagram of the free-body meter with no ground connection of a sensor plate is shown as Figure 3.3-1. It is important to note that an assumption made for the derivation of the circuit model requires that the current entering a port is equal to the current leaving that port. Thus, it is not possible to predict the behaviour of a sensor which has a separate ground connection which would imply that this assumption of the circuit model would be invalid. Hence, the model cannot predict the outcomes of a "ground-reference" type meter.

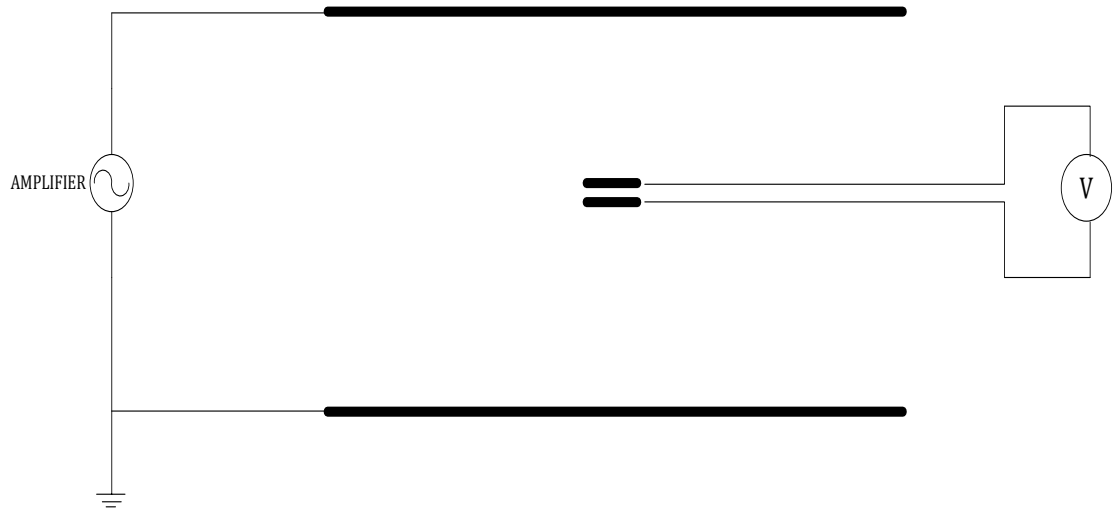

Figure 3.3-1: Free-body meter in the measurement system.

In other words, making a ground connection to one of the sensor plates, essentially would mean that the grounded outer plate and the grounded sensor plate are being forced to be at the same potential and this would mean that the field between these two plates becomes zero or close to zero. The diagram of a ground reference type meter with a sensor plate connected to ground is showed in Figure 3.3-2. The distortion of the electric field is shown graphically in the FEM simulation as Figure 3.3-3. Note that the shades move from black to grey where black indicates a zero field and the lighter shades indicate a higher field.

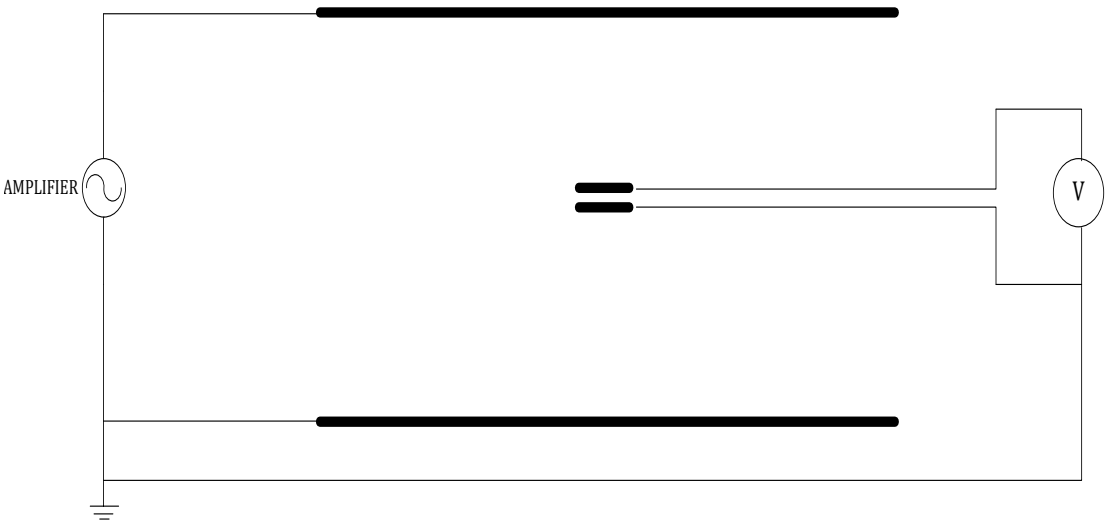

Figure 3.3-2: Ground-reference type meter in the measurement system.

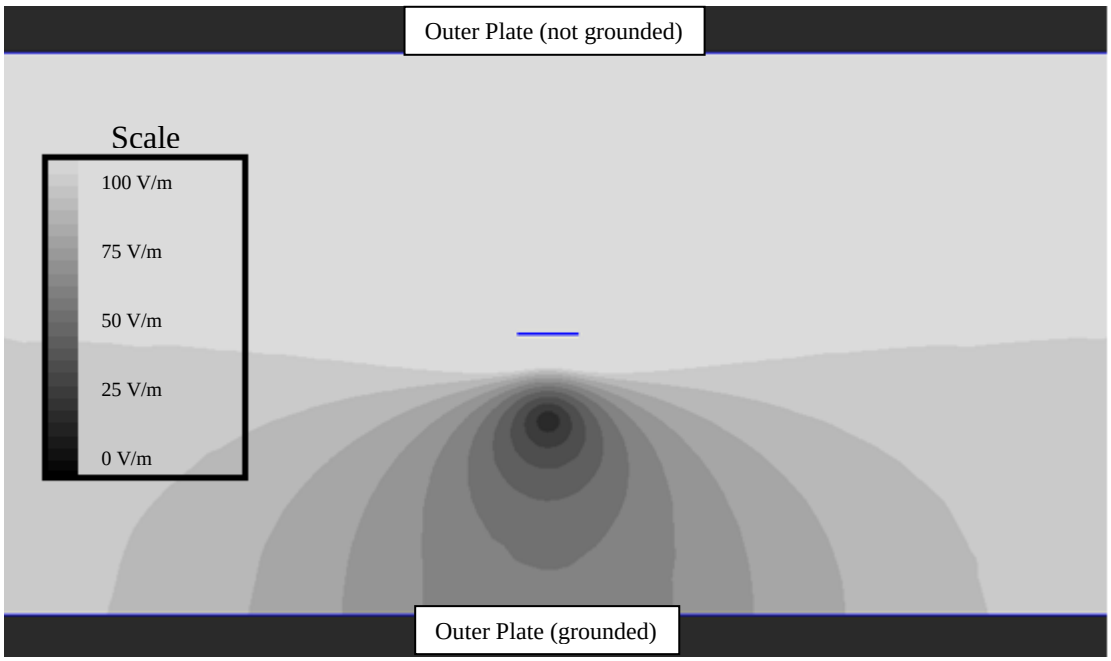

Figure 3.3-3: FEM simulation of experimental setup with lower sensor plate at ground potential.

It is also important to have the sensor plates parallel to the plates generating the field since a deviation will cause a smaller area to be exposed and hence a smaller

measurement will result. The device was therefore suspended by plastic wire from all four corners within the structure.

3.3.1 Voltage Measurement

The parameter chosen for measurement was voltage. This was because the expected currents were shown to be in the Nano-Amp range, and measurements of these currents would be possible but much more complicated than the voltage measurements.

Another important consideration is that of the voltage measurement device. Recall from chapter two, the model predicts a voltage between the sensor plates for a particular field strength. The connection between the sensor and the voltage measurement device is also important since the sensor is a very "weak" source. This means that the current and voltage produced by the sensor are both very small and can be easily influenced by external interference and parasitic effects, in particular, the self-capacitances of the wires connecting the sensor to the voltage measurement device, as well as that of the terminals of the voltage measurement device. The circuit representation of this is shown as Figure 3.3-4.

In Figure 3.3-4, the source capacitor, C_{34}, is a very small capacitor, which means that the voltage measured between points A and B is separated by a high impedance from the voltage at the source (between points X and Y). In other words, the current generated by the dependent source is very small. This implies that because of the self-capacitances of the wires and terminals of the voltage measurement device (lumped together as C_{AG} and C_{BG}) the voltage that will be measured between points A and B becomes dependent on these capacitances. C_{AG}, is the lumped self-capacitance of the wire from the sensor and the terminal of the multimeter at point A, and C_{BG} is that of point B, and C_{33} and C_{44} are the self-capacitances of the sensor. This means that as the length or position of the wires change, the capacitances, C_{AG} and C_{BG}, will change.

This affects the measurement drastically and can cause the voltage measured to become dependent on the position, orientation and presence of an observer in close proximity of the voltage measurement device. A large discrepancy in the self-

capacitances of the voltage measurement device terminals could also cause a dependency on the position of this device relative to the experimental setup.

In other words, it is clear from Figure 3.3-4, that due to the presence of the self-capacitances C_{33}, C_{44}, C_{AG}, and C_{BG}, there will be a common-mode current (I_{CM}) present. As the sizes of these capacitors change, or as the position of the voltage measurement device changes, the path of the common mode current will also change. The presence of this common mode interference adversely affects the measurement and the subsequent section discusses this issue.

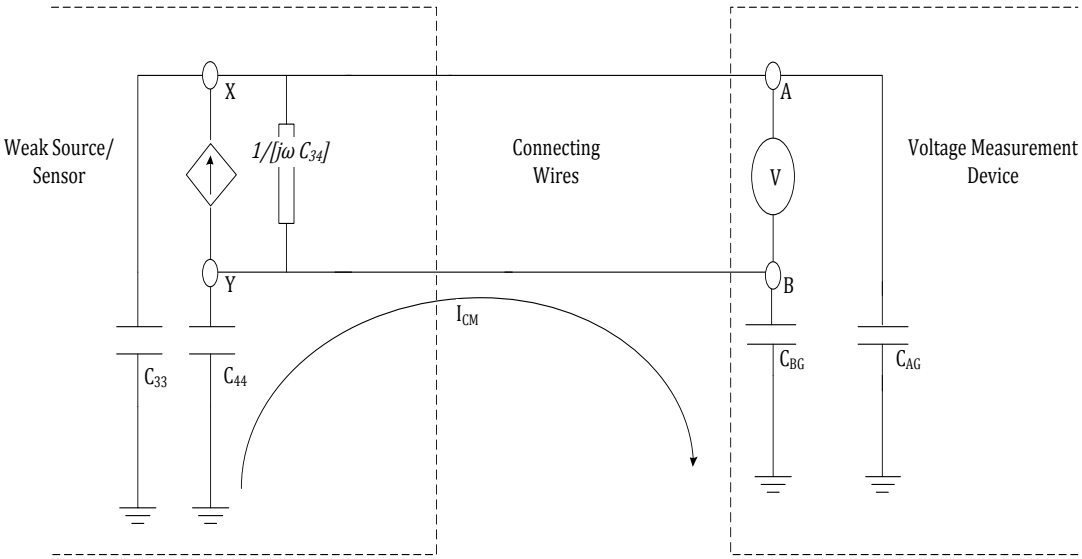

Figure 3.3-4: Lumped model of a weak source representing the sensor and the self-capacitances of the voltage measurement device

3.3.2 Minimization of the Common Mode Interference

In order to eliminate the effects of the parasitic self-capacitances of the wires connecting the plates to the voltage measurement device, which causes common-mode interference (refer to Figure 3.3-4), an instrumentation amplifier with a high CMRR (common mode rejection ratio) was used and positioned as close to the plates as possible. The amplifier was battery powered and the complete sensor system is shown diagrammatically in Figure 3.3-5.

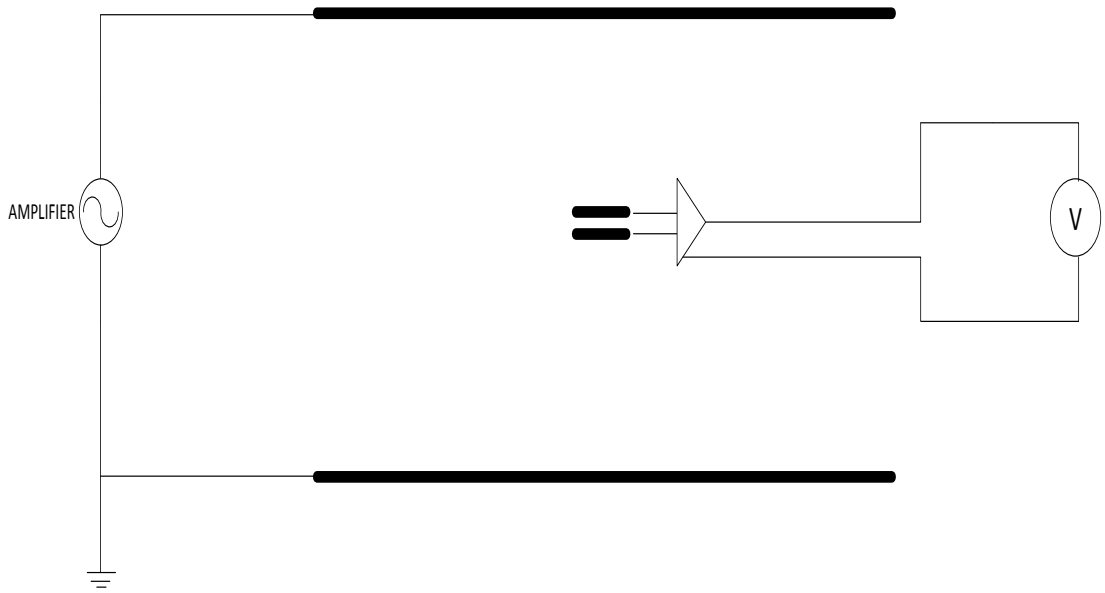

Figure 3.3-5: Complete free-body type system.

This minimized the size of self-capacitance of the wires from the plates and hence the common mode interference. The presence of this amplifier appears as a quasi-source, which is much stronger that the sensor itself. It is seen by the voltage measurement device to have a very small source impedance. Hence, with reference to Figure 3.3-6, the voltage which the sensor produces (between points D and E), becomes almost equal to the voltage measured (between points A and B).

By placing the amplifier close to the sensor plates the wire lengths of the connections from the sensor to the amplifier themselves were minimized (10 mm), and hence their self-capacitances were minimized. This means, referring to Figure 3.3-6, that the voltage between points X and Y is approximately equivalent to the voltage between points D and E, and because the gain of the amplifier is set to one, this voltage will be the voltage measured by the measurement device between points A and B.

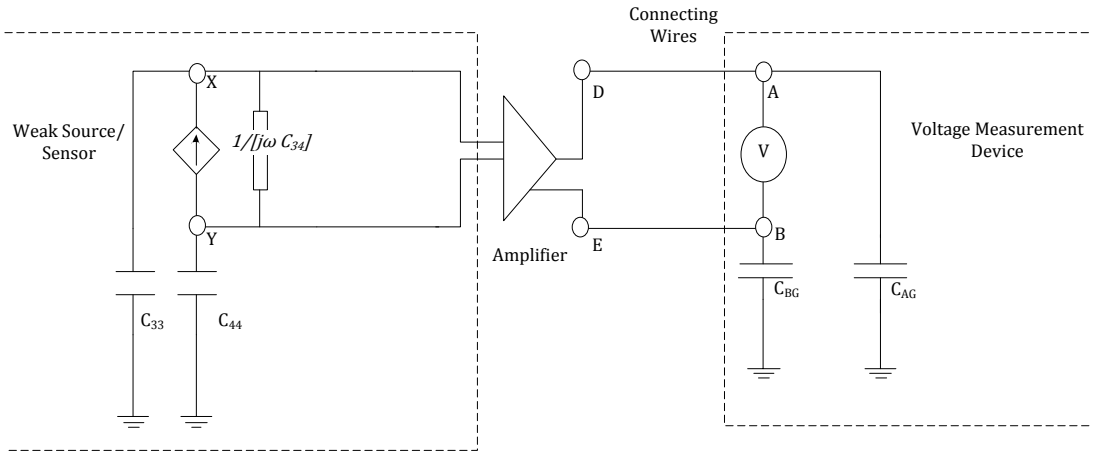

Figure 3.3-6: Circuit representation of the amplifier included in the system.

Figure 3.3-7 shows the circuit level representation of the model for the sensor connected to the amplifier circuit. There are two 10 MΩ resistors at each of the differential inputs of the amplifier. This prevents the input current from drifting out of the operating range of the amplifier. These resistors can be termed as bias resistors since they allow for a balanced input and because they provide a path for the bias current for the inputs, resulting in a lower input offset voltage and improving the common mode rejection of the amplifier [4]. If these resistors are removed, the input terminals of the amplifier will drift out of its operational common-mode range [4], meaning that internal components of the amplifier will saturate.

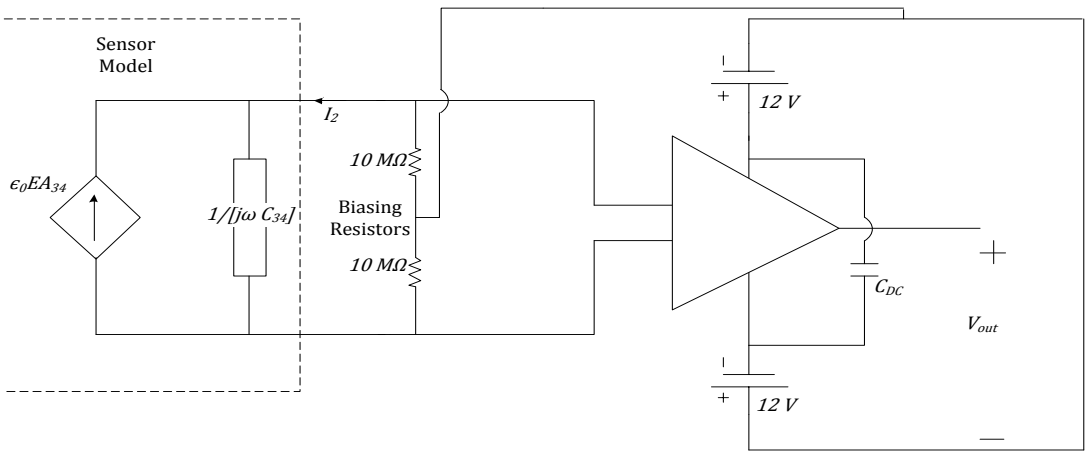

Figure 3.3-7: Circuit diagram of amplifier connected to sensor model.

The capacitor across the supply of the amplifier, C_{DC}, is simply for supply filtering, and is commonly referred to as a DC bus capacitor. It is required since the amplifier is battery operated, meaning that it has a floating supply. The amplifier chosen for the measurement device was an INA114. A high gain was not required and therefore the gain was set at one.

The amplifier circuit also allowed for the connection to the multimeter to be as long as necessary with minimal consequences. Moreover, it allowed for an observer to move into proximity and even handle the multimeter with no significant effects to the measurement. The length of the wires connecting the amplifier to the voltage measurement device was 3450 mm. This length allows for measurements to be taken at different positions around the field generation device.

The symbols of Figure 3.3-7 are as they were described in chapter two, with C_{34} the sensor capacitance, A_{34}, the overlapping area of the parallel plates of the sensor resulting in this capacitance, ε_0 is the permittivity of free space. The term ε_r has been excluded from the source since the separating dielectric between the sensor and the outer plates is air, which has a relative permittivity of approximately one.

A photograph of the complete measurement device (sensor and amplifier) excluding the multimeter is shown as Figure 3.3-8. The device is 133 mm long and 100 mm wide. It has a total thickness of 21 mm.

Due to the two bias resistors present as well as the input characteristics of the amplifier (i.e. input impedance and capacitance), it is evident that the model can be used in order to accurately predict what the output voltage of the measurement circuit will be. This is because the output voltage would be dependent on the parallel equivalent impedance of the capacitor branch, the branch with the two resistors and the input impedance of the amplifier.

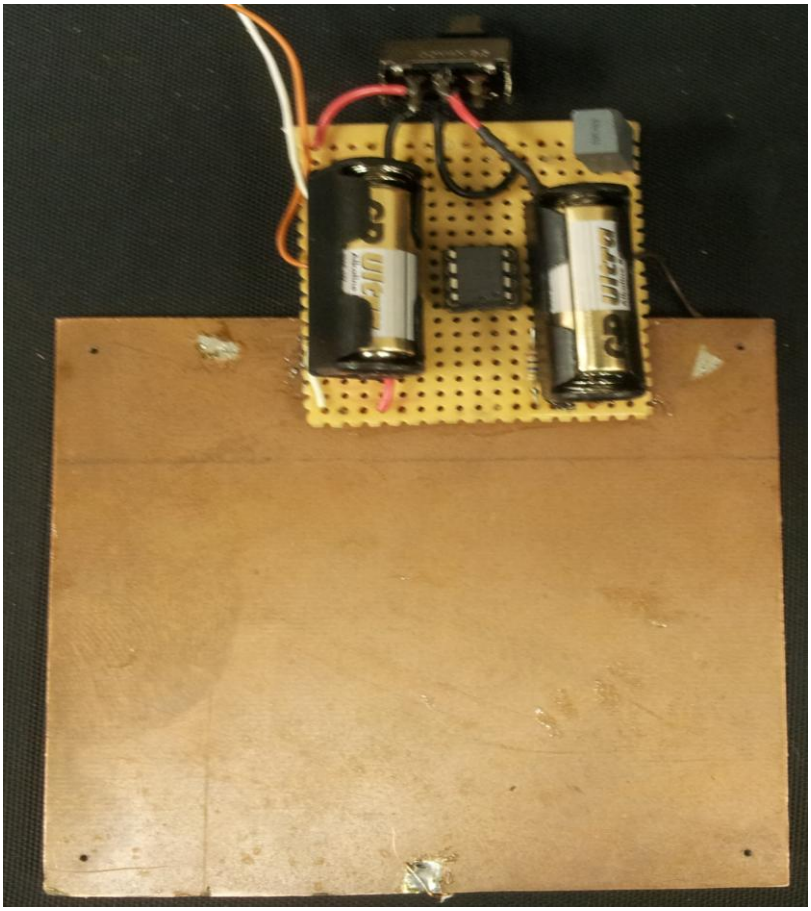

Figure 3.3-8: Complete measurement device.

A Fluke 189 true RMS multimeter was chosen for the task of measuring the voltage, this device worked well at the desired specifications. The inter-terminal capacitance and self-capacitances of the terminals were also measured. The self-capacitances were well matched and the inter-terminal capacitance was found to be insignificant towards the measurement. The results and procedure of this measurement are shown in Appendix B.

The complete device adheres to the IEEE standards [1, 2] which describe the desirable characteristics for a field meter. It is lightweight and durable, and portable. The voltage measurement device clearly displays the measured value, and has just one switch to turn the device on. The temperature and humidity effects were not extensively tested; however, the printed circuit board material, amplifier, components and wires used to construct the device are all expected to perform well under a wide range of temperatures.

3.4 Conclusion

A parallel plate capacitive electric field probe was designed and constructed in order to experimentally verify the model derived in chapter two. The effects that would adversely disturb the measurement were addressed and were taken into account in the design of a complete measurement device, which will be tested using a parallel plate uniform field generation apparatus. Some of those effects include positioning of the sensor in the field, parasitic self-capacitances resulting in common mode interference and the drift current on the sensor plates. The final design of the measurement device incorporated an instrumentation amplifier, which significantly increases the accuracy of the measurement by minimising the common mode interference. Chapter four contains the measurements that were taken using the system designed.

3.5 References

[1] IEEE Standard Procedures for Measurement of Power Frequency Electric and Magnetic Fields From AC Power Lines, Transmission and Distribution Committee Of The IEEE Power Engineering Society, IEEE Std. 644™-1994 (R2008) December 1998.

[2] IEEE Recommended Practice for Magnetic Flux Density and Electric Field Strength Meters—10 Hz to 3 kHz, Transmission and Distribution Committee Of The IEEE Power Engineering Society, IEEE Std. 1308™-1994, August 2011.

[3] *Transmission Line Reference Book-45 kV and Above*, second edition, Palo Alto, Calif.: Electric Power Research Institute, 1982.

[4] Burr-Brown, "Precision Instrumentation Amplifier," INA114 datasheet, October 1993.

Chapter 4

Experimental Validation and Analysis

4.1 Introduction

The measurement device designed and described in chapter three was used in order to confirm the validity of the circuit model derived in chapter two and the boundaries of its application.

The sensor was placed in a uniform electric field with varying field strengths and frequencies. The resulting output was measured and then compared to the expected results using the model derived in chapter two.

Measurements were also taken in order to determine the frequency characteristics of the sensor plates, which is essentially a parallel plate capacitor.

This chapter documents the methodology of the experiments undertaken as well as their results. It also contains a critical discussion of these results and an analysis of possible improvements to the sensor and model.

4.2 Experimental Methodology

The AC field generated using the device described in section 3.2 of chapter two was varied by simply changing the supply voltage between these two plates. This input voltage waveform was monitored using an oscilloscope, while the output voltage was monitored using the Fluke 189 true RMS multimeter.

The measurements were taken iteratively, varying the voltage across the outer plates in steps through the voltage range at each frequency. The same approximate voltages were used at each frequency, where the measurements were taken at 50 Hz, 100 Hz,

200 Hz, 300 Hz, 400 Hz and 500 Hz. The field strengths are calculated using equation 4.1. The field, *E*, was varied from 0 to 1400 V/m.

$$E = V/d \tag{4.1}$$

The exact measured values that were generated for each testing frequency are documented in Appendix C. These exact input values were used in the calculation of the predicted output voltage of the sensor circuit. All of the electric field and voltage values presented in this chapter are shown in RMS.

It can therefore be understood that the input to the measurement system is a variable electric field generated by the outer plates, and the output will be the measured voltage at the output of the sensor circuit which, as described in chapter three, is voltage at the output of the amplifier.

4.3 Calculated and Measured Results

The values that were calculated which are labelled as the results expected from the contemporary theory are predicted using the theory described in section 2.4 of chapter two.

4.3.1 Calculation of Results Using the Model

Figure 4.3-1 shows the circuit diagram of the sensor model connected to the amplifier with the internal impedances of the amplifier.

The symbols used in Figure 4.3-1 are consistent with those used in the preceding chapters. The voltage, V_{in}, is the voltage at the input of the amplifier, R_{in}, the input resistance and C_{in} is the input capacitance. This is the voltage which is calculated and compared to the experimental measurement since the output voltage of the amplifier is expected to be approximately equal to this voltage (the amplifier has a gain of one as mentioned in chapter three).

By simple circuit analysis, V_{in} can be calculated using equation 4.2. With reference to Figure 4.3-1, this voltage is simply the current emanating from the dependent source multiplied by the equivalent impedance of the parallel branches.

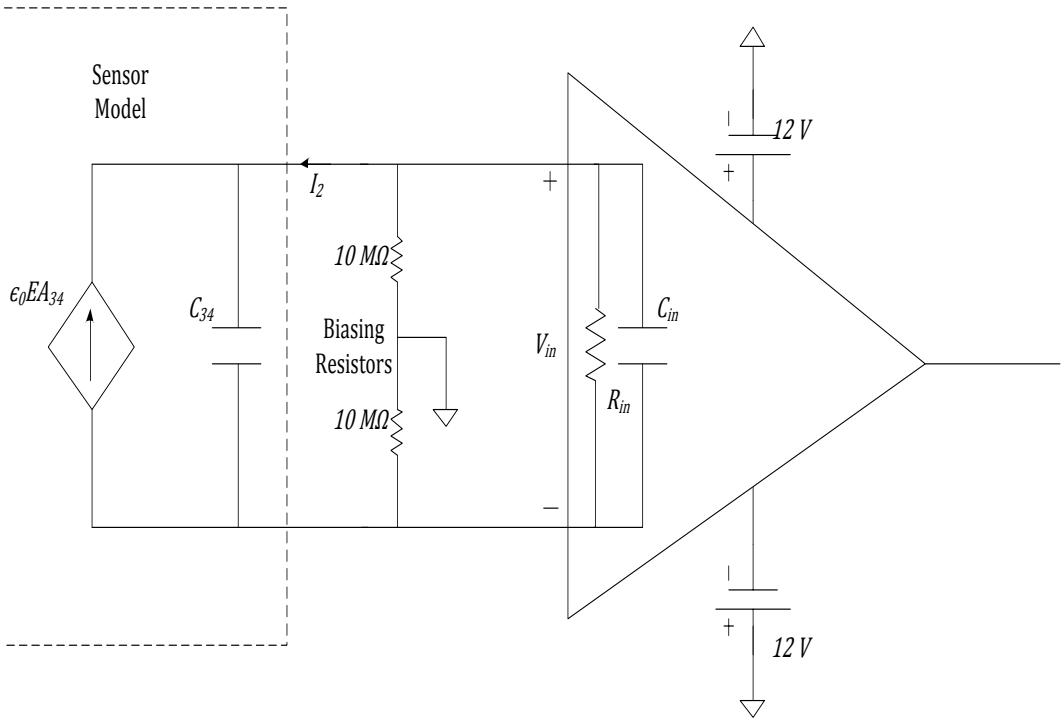

Figure 4.3-1: Sensor model and amplifier circuit diagram.

$$V_{in} = j\omega\varepsilon_0 EA_{34} \times \left[(Z_{C_{34}} || Z_{C_{in}}) \angle 90° || R_{in} \angle 0° || \ 20\ M\Omega \angle 0°\right] \tag{4.2}$$

By observing equation 4.2, it is evident that the input voltage to the amplifier, V_{in}, is dependent on the frequency of operation. This is because of the phase difference between the capacitive impedance terms (Zc_{34}, as well as Zc_{in}) and the resistive terms, R_{in}, and the bias resistors branch.

For the calculation of the impedance term of the model, the actual measured capacitance was used, and this was found to be approximately 275 pF. The device used for this measurement was a precision LCR meter. According to the manufacturer

datasheet [1], the input impedance of the amplifier is 100 GΩ, and the input capacitance is 6 pF. The measurements for the parallel plate sensor could have been taken using an oscilloscope and frequency generator as well, where the impedance could be calculated by simply using Ohm's law. The calculated values for the impedances, and the currents expected from the dependent source are shown in Appendix C.

4.3.2 Results of Experiment

A comprehensive comparison is documented in this section. For each testing frequency, thirteen measurements for voltage were taken and each measurement was compared to its corresponding calculated values using the contemporary theory prediction, as well as the model prediction.

The graphs are shown as Figure 4.3-2 up to Figure 4.3-7. On the y-axis of all the graphs, the input (varying electric field) is shown, and the output voltage of the sensor circuit is shown on the x-axis.

On all of the graphs, all three waveforms, the measured results and those predicted by the model and contemporary theory are clearly linear. The graphs also show a very close agreement, or a very small difference between the expected and measured waveforms. There is a clear difference in the gradients of the curves. There is also a clear frequency dependence on this difference in gradient, and this frequency dependence is significantly decreased in the model prediction, however, reasons for this, and the analysis of these graphs is shown in the subsequent section.

Table 4.3-1 shows the difference percentages of the gradients calculated for the respective frequencies and the frequency dependence of the gradients become more evident. Appendix C contains the numerical values that were calculated and measured. Figure 4.3-8 and Figure 4.3-9 show the curves which describe the difference percentages of the gradients of the contemporary theory prediction and the model prediction with respect to frequency. The gradients are calculated using the least squares fit straight line equation of the curves.

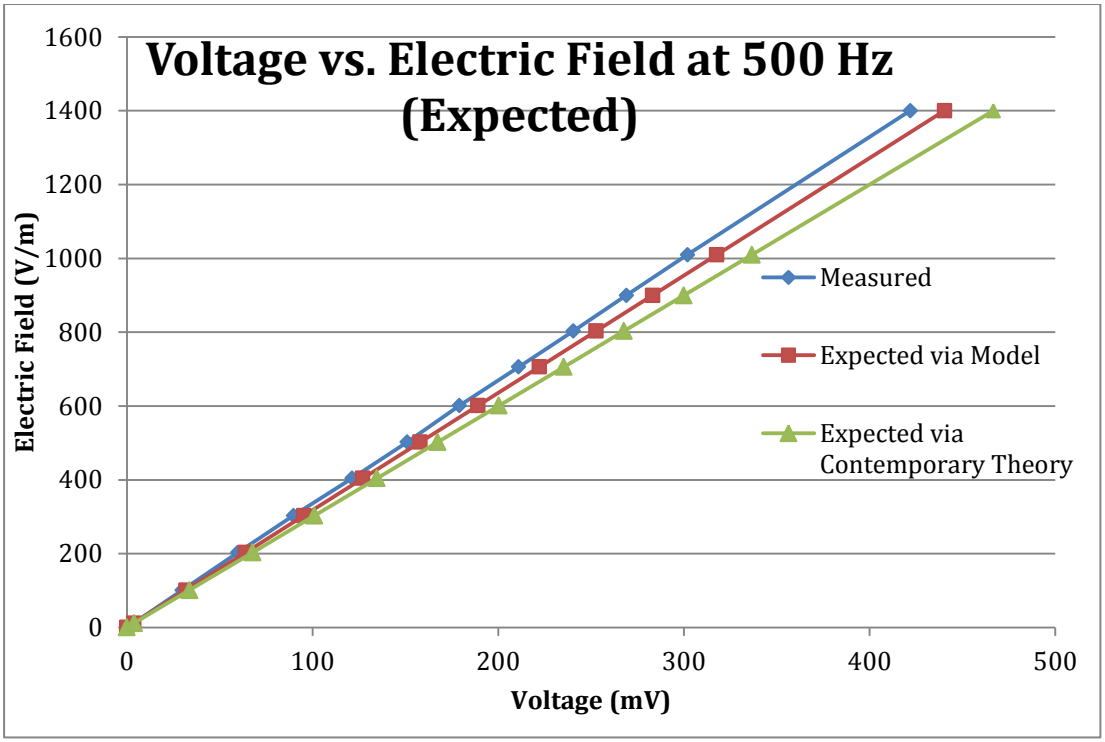

Figure 4.3-2: Graph showing the comparison of the expected output voltages for changing input field at 500 Hz.

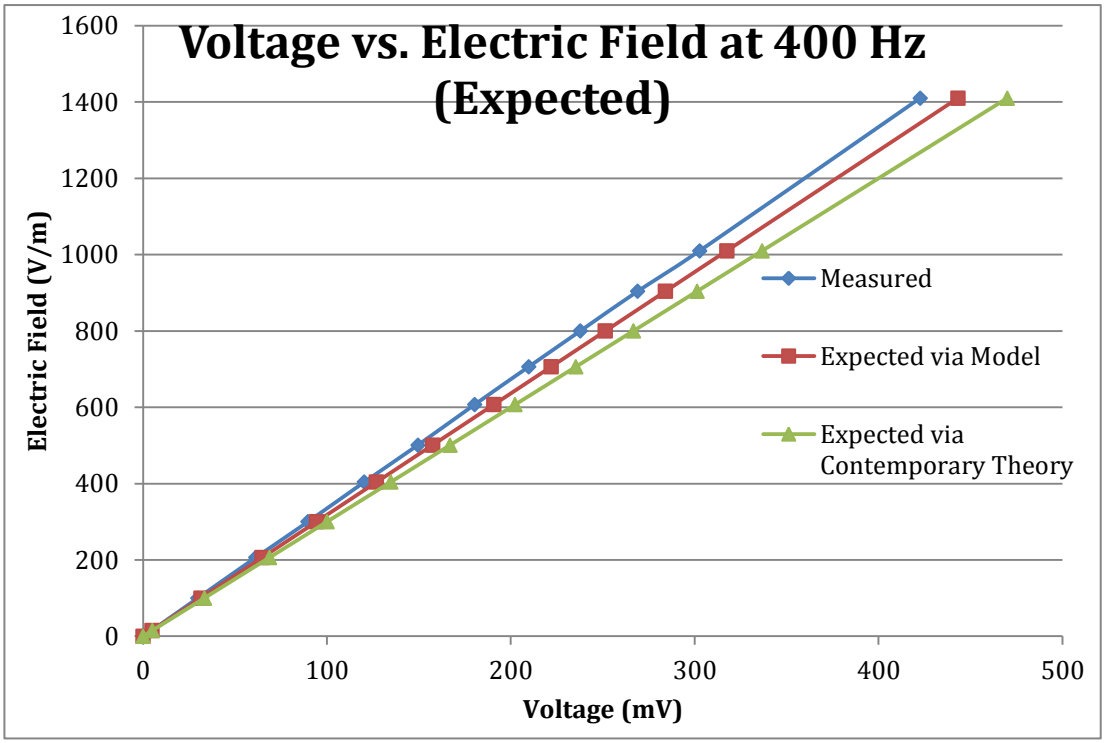

Figure 4.3-3: Graph showing the comparison of the expected output voltages for changing input field at 400 Hz.

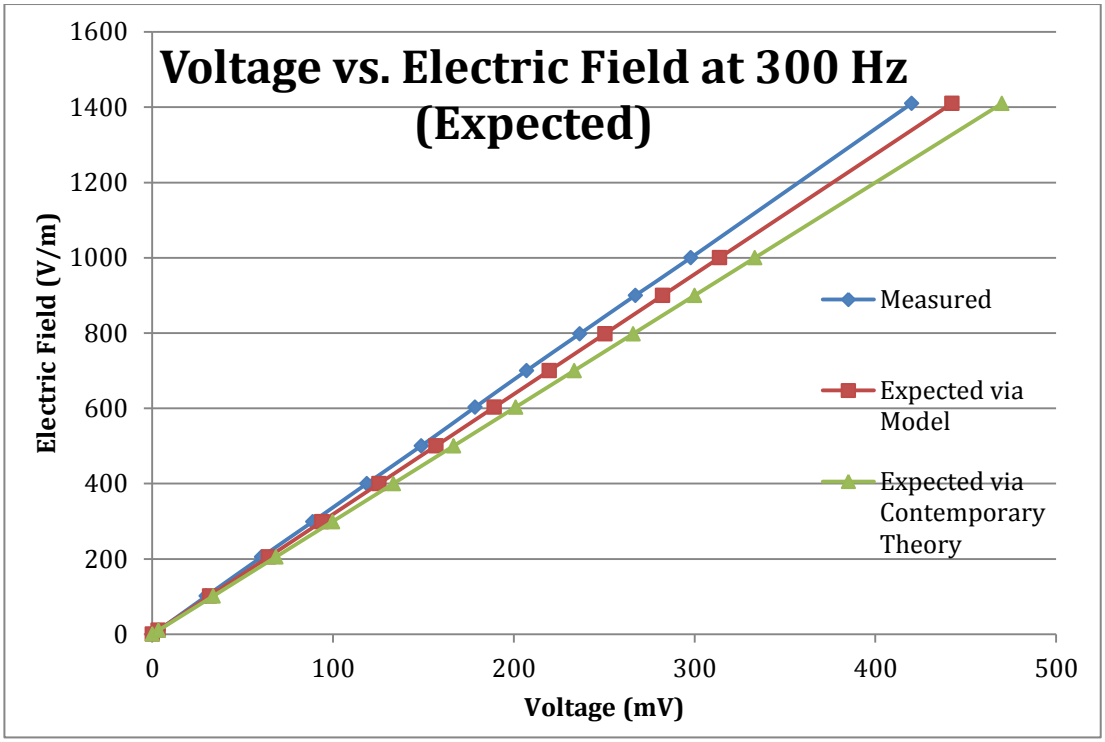

Figure 4.3-4: Graph showing the comparison of the expected output voltages for changing input field at 300 Hz.

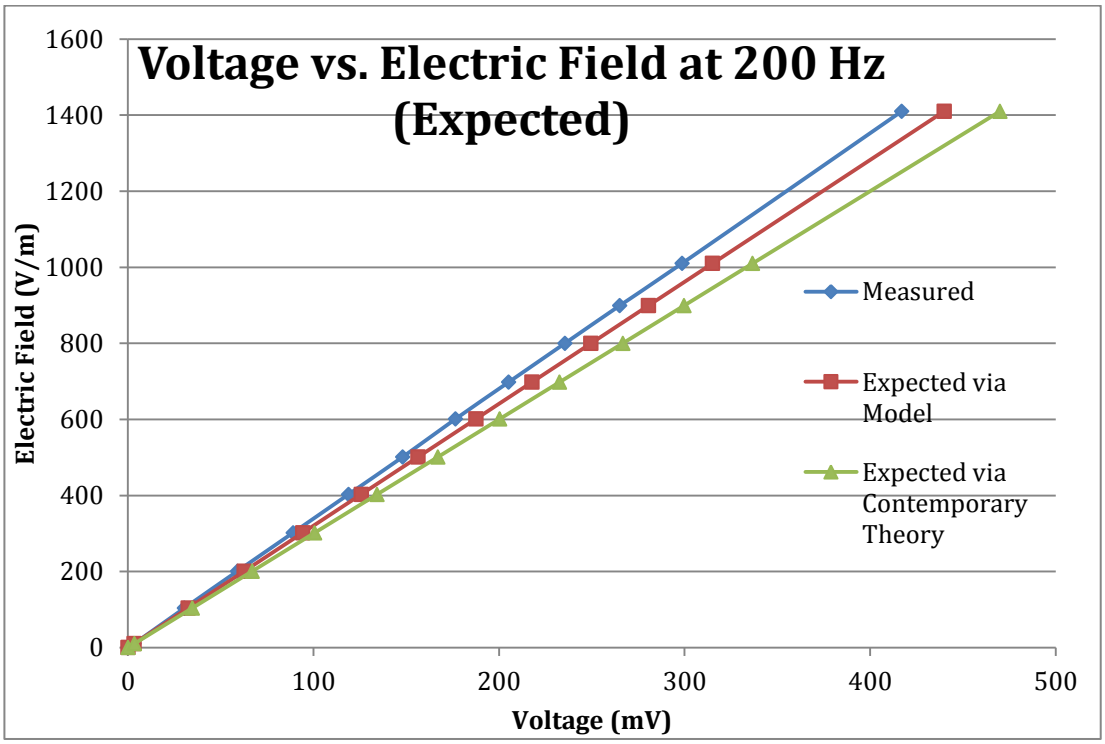

Figure 4.3-5: Graph showing the comparison of the expected output voltages for changing input field at 200 Hz.

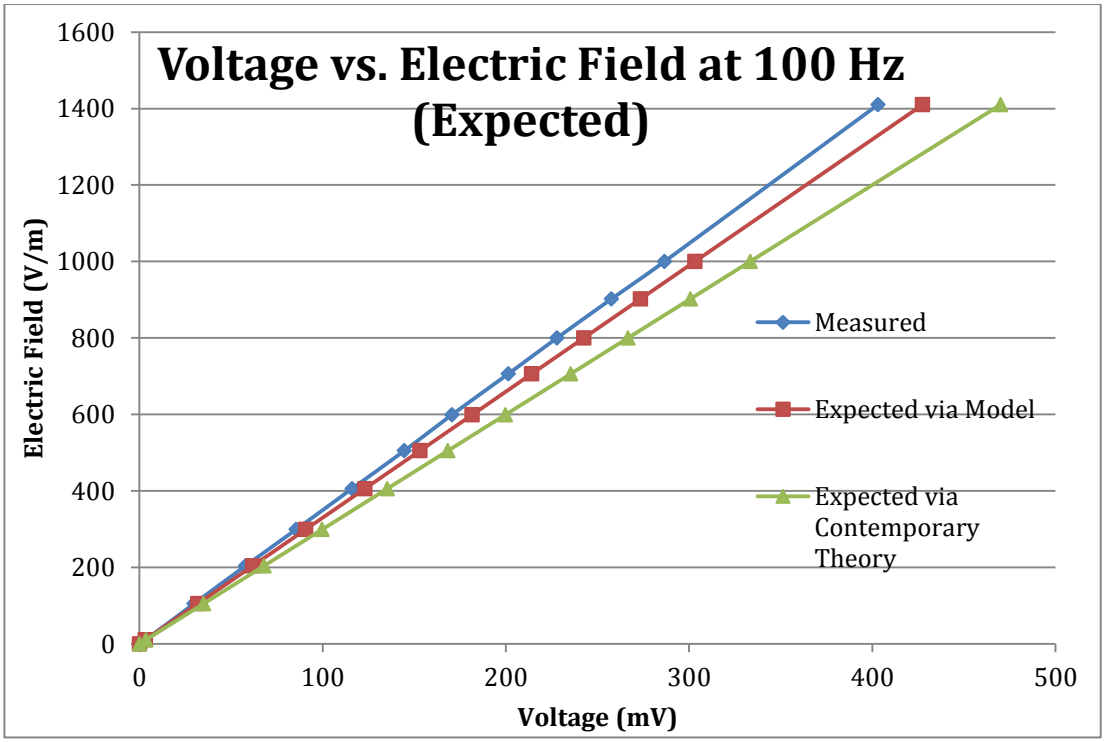

Figure 4.3-6: Graph showing the comparison of the expected output voltages for changing input field at 100 Hz.

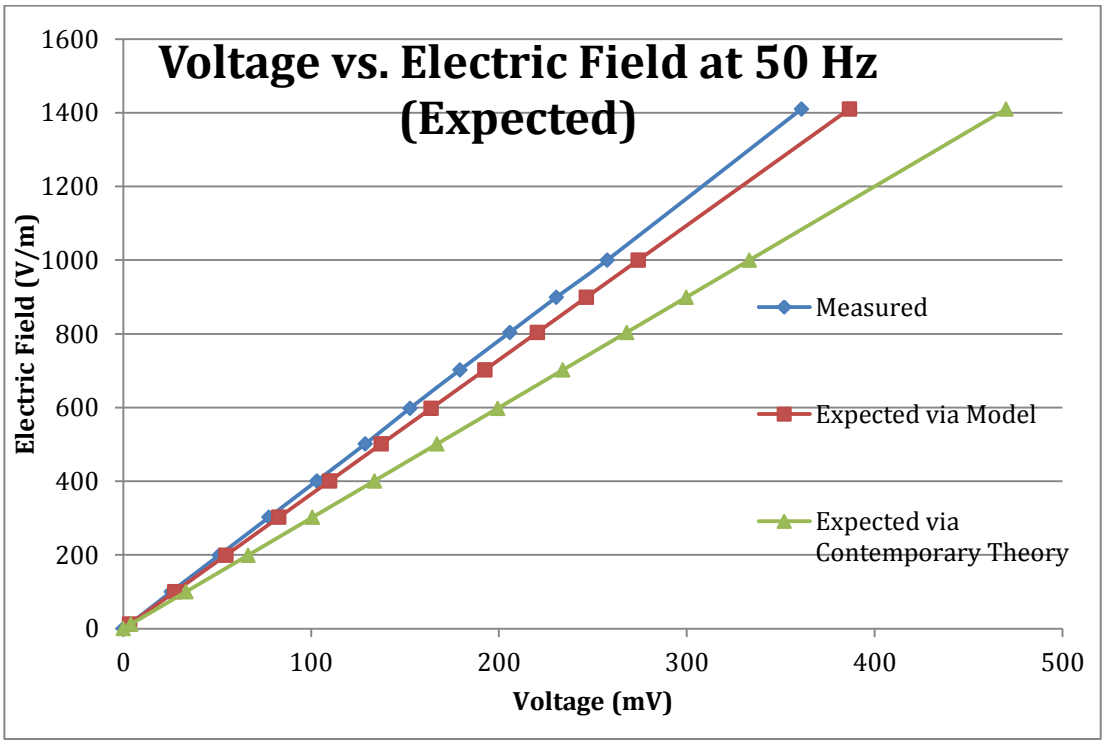

Figure 4.3-7: Graph showing the comparison of the expected output voltages for changing input field at 50 Hz.

Table 4.3-1: Gradient percentage differences between measured and predicted waveforms for their respective frequencies.

Frequency (Hz)	*% Gradient Difference between Contemporary Theory Prediction and Measured Voltages*	*% Gradient Difference between Model Prediction and Measured Voltages*
50	30.00	6.85
100	16.67	6.06
200	12.83	5.78
300	12.00	5.40
400	11.33	5.03
500	11.00	4.72

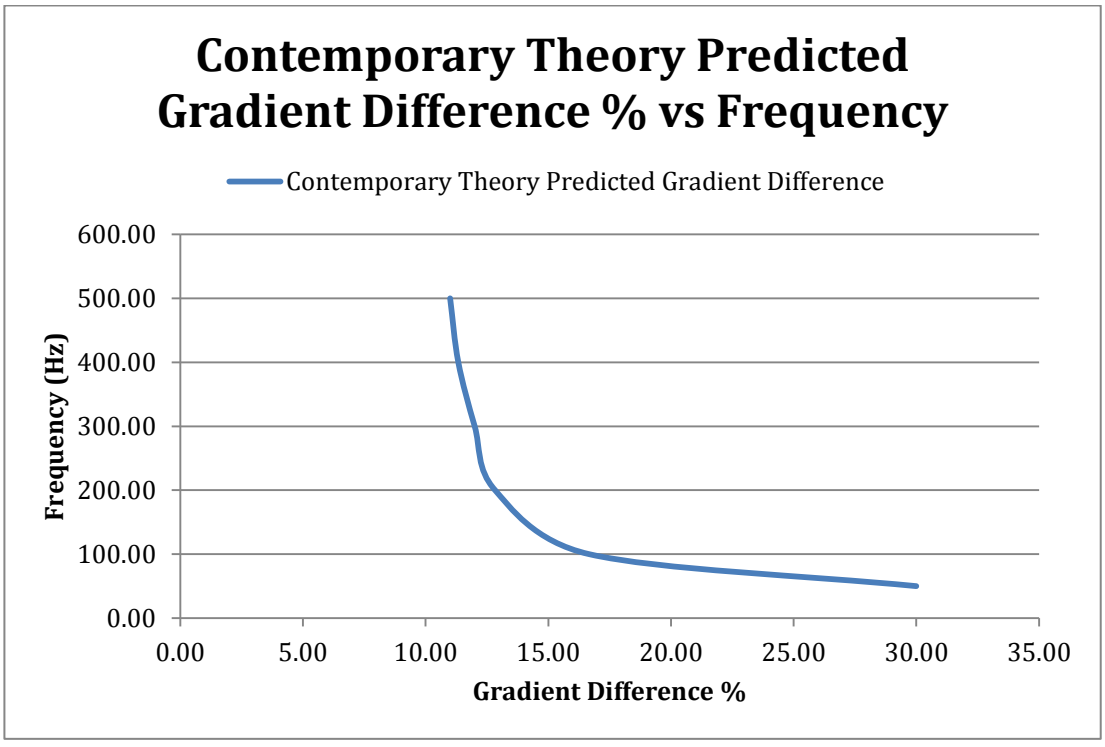

Figure 4.3-8: Gradient difference percentage of the contemporary theory prediction with respect to frequency.

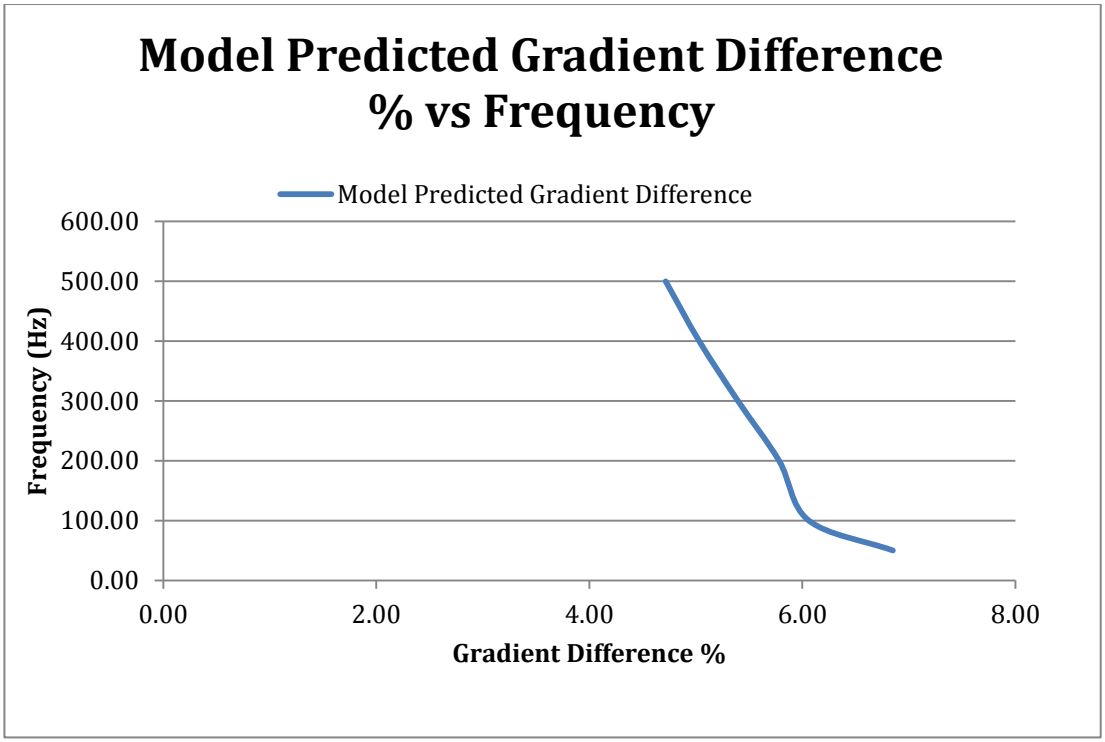

Figure 4.3-9: Gradient difference percentage of the model prediction with respect to frequency.

4.3.3 Analysis of Results

It is clear that the model prediction was less frequency dependant and agreed better with the experimental results than the contemporary prediction. Both provided a linear relationship between the system input and its output, i.e., the electric field and the resulting measured voltage.

The reason for which the contemporary theory differed more than the model prediction from the measured values is the lack of accountability for the capacitive and resistive impedances which are present at the output of the model. This is a frequency dependant impedance and hence the deviation from the measured waveform was also dependant frequency. This is shown by Table 4.3-1 and Figure 4.3-8. The model clearly provided better results since it allowed for the simple accountability of this impedance, as shown in section 4.3.1.

The model prediction, however, still showed a considerable difference in gradient from the measured waveform, with a small frequency dependence, as shown by

Figure 4.3-9 and Table 4.3-1. This can be attributed to the fringing fields in the region of the sensor.

By taking into account the approximate fringing field in the model, shown by Figure 4.3-10; it is possible to reduce the deviations between the expected and measured waveforms. The approximated fringing effect on the model is derived in chapter two, and is partially shown as the source current modification written as $\varepsilon_0 E_1 A_f$, as well as an added capacitance in parallel to the sensor plate, C_f. It is difficult to account for the exact percentage distribution of this total difference caused by fringing to the source and to the capacitance. By modifying either of these values separately (either the capacitance or the source current), the approximated effect of fringing can be accounted for.

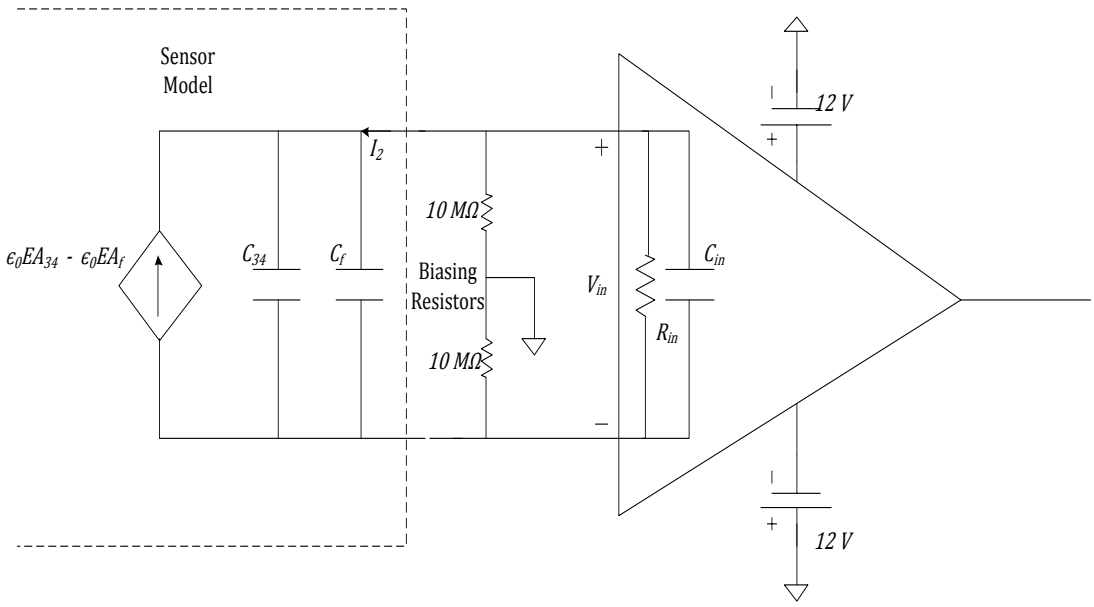

Figure 4.3-10: Sensor model with the approximated fringing effects and the amplifier circuit diagram.

Therefore, by approximating that the fringing effects can be attributed to the parallel capacitance, C_f, it is possible to reduce the deviations in gradient between the measured and expected waveforms. Thus, the compensated voltage calculated for V_{in} is shown as equation 4.3. The compensated waveforms compared to the model prediction as well as the measured results are shown as Figure 4.3-11 to Figure 4.3-16.

$$V_{in} = j\omega\varepsilon_0 E A_{34} \times \left[(Z_{C_{34}} || Z_{C_f} || Z_{C_{in}}) \angle 90° || R_{in} \angle 0° || \ 20\ M\Omega \angle 0°\right] \quad (4.3)$$

The approximated value for the fringing capacitance, C_f, is assumed to be 7 % of the capacitance between the sensor plates, C_{34}. This is the value which provides the least average difference in the gradients of the graphs throughout the range of frequencies. Thus, C_f is calculated to be 19.3 pF. The fringing that occurs is geometrically dependant on the structure and not frequency dependant, and hence this capacitance is the same throughout the frequency range.

The difference percentages calculated between the gradients of the measured and compensated as well as the original model predictions is shown as Table 4.3-2. It is now evident that the differences are very small, i.e. below 2 %, and the graphs shown as Figure 4.3-11 to Figure 4.3-16 indicate that the fringing compensated and measured waveforms are much closer together. However, by carefully observing the differences in gradient, it is possible to notice a frequency dependence still present.

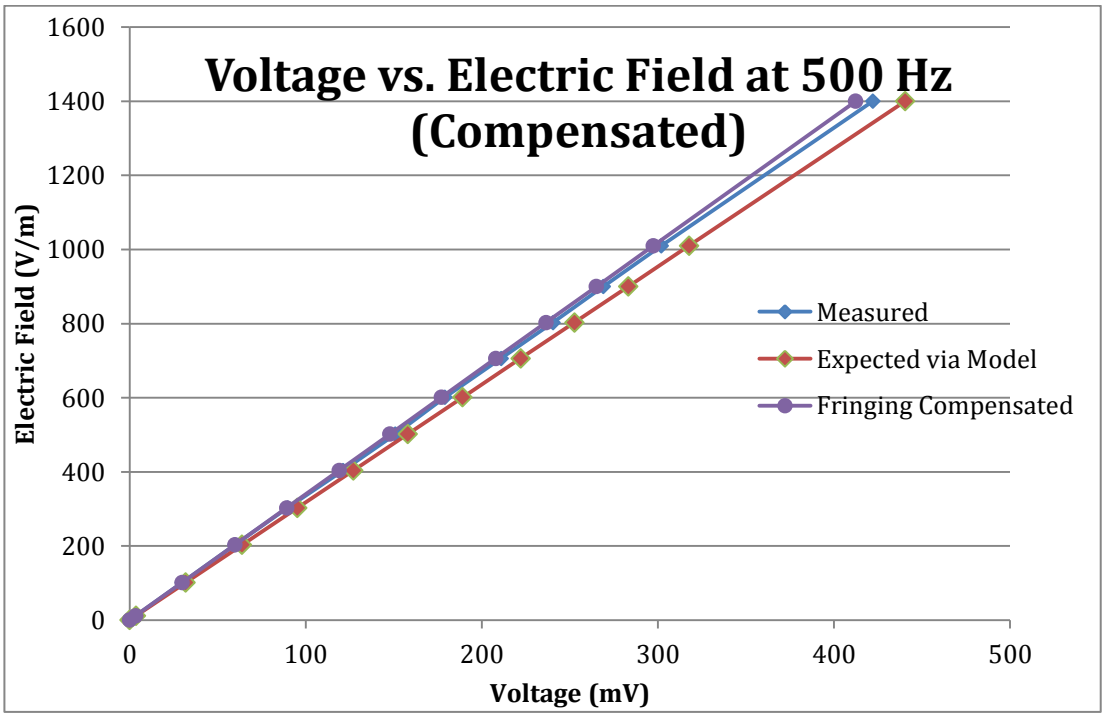

Figure 4.3-11: Graph showing the comparison of the compensated output voltages for changing input field at 500 Hz.

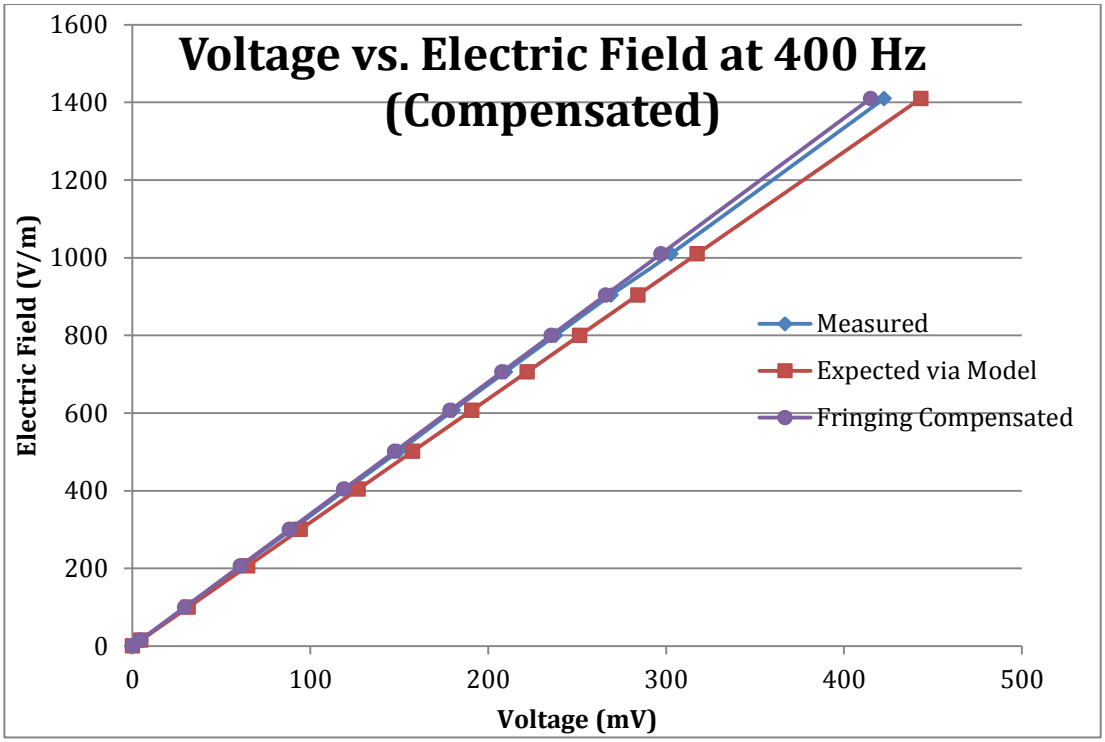

Figure 4.3-12: Graph showing the comparison of the compensated output voltages for changing input field at 400 Hz.

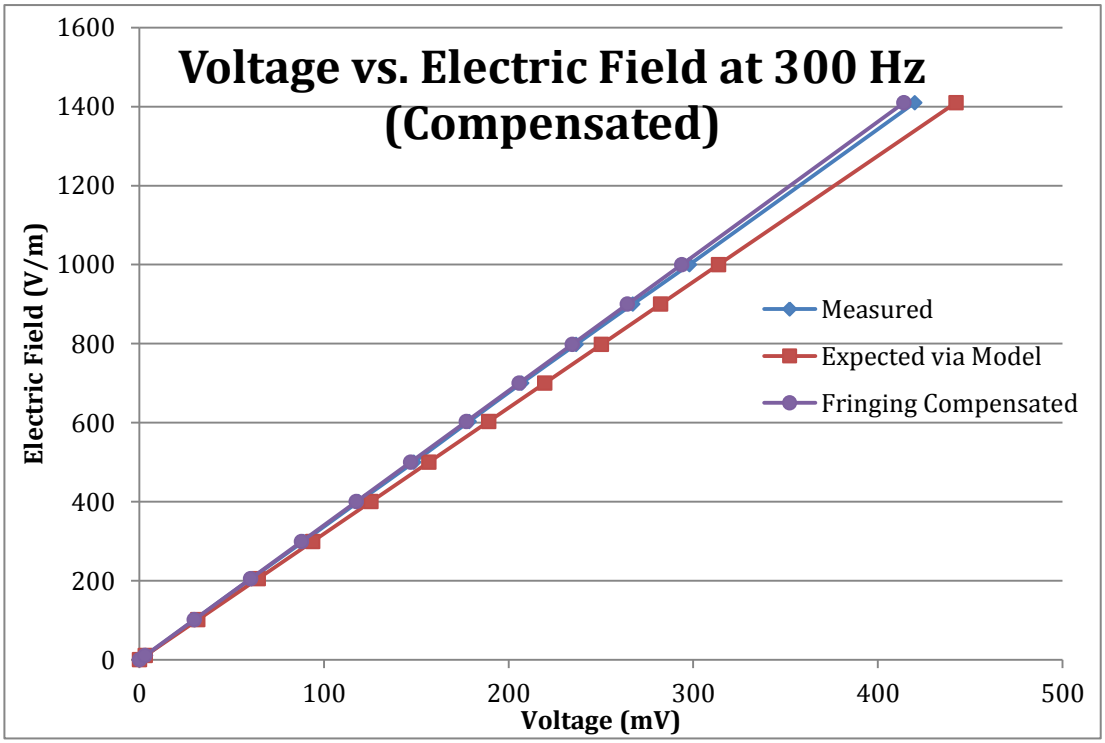

Figure 4.3-13: Graph showing the comparison of the compensated output voltages for changing input field at 300 Hz.

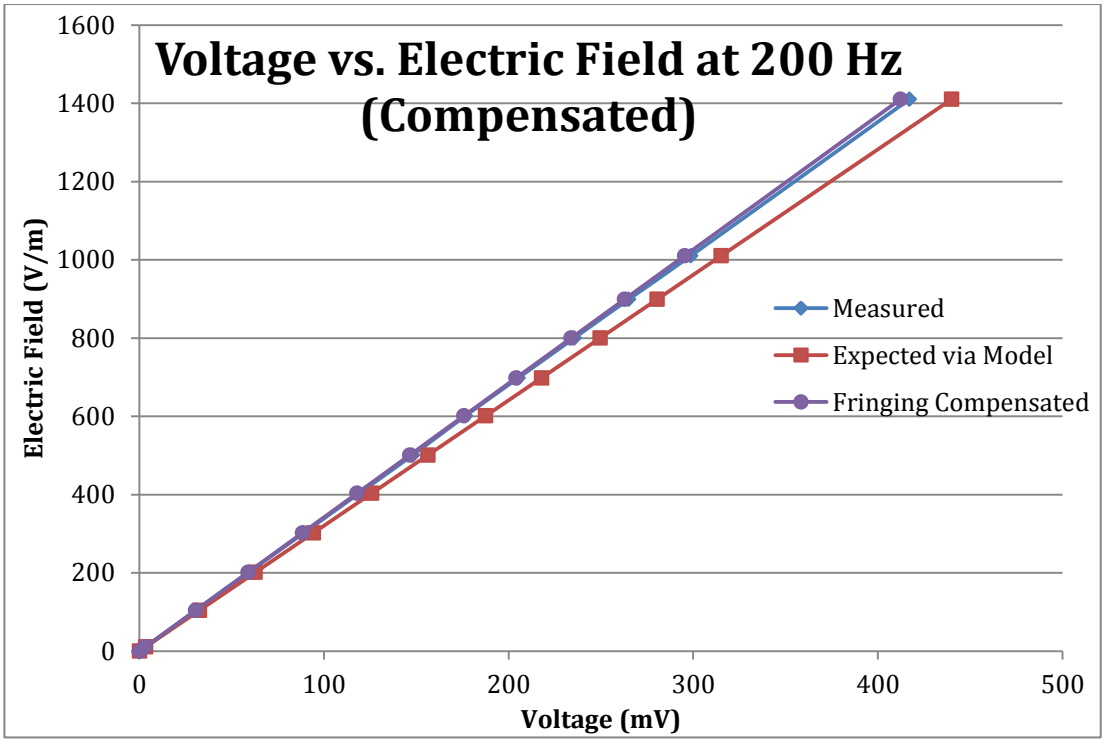

Figure 4.3-14: Graph showing the comparison of the compensated output voltages for changing input field at 200 Hz.

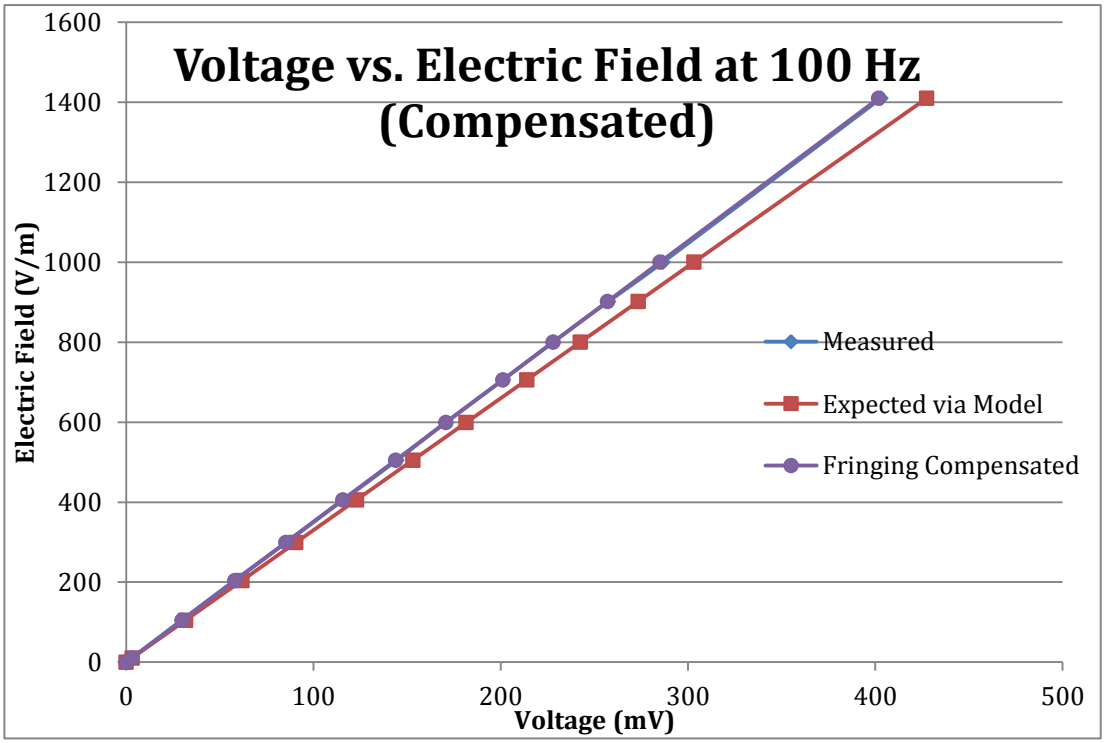

Figure 4.3-15: Graph showing the comparison of the compensated output voltages for changing input field at 100 Hz.

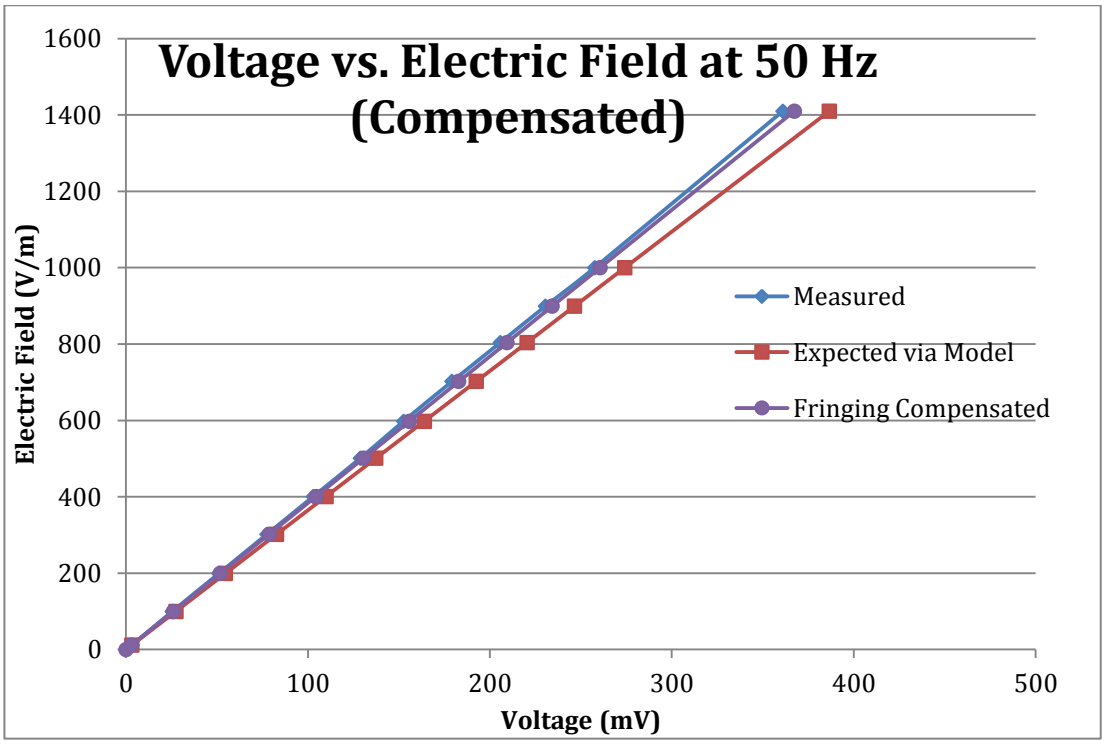

Figure 4.3-16: Graph showing the comparison of the compensated output voltages for changing input field at 50 Hz.

Table 4.3-2: Gradient percentage differences between measured, compensated and predicted waveforms for their respective frequencies.

Frequency (Hz)	***% Gradient Difference between Model Prediction and Measured Voltages***	***% Gradient Difference between Compensated Prediction and Measured Voltages***
50	6.85	1.56
100	6.06	-0.28
200	5.78	-1.02
300	5.40	-1.18
400	5.03	-1.74
500	4.72	-1.77

Figure 4.3-17 shows that the non-linear frequency dependant difference in gradient is still present, however, the difference percentages are much smaller when the model is used to compensate for fringing.

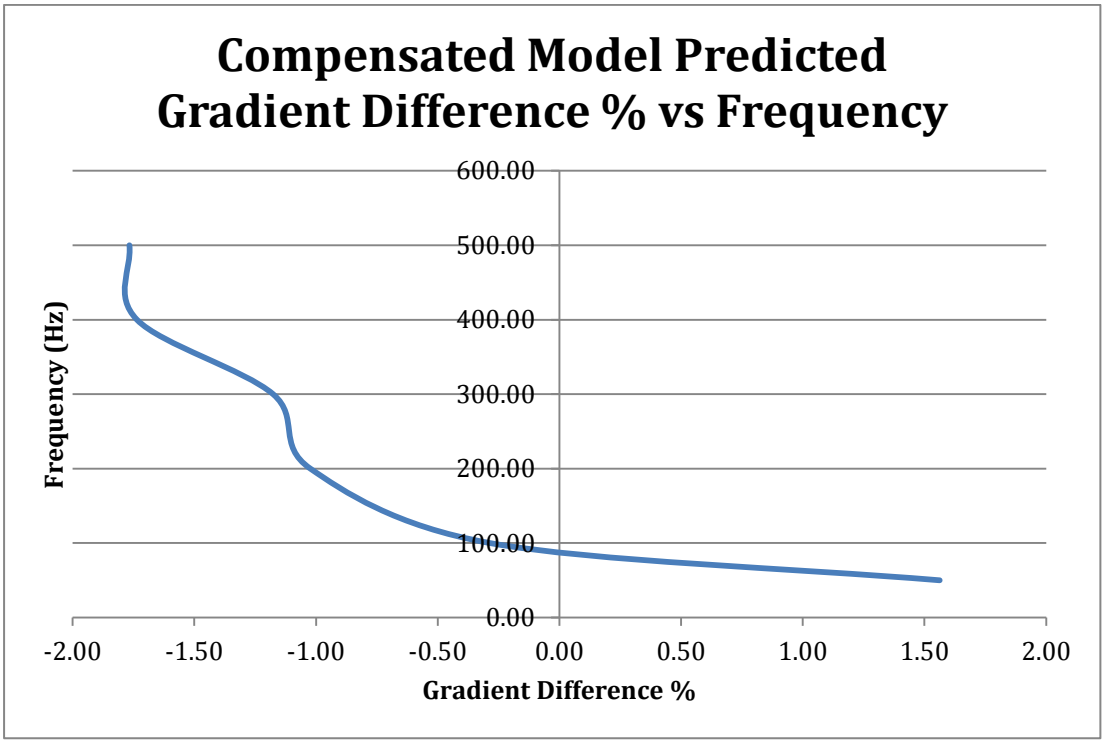

Figure 4.3-17: Gradient difference percentage of the model prediction with respect to frequency.

The input characteristics of the amplifier were tested in order to verify if this non-linear frequency dependant difference in gradient can be attributed to them. The measurement circuit is shown as Figure 4.3-18.

By varying the input voltage and frequency in the range of the measured output voltages of the sensor, and monitoring the current at the input of the amplifier, it was possible to validate if the input to the amplifier is non-linear.

The current measured at the input of the amplifier was consistently approximately 0.3 nA while the voltage was varied between 7.07 mV and 400 mV throughout the frequency range (50 Hz to 500 Hz).

It can therefore be deduced that the input characteristics of the amplifier perform as expected and are not responsible for the non-linear frequency dependant difference in gradient between the measured and expected waveforms.

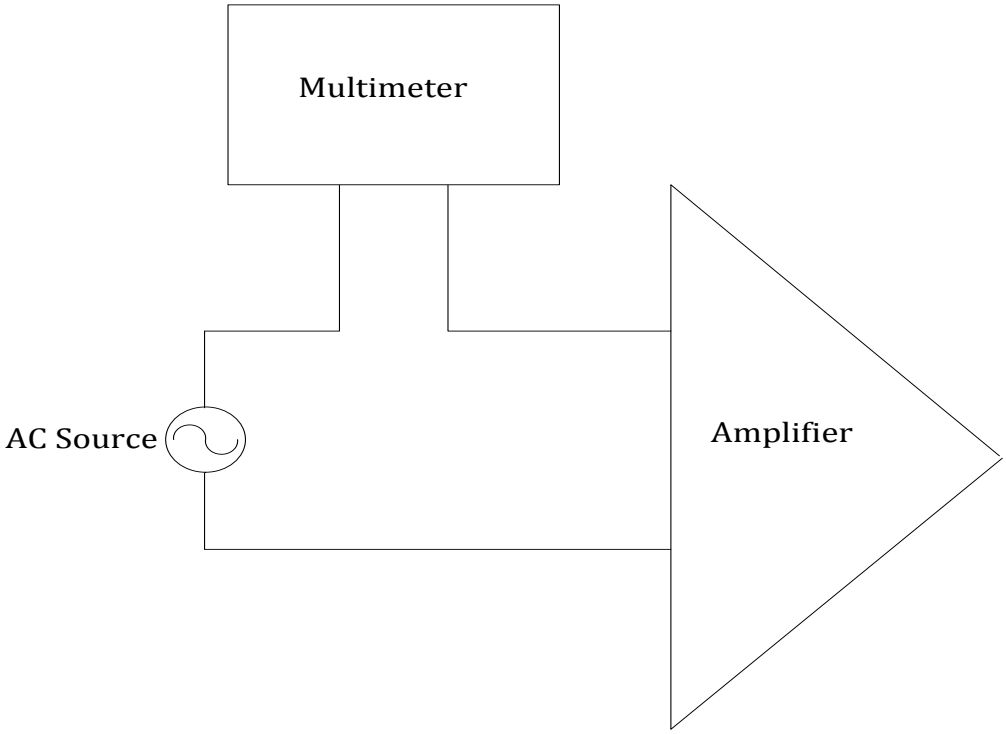

Figure 4.3-18: Circuit used to verify the input characteristics of the amplifier.

The remaining difference, which is small (below 2 %), is therefore suspected to be due to the external field modifying the characteristics of the amplifier circuit. It could also be due to inaccuracies in the voltage measurement device at the output of the amplifier.

The compensation for fringing effects are generally eliminated by calibration of the electric field measurement device, however, the model provides the opportunity to approximate these effects on a circuit level and hence take them into account.

4.3.4 Frequency Characteristics of the Sensor

The characteristics of the sensor were evaluated using a precision LCR meter. The phase and impedance plots are represented by Figure 4.3-19 and Figure 4.3-20 respectively.

The parallel plates which form the sensor form a well-defined capacitor, with a measured capacitance of approximately 275 pF. It was expected to perform well throughout the frequency sweep range of the LCR meter, which was limited to 2 MHz.

The phase plot of Figure 4.3-19 shows that the angle of impedance of the capacitor remains almost constant up to 2 MHz. The magnitude of the phase angle was plotted (its actual value is negative) against the frequency logarithmically. This means that it can perform well out of its required operating frequency range (50 Hz to 500 Hz) as specified in chapter three.

The logarithmic scaled impedance plot also indicates that the frequency modifies the impedance as expected throughout the testing range. This means that the impedance is purely capacitive and that resonances due to the parasitic inductance do not affect the sensor at these frequencies. If this inductance does produce resonances, the circuit model of the sensor will no longer be able to predict the outcomes of the system as it does not account for this effect.

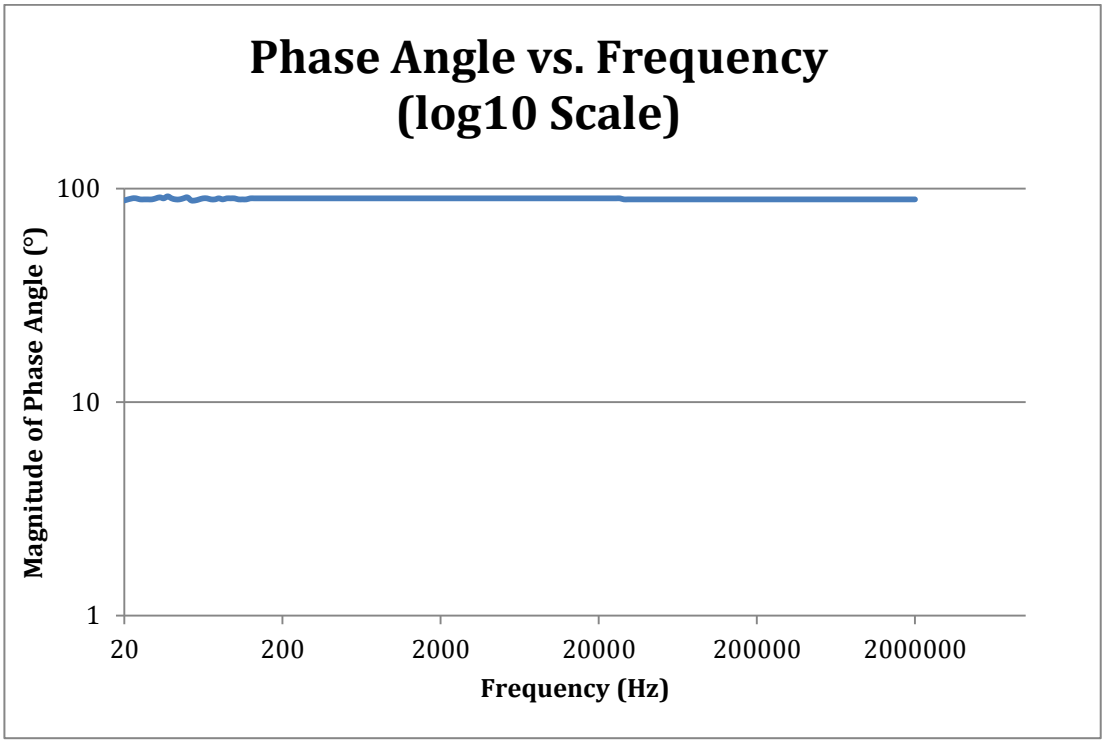

Figure 4.3-19: Phase plot of the parallel plate sensor.

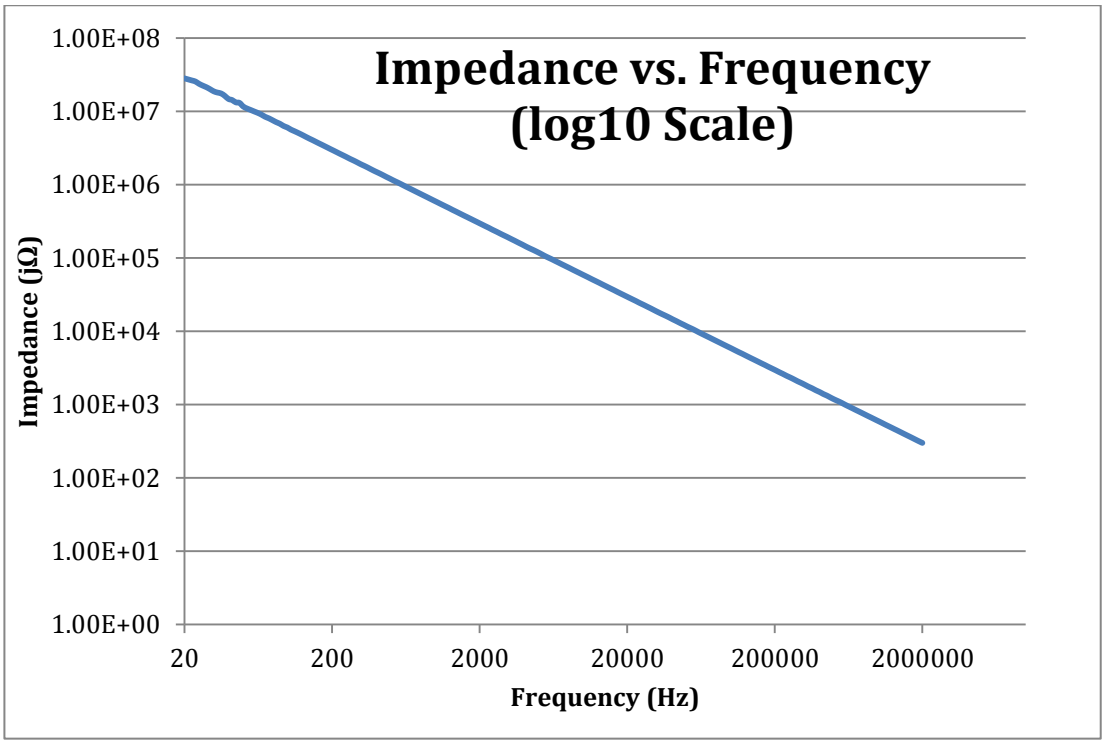

Figure 4.3-20: Impedance plot of the parallel plate sensor.

4.4 Possible Improvements and Future Work

There are various improvements that can be made to the design of the measurement system. Some of these are provided below.

- A robust positioning enclosure or attachment can be used which allows for more maneuverability of the sensor.
- The circuit could be assembled in more economically allowing for a more compact design where the area of the circuit does not overlap the sensor plates.
- The inclusion of a microprocessor and storage chip which could store the measured fields digitally.

Future work could include the extensive study of the device characteristics with respect to humidity and temperature. The actual quantification of the input characteristics of the amplifier in the field environment could be conducted

experimentally and this could possibly improve the model prediction and account for the difference in gradients between measured and predicted waveforms. This would require the amplifier to be present in the field, while its external input current would be monitored for changes as the field frequency is varied. This would be done without the sensor present.

A more detailed investigation into the fringing approximation of the model could be conducted. This would entail the investigation of sensor structures with the deliberate geometrical design of maximizing the fringing fields in the region of the sensor, for example, plates that are extended on both sides, or plates that are curved at the edge. This would increase the amount of fringing and the model approximation could be further verified and improved.

Measurements of non-uniform fields could be taken in three-dimensions where the magnitudes of the field can be vectorially added in each dimension. This could be experimentally verified and compared to the prediction by the model in this environment.

The device could be isolated using a well-designed isolation transformer which operates well at the desired frequencies and hence a grounded instrument can be used to measure the exact waveforms that the device produces. The design of this device would entail careful consideration of the measurement characteristics of the oscilloscope probes. This would prevent the problem described in chapter three where the device would distort the electric field and hence cause an unreliable measurement.

4.5 Conclusion

The device described in chapter two was used in order to experimentally verify the model derived in chapter two. The results show that the difference in gradient between the measured and expected waveforms was small, but indicated that there was a frequency dependant issue which was compensated for using an approximation for fringing. The deviation between the waveforms was significantly reduced, however, it was deduced via further analysis that the remaining difference can be attributed to modification of the characteristics of the measurement circuit by the field

(non-ideal performance of the amplifier when placed in the field environment) or to inaccuracies in the measurement device. The parallel plate sensor frequency characteristics show that it performs well throughout its required operating frequency range and can even be operated up to 2 MHz. The model was useful in the analysis of the results. Future work includes broadening the scope of the model investigation in order to include various other topologies and geometries which can improve the fringing approximation of the model, hence allowing for a model that is less dependent on geometries.

4.6 References

[1] Burr-Brown, “Precision Instrumentation Amplifier,” INA114 datasheet, October 1993.

Chapter 5

Conclusion

This chapter concludes the research presented in this document by presenting the methodologies employed and the outcomes of the preceding chapters.

A comprehensive literature review on the topic of electric field detection, and in particular the devices used for uniform AC fields. Some applications of electric field detection were presented. The basic principles of operation of typical devices that are used for AC electric field detection are discussed, these are the two capacitive types, i.e., free-body meters and ground reference meters, as well as the optical field probe. A summary is also included which describes devices that are used for DC field detection. The lack of a simple circuit model which represents a parallel plate sensor in a uniform electric field from the current theory was highlighted. Some applications of electric field detection are mentioned and include wireless voltage detection and live line maintenance. The theory which describes a four bodied system in terms of a two port network circuit model showed prospect in the derivation of an electric field sensor model.

An intensive exploration of the contemporary theory available to analyse free-body sensors is shown and some of its limitations are described, they include the inability to design sensors for specific applications and a method of analysis which is complicated and physics based. A detailed explanation of the derivation of the four bodied system model which includes the description of the inter-capacitances that arise due to the proximity of conductive bodies is portrayed. Using FEM simulations, a simple model was derived which represents a parallel plate sensor in a uniform electric field. This model, under the assumption that the bodies generating the uniform field are sufficiently large and far apart, is shown to be equivalent to the four bodied system model. Approximations were made for the consideration of the effects

of fringing and self-capacitances of the sensor plates. Limitations include the lack of accountability for external interference.

In order to verify the model that was derived, a measurement system was designed. This system had to include a uniform field generation device, these were large parallel plates separated by a small distance relative to the size of the plates. This field generation system was energised using a grounded supply system. This meant that in order to not distort the field, the measurement device could not be grounded and had to be designed to operate as a free-body meter. In the derivation of the circuit model, the assumption which states that the currents at the input and output of each port must be equal, explains that the model cannot be applied to a ground-reference meter. The measurement system was comprised of the sensor, an amplifier and a voltage measurement device. The amplifier was introduced so as to remove the common mode interference present in the circuit, thus increasing the precision of the measurement of the sensor plate voltage.

Measurements were taken with iterations through voltages and frequencies. The results of the measurements were presented in comparison to the expected values predicted by the model. There was good agreement between these values; however, by accounting for the approximate amount of fringing fields in the region of the sensor, the results were improved significantly. The reason for the remaining difference is examined with the use of the model and can be attributed to the non-ideal characteristics of the amplifier in the field environment and the voltage measurement device errors.

Possible improvements include the adaptation of the model to account for various geometries and conductor arrangements in the investigation of the effects of increasing the fringing fields in the system. It would also be useful to verify the amplifier input characteristics in a field environment.

This chapter concludes the research undertaken in order to derive and verify a general circuit model which can be used for the design and prediction of performance of parallel plate uniform electric field sensors. Furthermore, this circuit model can be

used to compensate for the approximate amount of fringing electric fields present in the region of the sensor.

Appendix A

Electromagnetic Fundamentals

A.1 The Concepts of Charge and Electric Field

In order to establish a firm understanding of how electric fields are defined and how they affect conductors, the concept of charge must be defined. The theory described in this section is adapted from [1].

Charge is simply a property, like mass, that is assigned to particles. Particles are defined to possess positive or negative charges, and like charges will repel each other, while unlike, or opposite charges will be attracted to each other. This is illustrated by Figure A.1-1.

Figure A.1-1: Charged particles.

The fundamental quantity of charge is that of a proton, denoted by *e*, this is the same as the negative of the charge of an electron and is specified in units of Coulombs (C). An object that has more positive charge than negative charge is defined as a positively charged object, and similarly for a negatively charged object.

It is worthwhile to note that a change in charge on a body means that a current is flowing through that body and the direction of the current indicates whether the change in charge is positive or negative. Thus the concept of current is defined as the rate of flow of charge.

The force that these charged particles will attract or repel each other is defined by Coulomb's law. This force, *F*, with units of Newtons, N, is called the electrostatic force and is given by equation 1.1.

$$F = \frac{kq_1q_2}{d^2} \tag{1.1}$$

Where *k* is Coulomb's constant, q_1 and q_2 are the charges of the respective particles and *d* is the distance between these particles.

It can therefore be deduced that there is some form of influence from a particle due to its charge that surrounds the particle. This means that because of the property of charge that a particle has, by placing another particle close to it, within in range of this field that surrounds it, this particle will be affected by it. This is called an electric field. Another way of describing this phenomenon is stating that for a specified charge present on particle A, the force that will be exerted onto another particle, particle B in its vicinity at a particular distance from it, is due to the electric field of particle A. This is shown mathematically in equation 1.2. So it can be said that the field is dependent on the charge generating the field, q_A, Coulomb's constant, and the distance between the particles. This electric field has the units of Newtons per Coulomb (N/C).

$$E = \frac{F}{q_B} = \frac{kq_A}{d^2} \tag{1.2}$$

It is therefore possible, depending on the geometry to draw the electric field pattern around a charged particle or object. An example of this is shown in Figure A.1-2.

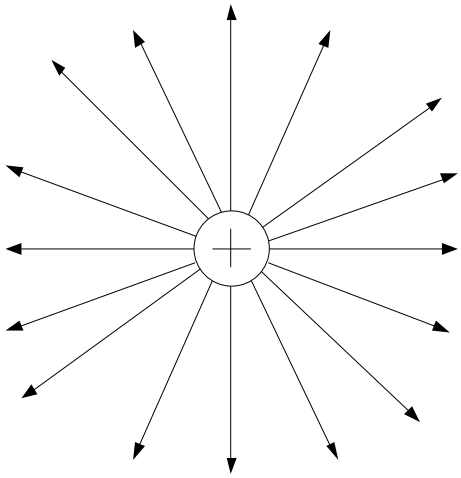

Figure A.1-2: Field pattern around a positive charge.

Electric flux lines are a representation of electric flux density. This means that for a particular closed surface, the electric field gives rise to a particular electric flux flowing through that surface and this can be shown by a surface with lines emerging from it, transverse to it. Another method of describing electric flux using Gauss' law is that the total amount of electric flux lines emerging from the closed surface is equal to the charge enclosed by that surface. Electric flux lines are always drawn to originate on a positive charge and end on a negative charge. Electric flux may be written in terms of the electric field or in terms of the enclosed charge on a surface and this is shown by 1.3. Where *E* is the electric field, *dA* is the differential area, ϵ_0 is the permittivity of free space, and Q_S is the charge on the closed surface *S*. It may also be written in terms of the flux density *D* as shown by 1.4.

$$\phi_{electric} = \oint_S E.dA = \frac{Q_s}{\epsilon_0} \tag{1.3}$$

$$\phi_{electric} = \int_S D.dS \tag{1.4}$$

When a charge is placed in an electric field, it has a potential energy to move from one point to another in the field. This potential energy is basically the force that is

exerted on the charge by the field over the distance which it has to move and is represented mathematically by equation 1.5.

$$W_{x1\ to\ x2} = \int_{x1}^{x2} F.dx = q_B \int_{x1}^{x2} E.dx \tag{1.5}$$

Where x denotes position in space, and $W_{x1\ to\ x2}$ is the work done (with the units of Joules) to move the charge from x_1 to x_2 (the start and end points respectively). The other variable definitions are consistent with those from equation 1.2. Simply, this electric potential energy is the amount of work required to move a charge from the point x_1 to the point x_2 and is measured in Joules (J).

The amount of work done per unit charge is defined as the electric potential. This means that the electric potential is independent of the charge of the particles. It is the potential relative to position in space. The unit for this quantity is Joules per Coulomb (J/C) or Volts (V). This implies now that the electric field can have the units of Volts per meter (V/m).

A.1.1 Capacitance from a Fundamental Perspective

Capacitance is a constant describing the interaction between voltages and charges between conductors and this can be shown by observing two conductors in free space which are oppositely statically charged. This situation causes the charges to reside on the outer surface of the conductors and the flux density becomes equal to the charge density. Thus all the flux lines that originate from the one conductor end on the other, and from the flux density, the electric field strength can be calculated. This means that the voltage between the conductors can also be determined. Thus by doubling the charges, the voltage will be doubled as well.

Thus capacitance between two conductors in a vacuum can be represented by 1.6 and is a good measure of charge storage capability. This because, as mentioned in the preceding section, voltage, *V,* can be described as measure of the electric potential energy for a unit charge to move from one point to another. *Q* is the surface charge.

$$C = \frac{Q}{V} \tag{1.6}$$

The units for capacitance are Farads and it can be expressed in independently in terms of the geometry of the interacting conductors.

A.2 References

[1] R. S. Elliot, *Electromagnetics: History, Theory and Applications*. IEEE Press, New York, first edition, chapter 3, pp. 98- 215, 1999.

Appendix B

Measurements of the Multimeter Capacitances

B.1 Inter-terminal Capacitance

The specifications of the Fluke 189 true RMS multimeter indicate that the inter-terminal capacitance is less than 100 pF. It does not provide an exact value; hence a measurement of this capacitance is required in order to determine the self-capacitances of each of the terminals. For all the measurements shown in this chapter, the multimeter was operated in voltage measurement mode, because of this, a measurement bridge cannot be used since the bridge and multimeter signals will interfere with each other.

This measurement is simple and is operates on the principles of Ohms law. A voltage waveform is supplied via a known impedance and a simple voltage divider is formed. The input voltage is measured separately without the impedance and compared to the voltage measured with the impedance present. The leads of the multimeter were removed for increased measurement accuracy.

The circuit diagram is shown as Figure B.1-1.

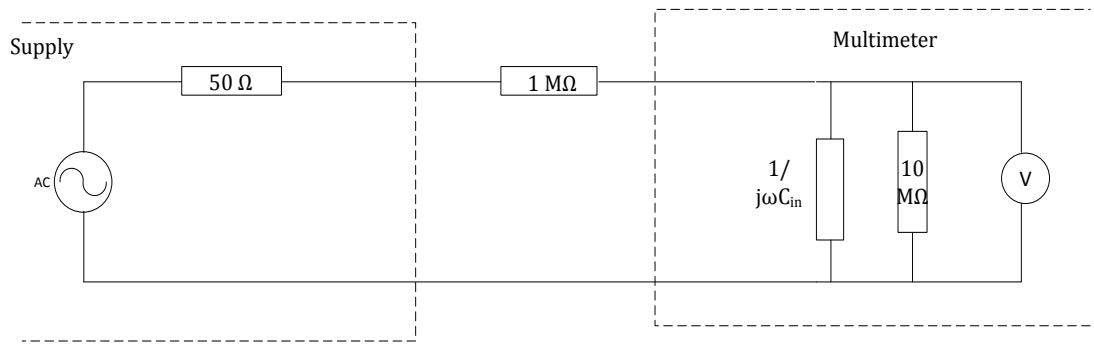

Figure B.1-1: Circuit diagram used for measurement of internal capacitance of multimeter.

The impedance of 1 MΩ was specifically chosen to be much smaller than the 10 MΩ internal impedance of the multimeter. A high frequency, i.e., 100 kHz was chosen so as to cause the impedance of the capacitor to be much smaller than that of the 10 MΩ resistor.

The voltages were measured and a simple voltage divider calculation showed that the magnitude of the impedance of the capacitor is 26.62 kΩ at the chosen frequency. This results in a capacitance of 59.77 pF which is within the specification of the multimeter.

A second measurement was taken in order to verify this value. This was done at 50 kHz. The value calculated for the magnitude of impedance at this frequency was 54.40 kΩ. This resulted in a capacitance of 58.51 pF.

For further confirmation, capacitors with known values, i.e., 10 pF were added to the circuit in parallel to the inter-terminal capacitor. The measurement showed that the values for the total parallel capacitances at 100 kHz and 50 kHz were 70.20 pF and 68.57pF respectively. These values are greater than the initial values by almost exactly 10 pF. It can therefore be concluded that the measurements were correct.

B.2 Self-Capacitances of the Terminals

For this setup a pseudo ground plane had to be defined. A large copper plate was used for this task. The Fluke 189 multimeter was placed above this plane, and with one lead removed, the remaining lead was energized at a sufficient voltage which allowed current to flow through the self-capacitances of the terminals. A photograph of the experimental setup is shown as Figure B.2-1.

The dimensional diagram is shown as Figure B.2-2 and the conceptual circuit diagram as Figure B.2-3.

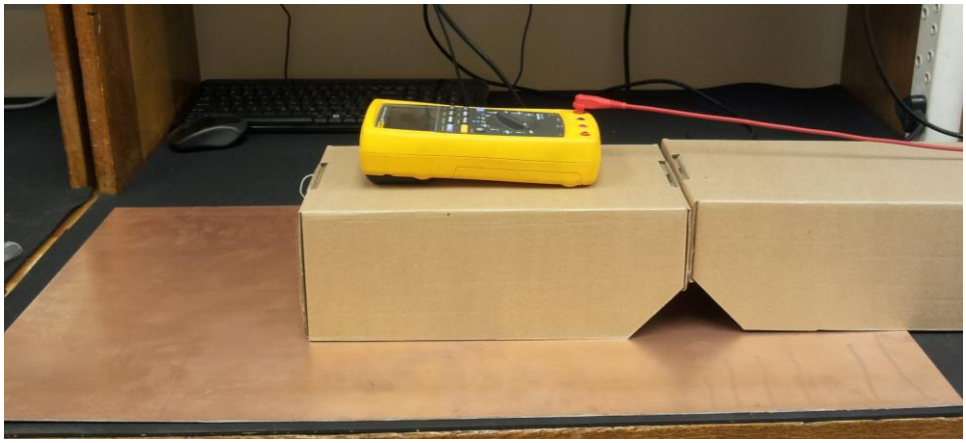

Figure B.2-1: Experimental setup used in order to measure the self-capacitances of the multimeter terminals

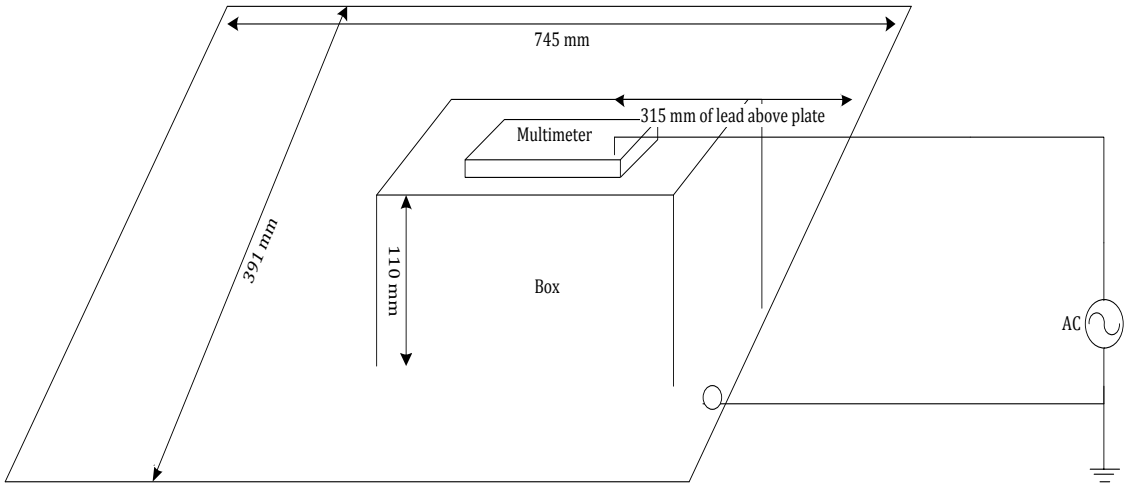

Figure B.2-2: Dimensional drawing of the setup used to measure self-capacitances.

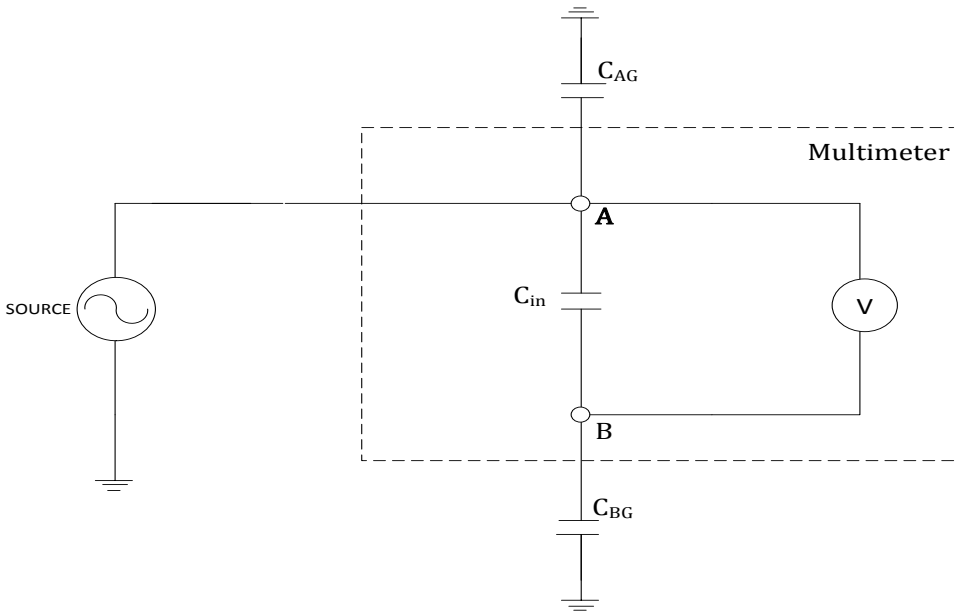

Figure B.2-3: Conceptual circuit diagram of the measurement setup.

The frequency chosen for measurement is 100 kHz and the voltage was set at 71.38 V. This basically allows for the capacitive impedance to be low enough for current to flow. Current measurements were taken using a current probe on an oscilloscope.

The measurements taken firstly show that the current and voltage are 90° out of phase. This confirms that there is a capacitive load. For the measurement at terminal A, the equivalent capacitance was calculated as 18.2 pF, and the measurement at terminal B produced a capacitance of 19.6 pF. These capacitances are well matched, hence, the multimeter was deemed suitable as the voltage measurement device for the measurement system.

Appendix C

Detailed Results

C.1 Numerical Values for Experimental Validation

The numerical values that were used in order to plot the graphs shown in chapter four are documented in tabular form. This is shown from Table C.1-1 to Table C.1-6. These tables simply contain the exact field strengths that were generated and the expected and measured voltages.

Table C.1-1: Numerical values obtained at 500 Hz.

Input Field Strength (V/m)	***Expected Output Voltage using Model (mV)***	***Expected Output Voltage using Contemporary Theory (mV)***	***Expected Output Voltage Compensated Fringing Model (mV)***	***Measured Output Voltage (mV)***
0	0	0	0.00	0
11.6	3.65	3.87	3.47	3.6
101	31.77	33.67	30.21	29.8
203	63.86	67.67	60.72	59.73
303	95.32	101	90.63	89.7
404	127.09	134.67	120.84	121.3
502	157.92	167.33	150.16	150.9
601	189.07	200.33	179.77	179
706	222.10	235.33	211.18	211
803	252.61	267.67	240.19	240.4
900	283.13	300	269.21	269
1010	317.73	336.67	302.11	302
1400	440.42	466.67	418.77	422

Table C.1-2: Numerical values obtained at 400 Hz.

Input Field Strength (V/m)	***Expected Output Voltage using Model (mV)***	***Expected Output Voltage using Contemporary Theory (mV)***	***Expected Output Voltage Compensated Fringing Model (mV)***	***Measured Output Voltage (mV)***
0	0	0	0	0
11.6	4.81	5.1	4.57	3.47
101	31.43	33.33	29.89	30.21
203	64.75	68.67	61.57	60.72
303	94.29	100	89.66	90.63
404	126.98	134.67	120.75	120.84
502	157.47	167	149.74	150.16
601	190.78	202.33	181.42	179.77
706	221.90	235.33	211.01	211.18
803	251.44	266.67	239.10	240.19
900	284.13	301.33	270.18	269.21
1010	317.44	336.67	301.86	302.11
1400	443.17	470	421.41	418.77

Table C.1-3: Numerical values obtained at 300 Hz.

Input Field Strength (V/m)	***Expected Output Voltage using Model (mV)***	***Expected Output Voltage using Contemporary Theory (mV)***	***Expected Output Voltage Compensated Fringing Model (mV)***	***Measured Output Voltage (mV)***
0	0.00	0	0.00	0.00
11.6	3.23	3.43	3.07	3.47
101	31.68	33.67	30.13	30.21
203	64.31	68.33	61.16	60.72
303	93.79	99.67	89.21	90.63
404	125.48	133.33	119.34	120.84
502	156.85	166.67	149.18	150.16
601	189.16	201	179.91	179.77
706	219.59	233.33	208.85	211.18
803	250.33	266	238.09	240.19
900	282.32	300	268.52	269.21
1010	313.69	333.33	298.35	302.11
1400	442.31	470	420.68	418.77

Table C.1-4: Numerical values obtained at 200 Hz.

Input Field Strength (V/m)	***Expected Output Voltage using Model (mV)***	***Expected Output Voltage using Contemporary Theory (mV)***	***Expected Output Voltage Compensated Fringing Model (mV)***	***Measured Output Voltage (mV)***
0	0.00	0	0.00	0.00
11.6	3.28	3.5	3.12	3.47
101	32.45	34.67	30.87	30.21
203	62.71	67	59.67	60.72
303	94.22	100.67	89.66	90.63
404	125.73	134.33	119.64	120.84
502	156.30	167	148.73	150.16
601	187.50	200.33	178.42	179.77
706	217.76	232.67	207.22	211.18
803	249.58	266.67	237.50	240.19
900	280.47	299.67	266.89	269.21
1010	315.10	336.67	299.84	302.11
1400	439.89	470	418.59	418.77

Table C.1-5: Numerical values obtained at 100 Hz.

Input Field Strength (V/m)	***Expected Output Voltage using Model (mV)***	***Expected Output Voltage using Contemporary Theory (mV)***	***Expected Output Voltage Compensated Fringing Model (mV)***	***Measured Output Voltage (mV)***
0	3.18	0	0.00	0.00
11.6	31.83	3.5	3.04	3.47
101	61.85	35	30.37	30.21
203	90.65	68	59.01	60.72
303	123.08	99.67	86.49	90.63
404	153.10	135.33	117.43	120.84
502	181.59	168.33	146.07	150.16
601	214.03	199.67	173.26	179.77
706	242.53	235.33	204.21	211.18
803	273.45	266.67	231.40	240.19
900	303.16	300.67	260.90	269.21
1010	427.46	333.33	289.25	302.11
1400	3.18	470	407.84	418.77

Table C.1-6: Numerical values obtained at 50 Hz.

Input Field Strength (V/m)	***Expected Output Voltage using Model (mV)***	***Expected Output Voltage using Contemporary Theory (mV)***	***Expected Output Voltage Compensated Fringing Model (mV)***	***Measured Output Voltage (mV)***
0	0.00	0	0.00	0.00
11.6	3.29	4	3.16	3.47
101	27.42	33.33	26.37	30.21
203	54.56	66.33	52.48	60.72
303	82.79	100.67	79.65	90.63
404	109.94	133.67	105.76	120.84
502	137.35	167	132.13	150.16
601	163.94	199.33	157.71	179.77
706	192.46	234	185.14	211.18
803	220.42	268	212.04	240.19
900	246.46	299.67	237.10	269.21
1010	274.15	333.33	263.74	302.11
1400	386.56	470	371.87	418.77

C.2 Values Calculated for Current

In order to calculate the voltages predicted by the model, the current calculated by the dependent source needed to be calculated. These are shown together with their corresponding frequencies as Table C.2-1 and Table C.2-2.

Table C.2-1: Fields and their resulting currents from 50 Hz to 200 Hz

Frequency (Hz)	***50***		***100***		***200***	
	E (V/m)	***I (A)***	***E (V/m)***	***I (A)***	***E (V/m)***	***I (A)***
	0	0	0	0	0	0
	12	3.34E-10	10.5	5.84E-10	10.5	0.00E+00
	100	2.78E-09	105	5.84E-09	104	1.17E-09
	199	5.54E-09	204	1.13E-08	201	1.16E-08
	302	8.40E-09	299	1.66E-08	302	2.24E-08
	401	1.12E-08	406	2.26E-08	403	3.36E-08
	501	1.39E-08	505	2.81E-08	501	4.48E-08
	598	1.66E-08	599	3.33E-08	601	5.57E-08
	702	1.95E-08	706	3.93E-08	698	6.69E-08
	804	2.24E-08	800	4.45E-08	800	7.77E-08
	899	2.50E-08	902	5.02E-08	899	8.90E-08
	1000	2.78E-08	1000	5.56E-08	1010	1.00E-07
	1410	3.92E-08	1410	7.84E-08	1410	1.12E-07

Table C.2-2: Fields and their resulting currents from 300 Hz to 500 Hz

Frequency (Hz)	***300***		***400***		***500***	
	E (V/m)	***I (A)***	***E (V/m)***	***I (A)***	***E (V/m)***	***I (A)***
	0	0	0	0	0	0
	10.3	1.72E-09	15.3	3.40E-09	11.6	3.23E-09
	101	1.69E-08	100	2.23E-08	101	2.81E-08
	205	3.42E-08	206	4.58E-08	203	5.65E-08
	299	4.99E-08	300	6.68E-08	303	8.43E-08
	400	6.68E-08	404	8.99E-08	404	1.12E-07
	500	8.34E-08	501	1.11E-07	502	1.40E-07
	603	1.01E-07	607	1.35E-07	601	1.67E-07
	700	1.17E-07	706	1.57E-07	706	1.96E-07
	798	1.33E-07	800	1.78E-07	803	2.23E-07
	900	1.50E-07	904	2.01E-07	900	2.50E-07
	1000	1.67E-07	1010	2.25E-07	1010	2.81E-07
	1410	2.35E-07	1410	3.14E-07	1400	3.89E-07

C.3 Impedances

The impedances were calculated by taking the parallel equivalent of all the branches from the sensor to the input of the amplifier. Because the amplifier has such a high input resistance, resistive branches gave an equivalent impedance of 20 MΩ. This did not change with frequency. The capacitive branches, however, did. Their equivalent impedances are shown at the respective frequencies as Table C.3-1. This table documents these impedances before the approximate fringing was taken into account. Table C.3-2 shows the impedances calculated with fringing approximated as a capacitance.

Table C.3-1: Impedances and their frequencies.

Frequency (Hz)	***Equivalent Impedance of Capacitive Branches (Ω)***	***Total magnitude of equivalent impedance (resistive and capacitive) (Ω)***
50	-1.13E+07j	9.84E+06
100	-5.66E+06j	5.45E+06
200	-2.83E+06j	2.80E+06
300	-1.89E+06j	1.88E+06
400	-1.42E+06j	1.42E+06
500	-1.13E+06j	1.13E+06

Table C.3-2: Compensated impedances and their frequencies.

Frequency (Hz)	***Equivalent Impedance of Capacitive Branches (Ω)***	***Total magnitude of equivalent impedance (resistive and capacitive) (Ω)***
50	-1.08E+07j	9.48E+06
100	-5.38E+06j	5.20E+06
200	-2.69E+06j	2.67E+06
300	-1.79E+06j	1.79E+06
400	-1.35E+06j	1.34E+06
500	-1.08E+06j	1.08E+06